SOME STUDIES ON COMPOSITE SOLID ELECTROLYTES

by

ASHOK KUMAR

DEPARTMENT OF MATERIALS SCIENCE

INDIAN INSTITUTE OF TECHNOLOGY KANPUR

December, 1993

SOME STUDIES ON COMPOSITE SOLID ELECTROLYTES

A Thesis Submitted

in Partial Fulfilment of the Requirements

for the Degree of

DOCTOR OF PHILOSOPHY

by

ASHOK KUMAR

to the

DEPARTMENT OF MATERIALS SCIENCE

INDIAN INSTITUTE OF TECHNOLOGY KANPUR

December, 1993

यतः प्रवृत्तिः भूतानां येन सर्वमिदं ततम् ।
स्वकर्मणा तमभ्यर्च्य सिद्धिं विन्दति मानवः ॥

He from whom all these creatures proceed. Who pervades all this worshipping Him through the performance of His work, man attains success.

SRIMAD BHAGAVADGITA

CERTIFICATE

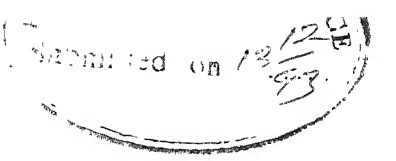

It is certified that the work contained in the thesis entitled, *"Some Studies on Composite Solid Electrolytes"* by *Ashok Kumar*, has been carried out under my supervision and that this work has not been submitted elsewhere for a degree.

K Shahi

K. Shahi

Professor, Department of Physics

and Materials Science Programme

I.I.T. Kanpur

December, 1993

SYNOPSIS

Name of Student : Ashok Kumar Roll No. : 8721261

Degree for which submitted	:	Doctor of Philosophy
Department	:	Materials Science Programme
Thesis Title	:	Some Studies on Composite Solid Electrolytes
Name of thesis supervisor	:	Prof. K. Shahi
Month and year of thesis submission	:	December, 1993

Considerable work has been done on composite solid electrolytes (CSEs) since the anomalous increase in the conductivity was discovered by Liang in LiI(Al_2O_3) composite system in 1973. The phenomenon has since been observed in a large number of systems involving matrix phases that exhibit Schottky (TlCl, LiCl, LiBr, LiI etc.) and Frenkel (AgCl, AgBr, AgI, CuCl, CaF_2, etc.) disorders, and a variety of dispersoids such as Al_2O_3, SiO_2, CeO_2, ZrO_2, Fly-ash etc. Almost all the models proposed to explain the enhancement in conductivity presume the formation of a high conducting space charge layer at the matrix/dispersoid interface. However, the exact mechanism of formation and the characterization of the space charge layer are still subjects of intensive research.

The present work reports a systematic study of the composite solid electrolyte effect on some cationic and anionic conductors. Lead halides which are anionic conductors, have been chosen

because unlike most other CSEs, $PbCl_2$-Al_2O_3 composites are reported to show a decrease in the conductivity. Alkali halides have been chosen because though the studies on CSEs are numerous and vigorous, the alkali halide based composites with the exception of lithium salts have not been investigated seriously. These may be more suitable materials to study the conduction mechanism in CSEs because they (i) generally do not undergo any solid-solid phase transition at ambient pressure, except cesium salts, and thus they provide a wider temperature range of study, (ii) have point defect (Schottky) type disorder having low concentration of defects thus show extrinsic effects appreciably, and (iii) are less hygroscopic except lithium salts. CsCl has been chosen because both of its B1 and B2 phases are normal ionic conductors. Thus the effect of Al_2O_3 on the phase transition can also be studied besides the composite solid electrolyte effect.

Chapter one reviews the historical development and classification of solid electrolytes. Besides, the properties of CSEs and different conduction mechanisms proposed to explain the enhancement in conductivity are discussed in this chapter.

Chapter two deals with the theoretical aspects of complex impedance analysis and general theory of ionic conductors. Also included in this chapter are the theory of heterogeneous doping as given by Jow and Wagner and developed by Maier and the Random resistor network percolation model.

Various synthesis and characterization techniques employed in the present work have been described in Chapter three. The details of the Conductivity set-up, Impedance analyzer, X-ray diffractometer, Differential thermal analyzer and Scanning electron microscope are given in this chapter. The conventional and solution casting methods of sample preparation have been described.

Chapters 4, 5 and 6 form the results and discussion part of the thesis. Chapter four presents the results of various measurements (XRD, DTA , SEM and Conductivity) on the PbX_2-Al_2O_3 (X = Cl, Br, I) composite systems. PbI_2-Al_2O_3 composites show enhancement in conductivity, whereas $PbCl_2$-Al_2O_3 and $PbBr_2$-Al_2O_3 composites show lowering in conductivity over their respective pure phases. These anomalous results are discussed in view of the fact that Pb^{2+} ions are virtually immobile in $PbCl_2$ and $PbBr_2$ whereas their mobility is appreciable in PbI_2.

Chapter five presents the results for MCl-Al_2O_3 (M = Na,K,Rb) composite systems. The composites containing up to 50 m/o Al_2O_3 have been synthesized by conventional and solution casting methods having three different particle sizes of Al_2O_3. The samples prepared by solution casting method show better conductivity results than those prepared by conventional method. The dependence of conductivity on composition, particle size and processing supports the space charge theory of conduction in CSEs. The calculated values of conductivity for different concentrations and

particle sizes of Al_2O_3 have been found to be in agreement with the observed values, suggesting the validity of Maier's theory. Macroscopically, the Random resistor network model explains the observed results adequately.

The conduction characteristics of CsCl-Al_2O_3 composites have been discussed in chapter six. The presence of space charge layer is evident in this system. Though the well known B1 (NaCl) $\longleftrightarrow$ B2 (CsCl) structural phase transition in CsCl is detected by the DTA of CsCl-Al_2O_3 composites, it is conspicuous by its absence in the conductivity vs temperature studies. This apparent suppression of B1$\longleftrightarrow$B2 transition in the CsCl-Al_2O_3 composites in the σ - T plots has been attributed to the fact that the conduction in the composites is dominated by the space charge region at the matrix-particle interface, and thus remains unaffected by the phase transition occurring in the bulk of the matrix phase.

Finally the summary and conclusions are given at the end. The following conclusions have been drawn from this work :

1. The conduction mechanism in the CSEs essentially involves the matrix-particle interface.

2. The anomalous results on PbX_2-Al_2O_3 composites are attributed to the fact that the mobility of Pb^{2+} ions is negligible in comparison to that of Cl^- and Br^- ions in $PbCl_2$ and $PbBr_2$ but comparable to that of I^- ions in PbI_2, and are in conformity with

the interface mechanism.

3. The enhancement in conductivity is attributed to the excess cation vacancies generated in the space charge region in the matrix phase surrounding the Al_2O_3 particles as a consequence of the stabilization of cations at the dispersoid due to internal adsorption. The samples prepared by solution casting method exhibit higher conductivity. These results are attributed to the increased rate of stabilization of cations at the interface during processing. NaCl-(30-40) m/o Al_2O_3 composites prepared by solution casting method show a conductivity of the order of 10^{-4} $ohm^{-1}cm^{-1}$ at $300^{o}C$.

4. The fact that the conductivity in CsCl-Al_2O_3 is totally unaffected by the B1$\longleftrightarrow$B2 transition provides additional concrete evidence for the conduction through interfacial mechanism.

5. The results obtained for various composite systems are consistent with the Random resistor network model. The agreement between the observed and calculated results suggests that the Maier's theory of heterogeneous doping provides a satisfactory description of interfacial mechanism of conductivity enhancement.

Dedicated

to

the fond memory of

my

beloved Parents

ACKNOWLEDGEMENT

I express my deep sense of gratitude to Professor K. Shahi who introduced me to the subject of composite solid electrolytes, for his consistent and meticulous guidance throughout the course of the present work.

I wish to acknowledge my deep regards for Prof. D.C. Agrawal, Prof. Jitendra Kumar and Prof. K.N. Rai of the department for their support and encouragement.

I would like to thank my colleagues and friends Dr. P Manoravi, Dr.Sujata Chaklanobis, Ms. Shiuli Gupta, Dr. G. Mangama, Mr. S.V. Sharma, Mr. Subhash Chand, Mr.V.P.N. Padmanabhan, Mr.Ajai Garg, Mr.Shantanu Bhattacharya and Mr.Subashish Mazumdar for their kind cooperation.

I am grateful to the staff members of the Institute Mr. J. N. Sharma, Mr. Vishwanath Singh, Mr. B.K. Jain, Mr. B. Sharma, Mr. Umashankar Singh, Mr. P.K. Paul, Mr. U.S. Lal and Mr. Jawar Singh for their technical and non-technical help in the present work.

Sincere thanks are also expressed to friends like Anup Kumar Verma, K.M. Dixit and Shiv Narayan who made my stay at I.I.T. Kanpur a memorable one.

Finally, my deepest thanks to my wife, Jyotsna for her forbearance and help.

Ashok Kumar

CONTENTS

LIST OF FIGURES

LIST OF TABLES

CHAPTER 1

INTRODUCTION

1.1 Historical Developments :

Materials in which charge transport occurs through the movement of ions, have been known since 1830's when Faraday observed the ionic conduction in nonmetallic solids Ag_2S and PbF_2. Faraday (1839) reported that PbF_2 at red heat conducts electricity about as well as Pt. However, it was Koulrausch (1882) who initiated a systematic study of ionic conduction in solids. His assembled set up for conductivity measurement was sensitive enough to measure a conductivity as high as ~ 1 $ohm^{-1}cm^{-1}$ at $150^{o}C$ in α-AgI. In their pioneering work Tubandt (1920) and his group verified and firmly established the Faraday's law for solid ionic conductors and also unambiguously demonstrated that α-AgI was a pure cationic conductor ($t_{Ag^+} \simeq 1$) (Tubandt and Lorentz, 1914) while $PbCl_2$ was essentially an anionic conductor ($t_{Cl^-} \simeq 1$) (Tubandt, 1932). Their measurements were precise enough to show that the ionic conductivity in AgI is actually more than 20% higher in the solid state near the melting point than in the molten state.

The theoretical models to explain the transport of electricity through ionic solids by the flow of ions were developed by Frenkel (1926), Wagner (1933) and Schottky (1935). Frenkel disorder, in which ions move from normal lattice sites to

interstitial sites, and Schottky disorder in which the vacancies are introduced in the normal lattice sites by moving the ions to the external surface, established a clear structural basis for the occurrence of ionic conductivity in a crystalline solid.

The first detailed study of the structural basis for high ionic conductivity in a crystalline solid was carried out by Ketelaar (1938) in Ag_2HgI_4, essentially a double salt of AgI and HgI_2. It undergoes a transition at ~ 50^oC to form a phase in which the Ag^+ ions are disordered among a much larger population of tetrahedral sites in the structure. The structural studies on AgI (Strock, 1934) revealed that the iodide sublattice remains rigid while silver ions are randomly distributed over the available symmetry sites in the *bcc* structure. Moreover, the entropy change per atom at the transition at ~ 147^oC (ΔS_t= 14.5 J mol^{-1} K^{-1}), which is comparable to the entropy change (11.3 J $mol^{-1}K^{-1}$) on melting (Perrott and Fletcher, 1968), is large enough to suggest the melting of the silver sublattice. Both the entropy changes are about half the entropy change at the melting (ΔS_f=24.2 J $mol^{-1}K^{-1}$) of the alkali halides (Lumsden, 1966). This suggests that one of the two sublattices melts at the solid-solid (β-α) transition temperature (O'Keeffe and hyde, 1976).

During the 1960's many new solid ionic materials were discovered. Reuter and Hardel (1961) synthesized a new material Ag_3SI, a double salt of Ag_2S and AgI, which showed exceptionally high ionic conductivity above 235^oC. A real breakthrough, however,

was the discovery of a new family of superionic conductors MAg_4I_5 (M=K, Rb, NH_4 etc.) by Bradley and Greene (1966, 1967) and Owens and Argue (1967) independently. These materials exhibit conductivities of $\simeq$ 0.3 $ohm^{-1}cm^{-1}$ at room temperature and the highly conducting phase persist down to about $-155^{o}C$. Around the same time, Yao and Kummer (1967) reported an unusually high ionic conductivity in the Na_2O-Al_2O_3 system. The highly conducting β-alumina long known in solid state and initially considered to be a further modification of Al_2O_3 but later identified by X-ray structure analysis as sodium oxa-aluminate $NaAl_{11}O_{17}$ (Ridgway et.al.,1936; Beevers and Ross, 1937; Peters et. al., 1971) is an exceptionally good and still unsurpassed sodium ion conductor. The actual motivating aspect of these workers, however, was the technological utilization of Na-β-Al_2O_3 in sodium/sulphur battery. Almost simultaneous discoveries of MAg_4I_5 and M-β-Al_2O_3 families of so called superionic conductors boosted the research and development activity tremendously.

Liang(1973) discovered that the dispersion of fine insulating Al_2O_3 particles in LiI enhances the Li^+ ion conductivity of LiI by about two orders of magnitude at room temperature from 10^{-7} to 10^{-5} $ohm^{-1}cm^{-1}$. Furthermore, Liang constructed cells using LiI(Al_2O_3) as solid electrolyte, lithium as the anode and a variety of two-phase iodide mixtures as cathode materials. In each case the open circuit voltage was virtually the theoretical voltage as calculated from the cell reaction. This showed that the electrical current was predominantly ionic. Moreover, one of the

cells, viz., $Li|LiI(Al_2O_3)|PbI_2/Pb$, was stored for two years after which it exhibited the same open circuit voltage and discharge characteristics as a freshly prepared cell. This again indicated a negligibly small electronic current in the composite solid electrolyte $LiI(Al_2O_3)$.

High conductivity solid electrolytes discovered so far include a large variety of materials; crystalline compounds, glasses, polymers and heterogeneously dispersed compounds. Moreover, high ionic conductivity in solids is not restricted to the motion of monovalent ions only. β''-Al_2O_3, for example, is a good conductor for a variety of divalent cations such as Pb^{2+}, Ca^{2+}, Ba^{2+}, Zn^{2+}, Sn^{2+} (Farrington and Dunn, 1982) as well as various trivalent lanthanide cations such as Nd^{3+}, Eu^{3+}, Sm^{3+}, Gd^{3+}, Er^{3+} etc. (Farrington et.al., 1983; Carrillo-Cabrera et.al., 1988).

All the highly conducting solid electrolytes share one common characteristic. They owe their conductivities to highly disordered regions in their structures. These regions may encompass an entire crystal (α-AgI), be restricted to the specific internal interfaces (Al_2O_3 dispersed in LiI), occur as highly disordered planes in a crystal (β-Al_2O_3's), or involve liquid-like disorder of an amorphous material (glasses and polymers).

1.2 Solid Ionic Conductors :

Ionic conductivity in solid ion conductors occurs due the

presence of disorder in the crystal structure. The disorder may take the form of ions appearing in the interstitial positions (Frenkel defects) or vacant lattice sites (Schottky defects). They fall into two groups; those in which the lattice defects are produced either thermally or by the introduction of foreign ions into the lattice, called *valency controlled doping* and, those in which a considerable number of defects occur naturally in the solid due to its structure. The first group is characterized by a low conductivity and a high activation energy of conduction. Since the experimentally determined activation energy is the sum of energies for migration and the formation of the defects, the concentration of defects at low doping levels ($\leq$ 1%) is often equal to the concentration of the dopant and thus the mobility of defects can be calculated. A typical example is KCl. In this crystal above 400^{o}C, both anions and cations participate to a comparable extent in the conduction process (Wagner and Hantelmann, 1950). Therefore, a Schottky disorder model involving an equal number of cations and anion vacancies to maintain electrical neutrality is indicated. This has been confirmed by the fact that the substitutional doping of K^{+} by a univalent ion, e.g. Na^{+} does not alter the conductivity markedly (Etzel and Maurer, 1950). Valency controlled doping of KCl by $PbCl_2$ (Lehfeldt, 1933) or $SrCl_2$ (Kiukkola and wagner, 1957) must lead to either an equivalent number of cation vacancies or less likely an equivalent number of anion interstitials. Doping KCl with $SrCl_2$ causes a marked increase in the conductivity by an amount proportional to the concentration of Sr^{2+} and the crystal becomes predominantly a

pure cationic conductor, and hence it allows the mobility of the vacancies to be estimated. Above 500°C, most of the alkali halides conduct via both cation and anion migration whereas at lower temperatures the conduction process is dominated by the ion of lower activation energy. Thus the sodium, potassium and rubidium chlorides are predominantly cationic conductors (Fuller and Reilly, 1967), while cesium chloride is an anionic conductor (Arends and Nijboer, 1967). Lead halides also conduct by virtue of Schottky defects. The anion vacancies are the only mobile charge carrier in $PbCl_2$ (Schwab and Eulitz, 1967) and $PbBr_2$ (Verwey and Schoonman, 1967), whereas the mobilities of anion and cation vacancies are comparable in case of PbI_2 (Tubandt, 1932; Lingras and Simkovich, 1978).

Ionic conductors in the second group are characterized by a high conductivity ($\sim 10^{-1} ohm^{-1} cm^{-1}$) at a suitable temperature, a low activation energy for conduction ($\simeq$ 0.1 eV) and a relative insensitivity of conductance to doping agents or impurities. The point defects (or disorder) necessary for conduction exist as a natural consequence of the lattice structure and an activation energy is necessary only for migration from one site to the other. It is the ionic conductors in this group, e.g., α-Li_2So_4, α-AgI, β-Al_2O_3 etc., which offer the greater possibility for the development of electrochemical devices.

Several conditions must be met for a solid to be a fast ion conductor at moderate temperatures. Firstly, the potentially

mobile species must be present as ions and not be trapped in strong covalent bonds. Secondly a population of alternative sites that the ions can potentially occupy and which are not their principal crystallographic positions must also exist. Thirdly, the energies of formation and migration of defects must be low. From a crystallographic point of view a perfect ionic crystal would be an insulator. The ionic solids falling into the second group have low defect formation energy, therefore the defect concentration is very high at moderate temperatures. The defect formation energy may be low for one of the several reasons. Some compounds such as AgI, Ag_2HgI_4, $RbAg_4I_5$ etc. undergo a specific order-disorder transition which involves a latent heat of transition similar to the latent heat of fusion. This latent heat represents the enthalpy required to disorder ions among the alternate sites in the crystal and therefore to create a large concentration of defects. Above the transition temperature the defect creation enthalpy is essentially zero. Other compounds such as β-Al_2O_3's owe their high conductivities to the ionic defects and disorders which are the result of specific compositional non-stoichiometry introduced during their formation.

1.3 Classification of Solid Ionic Conductors :

The ionic conductors can be classified in various ways depending upon the magnitude of conductivity, type of charge carriers, phase transitions and structure.

1.3.1 Based on Magnitude of Conductivity :

Ionic conductors can be classified into three groups based on their magnitude of conductivity at moderate temperatures.

(i) Poor or Normal Ionic Conductors :

These are conventional ionic solids in which the defect concentration is low. The number of mobile defects is ~ 10^{18} cm^{-3} and conductivity is < $10^{-6} ohm^{-1} cm^{-1}$. The transport is through Frenkel or Schottky defects which are thermally generated. As a result the number of defects is a strong function of temperature and the activation energy is very high ~ 1 eV or more. Examples : alkali halides, AgCl, AgBr, β-AgI etc.

(ii) Moderate Ionic Conductors :

These contain a large concentration of defects (~ 10^{20} cm^{-3}) which have coalesced into a coherent substructure or extended defects of submicroscopic dimensions. The range of conductivity is from 10^{-6} to < $10^{-3} ohm^{-1} cm^{-1}$. Examples : CaF_2 (Derrington et.al., 1975), PbF_2 (Schoonman et.al., 1975), $CaO.ZrO_2$ (Etsell and Flengas, 1970) etc.

(iii) Fast Ionic Conductors :

This is the case of *liquid like molten submattice* in which principally all the ions in a sublattice are available for movement. The number of mobile ionic charge carriers is ~10^{22} cm^{-3} and conductivity is > 10^{-3} $ohm^{-1} cm^{-1}$. Examples : α-AgI (Wiedersich and Geller, 1971), $RbAg_4I_5$ (Owens, 1971; Geller, 1976), α-Li_2SO_4

(Kvist and Lunden, 1965) etc.

This classification, however, is extremely broad since the range of temperature over which different materials may acquire some arbitrarily fixed value of conductivity is large. Thus while the conductivity of NaCl is ~ 10^{-15} ohm^{-1}cm^{-1}, that of $RbAg_4I_5$ is ~ 0.27 ohm^{-1}cm^{-1} at room temperature. Similarly the conductivity of NaCl changes from 10^{-8} to 10^{-3} ohm^{-1}cm^{-1} as the temperature changes from 300 to 800^{o}C (melting point), whereas the conductivity of $RbAg_4I_5$ does not change much with temperature.

1.3.2 Based on Type of Charge Carriers :

On the basis of the nature of mobile ions the solid ionic conductors can be classified into two categories.

(i) Cationic Conductors : Main cationic conductors are the following :

(a) Li^+ and Na^+ ion conductors, e.g., Li_3N (Huggins, 1977), LiI (Schlaikjer and Liang, 1973), Li_2SO_4 (Kvist and Lunden,1965), $LiI(Al_2O_3)$ (Liang, 1973), NASICON (Goodenough et.al., 1976), Na-β-alumina (Kennedy, 1977), etc.

(b) Cu^+ and Ag^+ ion conductors, e.g., AgI (Wiedersich and Geller, 1971), $RbAg_4I_5$ (Owens, 1971), CuI (Matsui and Wagner, 1977), CuCl (Joshi and Wagner, 1975), etc.

(c) Proton (H^+ ion) conductors, e.g., $HUO_2PO_4.4H_2O$ (Shilton and Howe, 1977), H_3O^+-β'-alumina (Farrington and Briant, 1978), etc.

(ii) Anionic Conductors : Main anionic conductors may be categorized as follows :

(a) O^{2-} ion conductors, e.g., stabilized ZrO_2, CeO_2, HfO_2 (Etsell and Flengas, 1970), etc.

(b) F^- ion conductors, e.g. PbF_2 (Schoonman et.al., 1975), CaF_2, BaF_2, SrF_2 (Derrington et.al., 1975), YF_3, LuF_3 (O'keeffe, 1973), etc.

1.3.3 Based on Phase Transitions :

The solid ion conductors may be classified into three categories on the basis of phase transitions.

(i) Normal Melting :

In this category, both cation and anion sublattices disorder simultaneously. Their is no solid-solid (nonconducting-conducting) transformation and the high conductivity is attained upon melting, e.g., alkali halides, AgCl, etc.

(ii) First Order Transition :

(a) Some solid ionic conductors notably certain silver and copper based materials like Ag^+ and Cu^+ salts exhibit a first order phase

transition to a high conducting phase. The lattice symmetry of both mobile and immobile sublattices changes at the transition. A large, discontinuous change occurs in the ionic conductivity at the solid-solid transition. A prototype material of this class is AgI. At the transition, the iodine array changes from f.c.c to b.c.c. and the silver ions become disordered and mobile. This is accompanied by a substantial change in the arrangement of the immobile ions.

(b) This class differs from the preceding one only in degrees. The solid-solid phase transition is first order but there is only a minor change in the immobile ion array, e.g., in Cu_2S the immobile array of sulphur remains approximately *hcp* and in Ag_2S it remains approximately bcc above the transition.

(iii) Faraday Transition :

In this type of transition, the disordering of the mobile array is spread over a substantial temperature range. There is no change in the immobile ion array. Crystals with the fluorite (CaF_2) structure are prime examples. The cations remain immobile upto the melting point. The conductivity passes smoothly from the values of normal salts ($< 10^{-8}$ $ohm^{-1}cm^{-1}$) to the values typical of ionic melts ($\sim 10^{-3} ohm^{-1}cm^{-1}$) through the transition temperature range.

1.3.4 Based on Structure :

The solid ionic conductors can be classified into four

categories depending on their structures.

(i) Crystalline Ionic Conductors :

The structure and composition of ionic solids are optimized for high ionic conductivity. The mechanisms by which the ions diffuse rapidly in these materials are related to those that lead to ionic conductivity in classical ionic solids such as NaCl, $BaCl_2$ and LiI (Ratner and Nitzan, 1988). Examples are Na-β-aluminas, NASICON, Stabilized ZrO_2, $RbAg_4I_5$, etc.

(ii) Amorphous Ionic Conductors :

Unlike crystalline solids wherein the carrier concentration may be defined as the density of defects with reference to the perfect lattice and each carrier is identically situated having the same mobility, in amorphous ionic conductors the large amount of free volume makes it hard to apply the concept of a point defect (Hughes and Isard, 1972) and the low defect concentration models (Haven and Verkerk, 1965; Ravaine and Souquet, 1977, 1978; Ingram, 1980; Moynihan and Lesikar, 1981). More satisfactory concept than the defect formation is to consider all the ions to be potentially conducting but in a broad distribution of states (Tuller et.al., 1980, Hughes and Isard, 1972). Lack of grain boundaries, isotropic and generally higher conductivities are the distinct advantages of amorphous (glassy) ionic conductors over their crystalline counterparts. Examples : alkali germanate glasses (Mundy and Jin, 1986, 1987).

(iii) Polymeric Ionic Conductors :

The dominant class of polymer electrolytes comprises the neutral polar polymer complexed with alkali metals, divalent transition metals, ammonium salts and acids. Fenton et.al.(1973) and Wright (1975) were the first to show that polyethylene oxide (PEO)-alkali metal salt complexes are ion conducting. Armand et.al.(1979) has shown the technological importance of these salt complexes in all-solid lithium batteries. Polymer electrolytes have since occupied an important place in Solid State Ionics, because of their unique properties, such as thin-film formation, easy processibility, flexibility, light weight and elasticity (Armand, 1986; Ratner and Shriver, 1988; Watanabe and Ogata, 1988).

(iv) Composite Ion Conductors :

Another group of ionic conductors includes the heterogeneously doped ionic solids, typified by LiI containing dispersion of Al_2O_3 that has been shown to be a good Li^+ ion conductor (Liang, 1973). In these materials, ionic conductivity is believed to occur in the thin interfacial regions surrounding the dispersed particles. Several phenomenologies have been invoked to explain the enhancement in the conductivity of these composites. Jow and Wagner (1979) proposed that the dispersion of the insulating particles in the host matrix produces a space charge layer at the matrix/particle interface, and thus facilitates the ionic motion. Maier (1984, 1985, 1986, 1987) formulated the space charge profiles in the interfacial region and developed a

quantitative model by employing the principle of parallel switching, while treating the space charge region as a separate phase.

1.4 Composite Solid Electrolytes :

There are two basic ways of optimizing the ionic conductivity in solids. First is to search for new structures and compounds and the second is to modify the properties of the known materials. The latter can be achieved in two basic ways.

1.4.1 Homogeneous Doping :

Homogeneous doping is the classical way to improve the ionic conductivity of a normal ionic conductor in which small amount of an appropriate material is dissolved in the host matrix normally in order to influence the defect concentrations. This can be further sub classified into two categories.

(i) Homovalent Doping :

Substitution of the ions having the same valency but different size influences the ionic conductivity of the host material. For instance the ionic conductivity of $KCl_{0.5}Br_{0.5}$ mixed crystals i.e. KCl doped with Br^- ion was found to be twice as large as that of pure KCl (Shulze, 1952). Several recent investigations on the *mixed crystals* have revealed that the effect of built-in wrong size of the homovalent ions depends strongly on the size difference between the host and the guest ion (Shahi and wagner, 1983; Johannesen and McKelvy, 1985,1986). A few tentative theories

and models have been suggested to explain the unusual transport properties of the mixed crystals. According to lattice loosening model (Lidiard, 1957; Shahi and wagner, 1983) the substitution of a homovalent ion which is either too large or too small (i.e. not of the same size as the host ion) introduces strain in the lattice that generally, if not invariably, results in the lowering of the melting point. This leads to the lowering of the formation and migration enthalpies, hence increases the concentration of mobile defects and thus results in an increase in the conductivity.

(ii) Aliovalent Doping :

An impurity ion whose valency is different from that of the corresponding host ion is referred to as aliovalent ion. Thus when an ionic solid (e.g. alkali(M)halide(X) MX) is doped with divalent cations (e.g. $M'X_2$, M'= Ca, Cd, Mg etc.) or divalent anions such as S^{2-}, CO_3^{2-} etc., the electrical charge neutrality requirement demands generation of excess defects of the compensatory type (cation or anion vacancies and/or anion or cation interstitials) which in turn increase the conductivity. The extraordinary influence of aliovalent doping on the concentration of point defects and hence on the charge carriers and conductivity was first realized by Koch and Wagner (1937) and subsequently demonstrated extensively by Kelting and Witt (1949) and Teltow (1949).

1.4.2 Heterogeneous Doping :

The qualitative effect that the overall conductivity of a two phase mixture may exceed the values for the pure constituent phases has been known for a long time (Jander, 1929). A lot of interest has been directed towards the phenomenon since Liang (1973) performed a systematic measurements on the enhancement of Li^+ion conductivity in LiI containing fine Al_2O_3 particles. This system belongs to a group of two-phase systems where a moderate ion conductor (for example, alkali and silver halides etc.) is mixed with a coexisting insulating oxide (mostly Al_2O_3). A *second group* of two phase materials consists of a mixture of two normal ionic conductors. Shahi and Wagner Jr. (1982) found a greatly increased overall conductivity in the miscibility gap of the system AgI-AgBr compared to the solid solubility regions. Table 1.1 lists some of the important composite solid electrolyte systems which show an appreciable enhancement in the conductivity. Such highly conducting materials have shown good promise for high energy density batteries.

The conductivity behavior of the composites is not well understood. Classical concepts such as doping are not applicable since the second phase particles are insoluble in the first phase (Liang et.al.,1978). The enhancement in the conductivity was found possible by assuming that a highly conducting layer of a few Angstrom thickness surrounds each insulating particle (Stoneham et.al., 1979).

Table 1.1

Some composite solid electrolytes with enhanced conductivity*

composite system	mole % disperoid	σ $(ohm\text{-}cm)^{-1}$	σ/σ_o	at T (^oC)	reference
$LiI(Al_2O_3)$	40	$1.0x10^{-5}$	100	25	Liang(1973)
$LiBr(Al_2O_3)$	20	$3.7x10^{-6}$	10	170	Khandkar and Wagner,Jr.(1986)
AgI(fly-ash)	13.5	$1.2x10^{-5}$	50	25	Shahi and Wagner,Jr.(1982)
$AgI(SiO_2)$	10	$1.1x10^{-5}$	45	25	Shahi and Wagner,Jr.(1982)
$AgI\begin{pmatrix}wet\\Al_2O_3\end{pmatrix}$	30	$6.0x10^{-4}$	2500	25	Shahi and Wagner,Jr.(1982)
$AgI\begin{pmatrix}dry\\Al_2O_3\end{pmatrix}$	30	$1.2x10^{-5}$	50	25	Shahi and Wagner,Jr.(1982)
$AgBr(Al_2O_3)$	15	$1.0x10^{-5}$	20	21	Maier(1985)
$AgCl(Al_2O_3)$	13	$1.0x10^{-6}$	10	21	Maier(1985)
$CuCl(Al_2O_3)$	10	$2.5x10^{-5}$	30	25	Jow and Wagner,Jr.(1979)
$CaF_2(Al_2O_3)$	4	$5.4x10^{-5}$	100	373	Vaidehi et.al. (1986)
$CaF_2(CeO_2)$	4	$3.9x10^{-4}$	1000	373	Vaidehi et.al. (1986)
$SrCl_2(Al_2O_3)$	25	$7.2x10^{-4}$	5	300	Fijitsu et.al. (1986)

*σ refers to the conductivity of the composite materials; σ_o of pure salt(host).

1.5 Properties of Composite Solid Electrolytes :

The composite solid electrolytes show some typical properties which are as follows :

(i) Fig.1.1 shows the conductivity versus composition (m/o) of

dispersoid for various composite systems. The ionic conductivity is typically enhanced by one to three orders of magnitude. The maximum in the conductivity is most often observed for composites containing 10 to 40 volume percent (v/o) dispersed particles. However, in many systems significant enhancement are also induced by the addition of only a few percent of the dispersed phase. For example 1 mole percent (m/o) Al_2O_3 enhances the conductivity of AgI threefold (Chowdhary et.al., 1985) and just 0.5 m/o CeO_2 enhances the conductivity of CaF_2 by a factor of 1000 (Wen et.al., 1983).

(ii) Most often the highest conductivities are reported for composites containing extremely fine (~ 0.1 μm) particle size of the dispersed phase, while a negligible effect is often observed for particles larger than a few microns. Many models have been presented to explain the observed dependence of the enhancement in conductivity on the particle size (Wagner, 1972; Jow and Wagner, 1979; Stoneham et.al., 1979; Pack, 1979). These models describe rather empirically the conductivity enhancement as a function of inverse of the radius of the dispersed particles. However, recent studies have emphasized the correlation between the enhancement in the conductivity and the effective surface area of the dispersed phase (Slade and Thompson, 1988). The large particles (~8 μm) with a very high surface area (200 m^2/gm) were found to enhance the conductivity as effectively as extremely small, nonporous particles with a similar effective surface area.

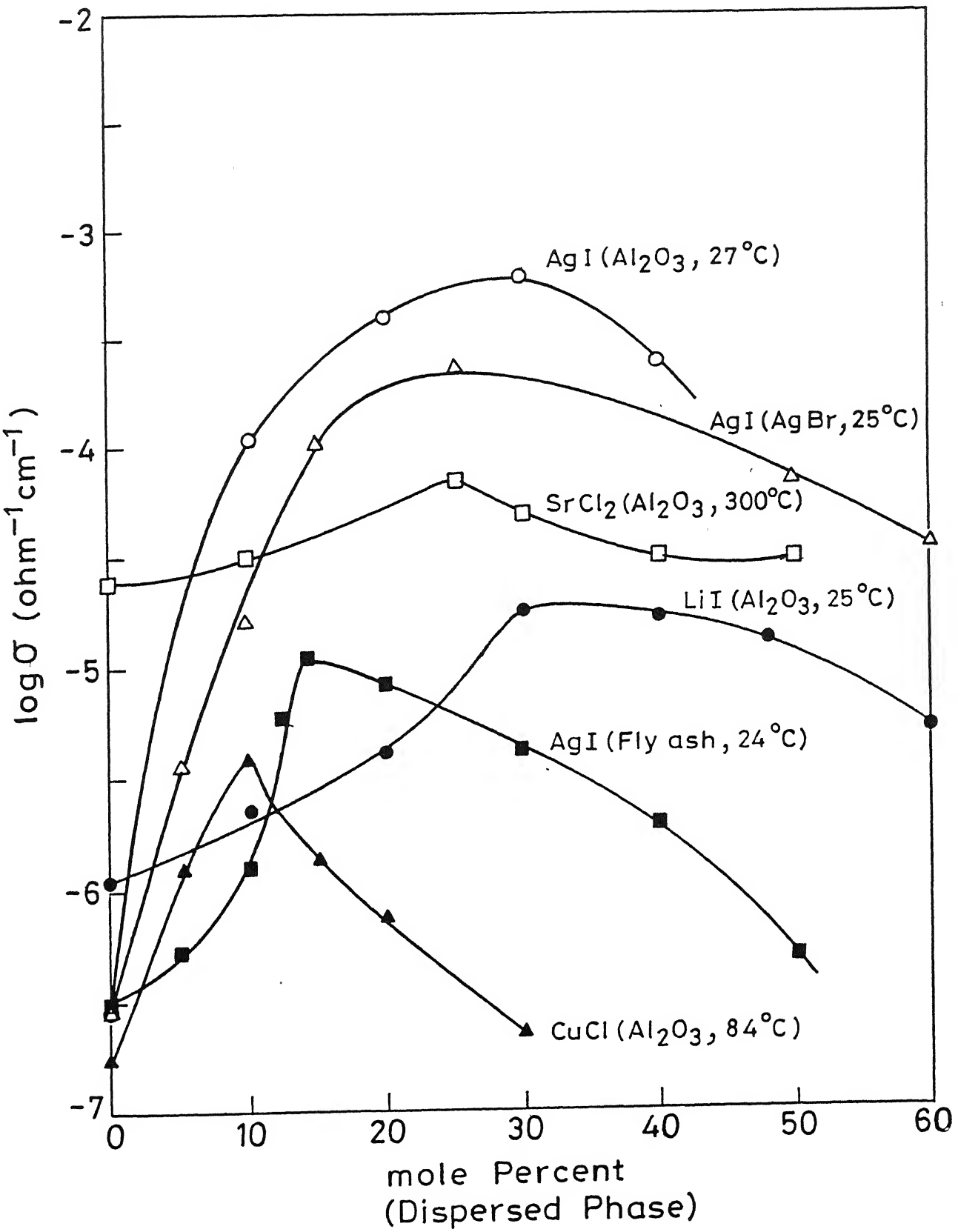

Fig.1.1 Conductivity vs composition (m/o of dispersoid) for various composites.

(iii) The composites prepared with undried alumina particles generally show higher conductivities than those prepared with predried alumina (Pack et.al., 1980; Shahi and Wagner, 1982). This is generally accepted as a proof of the water molecules or the hydroxyl groups adsorbed at the insulating particles. Several studies report that the enhanced conductivity is completely eliminated if the alumina particles are scrupulously dried before being added to the matrix phase (Maier,1985).

(iv) The largest conductivity enhancements are generally observed at lower temperatures, often near room temperature. This is explained in terms of decrease in the effective thickness of space charge layer (Debye length) with increase in temperature (Jow and Wagner,1979).

(v) The addition of a second phase may change the mechanism of conduction. In $AgI(Al_2O_3)$ composite the conduction mechanism changes to dominant transport via silver ion vacancies from the dominant transport via silver ion interstitials in pure AgI (Shahi and Wagner,1981). Maier and Reichert (1986) reported that dominant transport changed to conduction via the negatively charged cation vacancies in $TlCl(Al_2O_3)$ composites from the positively charged chloride ion vacancies in pure TlCl.

(vi) The addition of a second phase may change the temperature of a first order phase transition of the matrix electrolyte. Shahi and Wagner (1981) reported that the dispersion of Al_2O_3 changes

the α-β transition temperature in AgI. Chowdhary et.al.(1985) found that $\beta \rightarrow \alpha$ transition temperature was unaffected, whereas the $\alpha \rightarrow \beta$ transition temperature (during cooling cycle) decreased as the concentration of Al_2O_3 increased.

1.6 Conduction Mechanisms in Composite Solid Electrolytes :

Various mechanisms which may lead to the enhancement in conductivity in composites are as follows :

1.6.1 Interface Mechanisms :

The observed enhancement in conductivity by the dispersion of submicron insulating particles in a normal ionic conductor has been attributed to the matrix-particle interface by most researchers. Three possible processes that may lead to enhanced conduction along the interface between the matrix and the dispersed second phase have been identified. Of these the formation of a space charge layer at the matrix-particle interface is most widely accepted mechanism.

(i) Enhanced Carrier Concentration in the Space Charge Layer :

An interfacial space charge layer is formed when the interface has a net charge due to the preferential occupation of the interface sites by either cations or anions. Jow and wagner (1979) presented evidence for a space charge layer adjacent to the dispersoid in the composite solid electrolyte. They used the concept of a space charge layer at an electrolyte-vacuum interface, as was derived by Lehovec(1953) and Kliewer and Koehler

(1965). Maier has done the most extensive *quantitative* work investigating the possible formation of space charge layers along the interfaces in the composite solid electrolytes. In AgCl and AgBr based composites Maier (1985) found a good agreement between the experimental conductivities and those calculated by assuming a space charge layer at the interface. According to Maier (1984), the dispersoid acts as a nucleophilic surface, which attracts positively charged species. Shahi and Wagner (1981) studied $AgI(Al_2O_3)$ using the thermoelectric effect. They reported that the transport in the composite was via cation vacancies. But AgI exhibits Frenkel disorder and transport in pure AgI is predominantly via silver ion interstitials. The mechanism in the case of $AgI(Al_2O_3)$ composite changes from dominant transport via interstitials to the dominant transport via cation vacancies. This switching from chlorine vacancies in case of pure TlCl to thallium vacancies in $TlCl(Al_2O_3)$ composite has also been observed by Maier and Reichert (1986). On the other hand an electrolyte such as LiI exhibits Schottky disorder and the pure LiI conducts primarily via cation vacancies. The introduction of dispersoid causes the positively charged species to be attracted, leaving a depletion zone with a larger concentration of cation vacancies than in the bulk LiI, where the concentration of vacancies is given by the square root of the Schottky constant. Thus in LiI there is no change in mechanism but simply an increase in the number of cation vacancies.

Maier (1985) demonstrated that changing the chemical nature

of the surface of the alumina particles affects the conductivity of the composites. Alumina particles treated with either $(CH_3)_3SiCl$ or CH_3Li produced a significantly smaller enhancement in the conductivity than observed for untreated alumina particles. This is presumably due to a substitution reaction and a passivation of the surface hydroxides. Another observation suggesting the importance of the surface chemistry of the particles is the report by Slade and Thompson(1988) that in LiBr, SiO_2 particles are less effective in enhancing the conductivity than Al_2O_3 particles of similar size or surface area.

CaF_2 is an interesting example. It exhibits the anti-Frenkel disorder with equal concentrations of anion vacancies, $V_F^{\cdot}$ and anion interstitials F_i' (Ure, 1957). The activation energy for the motion of $V_F^{\cdot}$ is 0.51 eV, while that for motion of F_i' amounts to 0.91 eV (Bollmann and Henniger, 1972; Bollmann and Reimann, 1973). In pure CaF_2 the ionic current is, therefore, attributed to the fluorine ion vacancies. The enhanced conductivity in $CaF_2(Al_2O_3)$ composite has been attributed to the enhanced concentration of F_i' (Khandkar et.al.,1986). Some researchers, however, believe that the fluorine ions are attracted towards the interface and the enhancement in the conductivity occurs due to an increase in the fluorine ion vacancies $V_F^{\cdot}$ near the interface (vaidehi et.al.,1986; Akila and Jacob, 1987).

Other evidence for the space charge layer concept is provided by the influence of alumina dispersoids on the temperature of a

first order transition. Shahi and Wagner (1981) reported that the introduction of Al_2O_3 resulted in a change in the α-β transition temperature. Chowdhary et.al.(1985) observed that α to β (cooling cycle) transition temperature decreases as the Al_2O_3 concentration increases whereas β to α (heating cycle) transition temperature remains unaffected. Furthermore, the dispersion of Al_2O_3 particles in β phase increases the conductivity, whereas that in the α phase it reduces the conductivity. It is suggested that in the β phase, the cation vacancies tend to remain near the interface. Thus the transition is determined by the defects in the bulk AgI and the transition occurs at $147^{o}C$. On the other hand in the high temperature phase, the cation vacancies are more mobile and react with the interstitials. This results in a decreased ionic conductivity. According to Rice et.al.(1974) a critical concentration of defects is necessary to cause the transition. On cooling there is smaller concentration of lattice defects than in pure AgI. Hence the composite must be cooled below $147^{o}C$ because there is not enough concentration necessary to drive the α-β transition. These results clearly show that virtually insoluble dispersoid is not inert, but influences the concentration of defects in the electrolyte.

The interfacial space charge layer mechanism, however, has proven to be inadequate as an explanation for conductivity measurements on the thin-films of LiI (Schreck et. al., 1986) and AgCl (Muhlherr et.al., 1988) on Al_2O_3 substrate deposited by evaporation. Very near the interface the film conductivities are

larger than those reported for composite electrolytes. For both the materials the change in conductance as a function of film thickness does not decay to the bulk conductance of the pure material until the film thickness far exceeds the Debye length of the material. This is clearly inconsistent with the effect of a single space charge layer at the interface. For AgCl films it has been concluded that the conductivity must be determined by the microstructure of the films (Muhlherr et.al., 1988). Dudney (1985) has estimated the maximum likely space charge polarization that can be formed at an interface of LiI, β-AgI and AgCl based on defining an upper limit to the amount of excess charge that can be accommodated at an interface. This limit is close to a monolayer of excess anions or cations. It was found from these calculations that a space charge polarization along the alumina interface is not a large enough effect to account for the tremendously enhanced conductivities for composites of LiI and AgI. Even considering an extremely unrealistic model of an ideal layered composite containing 30-50 v /o of (50Å) sheets parallel to the direction of the current, the calculated enhanced conductivity due to the space charge layers along these alumina sheets is far less than the reported conductivities for the real LiI and AgI composite electrolytes (Dudney, 1988).

(ii) Enhanced Conduction at the Core of Interface :

Phipps et.al.(1981) and Phipps and Whitmore (1981) proposed that the lattice distortion is likely to give significant changes in the defect mobilities as well as in the defect concentrations

within the first one to three atomic layers near the interface. They solidified both pure and doped LiI films of 0.2 mm thick in a sandwich between silica plates. The interface contribution to the total conductivity of the LiI films was separated by subtracting the conductivity through the LiI films from the conductivity measured along the films. This mechanism, however, has not been accepted probably because the enhanced conductivity layer is confined to a few atomic layers. This is a much narrower distribution than predicted by most of the model calculations involving space charge layer where the high conductivity layer is calculated to be hundreds of angstroms wide. Besides, the enhanced conduction along the interface core require a dense continuous interface network through the composite which would be unlikely for very small volume fraction of dispersoid.

(iii) Interfacial Phase Formation :

There is a possibility that a highly conducting phase may form along the interface due to the reaction of the matrix with either the oxide particles or with the impurities adsorbed on the particles. Pack et.al.(1980) reported no enhancement in the conductivity of LiI(Al_2O_3) composite system. Although a third phase is generally not detected by X-ray diffraction, there is evidence that water can be a contributory factor to the enhanced conductivity for composites of those materials which are known to form a number of hydration compounds with bulk conductivities higher than those for the anhydrous compounds. However the bulk conductivities of the hydrated phase are simply not high enough to

account for the conductivity reported for the composites (Phipps et.al.,1981; Hartwig and Weppner, 1981 and Skarstad et.al.,1981). For example the value of σ for $LiI.H_2O$ has been reported from $2x10^{-7}$ to $1x10^{-5} ohm^{-1}cm^{-1}$ at $300^{o}K$ by various researchers (Pack et.al.,1980; Phipps et.al.,1981; Poulsen, 1982), but these are all lower than the highest conductivities of $4x10^{-5}$ and $10^{-5} ohm^{-1}cm^{-1}$ for $LiI.H_2O(Al_2O_3)$ reported by Liang (1973) and Maier (1985). In addition, the conductivities of the hydrated phases, $LiI.H_2O$ and $LiBr.H_2O$, are themselves enhanced by the addition of Al_2O_3/SiO_2 particles (Slade and Thompson,1988; Nakamura and Goodenough,1982). Clearly the enhanced conductivity in the composites cannot be attributed simply to the formation of an interface layer of one of the hydrated compounds.

1.6.2 Matrix Mechanisms :

Although it is widely accepted that matrix-particle interface is dominantly responsible for the enhanced ionic conductivity in dispersed phase composite solid electrolytes, there are several mechanisms by which conduction through the matrix can be enhanced by the presence of a dispersed phase.

(i) Conduction along Grain Boundaries and Dislocations :

It has long been known that the transport in polycrystalline single phase electrolytes may be faster than that in single crystal electrolytes, although for many ionic materials the detailed mechanism for this enhancement is not completely understood (Kingrey et.al., 1976; Peterson, 1983; Yan et.al.,

1977). The presence of rigid and inert particles is known to affect the microstructure that develops during sintering (Olgaard and Evans, 1986; Lange and Hirlinger, 1987) or recrystallization (Cotterill and Mould, 1976). For AgCl(Al_2O_3) composites, it appears that the role of alumina particles may be to stabilize the AgCl grain structure that forms the high conductivity paths (Dudney, 1988).

Model calculations of the conductivity for a composite, where the grain boundaries contribute to the high ionic conductivity path, reproduce quite well the typical trends observed for composites with respect to the composition and particle size dependence (Dudney,1988). The grain size is assumed to decrease as the volume fraction of the particles increases (Olgaard and Evans, 1986). As more particles are added to the composites, the density of the grain boundaries (and hence the conductivity) increases until alumina begins to have a significant blocking effect on the conductivity. In this model, unlike the interfacial models discussed above, a significant increase in the conductivity is likely for composites containing just ~ 1 v/o of well dispersed fine particles. This is consistent with a number of experimental observations on the composite solid electrolytes. However for composites of either LiI or β-AgI, calculations (Dudney,1985) indicate that a space charge polarization layer along the grain boundaries in the matrix cannot account for the observed conductivities of the composites, even if the matrix has an extremely fine si icron structure (Dudney, 1985).

2. Presence of a Highly Conducting Metastable Phase :

The presence of the second-phase particles in a composite may act to stabilize a metastable or a higher-temperature matrix phase during the processing. There are a number of experimental observations that suggest that the metastable (γ) phase of AgI might be present in the alumina composites. AgI transforms to the γ-phase under moderate pressures (Burley, 1967) or if cooled rapidly from near the melting temperature (Burley,1963). Comparison of the conductivity and thermoelectric power reported for AgI(Al_2O_3) composites (Shahi and Wagner,1981) and those reported for the γ-phase and the β-phase of pure AgI (Schiraldi, 1975) suggest that the presence of the more conductive γ-phase may,in fact, be responsible for the enhanced conductivity of the composites. Schmidt et.al.(1988) confirmed from the X-ray measurements the presence of γ-AgI containing 5 m/o Al_2O_3. For LiBr.H_2O(Al_2O_3) composite also, there is evidence that the high conductivity observed at and below room temperatures may be partially due to supercooling of the β-LiBr.H_2O phase (Schmidt and Bazan, 1988) which is stable above 34^oC and is characterized by disorder in the orientation of the water molecules. It appears that the presence of the dispersed Al_2O_3 stabilizes the high-conducting β-phase below the transition temperature.

Though it seems plausible that the second phase particles may stabilize a metastable phase or prevent a phase transition, perhaps by impeding the nucleation and growth processes, the possibility of having a metastable or supercooled phase of the

matrix materials has not been considered except for the above two cited examples.

(iii) Homogeneous Doping of the Matrix :

Most researchers argue that the homogeneous doping of the matrix by the dispersoid could not account for the continued increase in the conductivity for dispersoid concentrations well beyond the solubility limit. Though phase diagrams or solubility data are not available for the majority of the systems, yet this possibility is worth considering because small amount of dopants, specially aliovalent dopants, can have a profound effect on the conductivity of a material. This mechanism is suspected to contribute significantly to the enhanced conductivity in $CaF_2(Al_2O_3)$ composite system. Wen et.al.(1983) have pointed out that the enhancement may be the result of the formation of defects due to dissolution of very small amount of Al_2O_3 in CaF_2, although other researchers claimed that this occurs due to the interfacial mechanism.

Mechanism(s) responsible for the conductivity enhancement in composite solid electrolytes is(are) still a matter of some debate. More than one mechanisms may be operating simultaneously. Moreover one mechanism may be responsible in one concentration regime while another may be responsible in another concentration regime. A composite containing a significant volume fraction of well dispersed submicron size particles will have an extremely large matrix- particle interface area. In fact it has now become

matrix materials has not been considered except for the above two cited examples.

(iii) Homogeneous Doping of the Matrix :

Most researchers argue that the homogeneous doping of the matrix by the dispersoid could not account for the continued increase in the conductivity for dispersoid concentrations well beyond the solubility limit. Though phase diagrams or solubility data are not available for the majority of the systems, yet this possibility is worth considering because small amount of dopants, specially aliovalent dopants, can have a profound effect on the conductivity of a material. This mechanism is suspected to contribute significantly to the enhanced conductivity in $CaF_2(Al_2O_3)$ composite system. Wen et.al.(1983) have pointed out that the enhancement may be the result of the formation of defects due to dissolution of very small amount of Al_2O_3 in CaF_2, although other researchers claimed that this occurs due to the interfacial mechanism.

Mechanism(s) responsible for the conductivity enhancement in composite solid electrolytes is(are) still a matter of some debate. More than one mechanisms may be operating simultaneously. Moreover one mechanism may be responsible in one concentration regime while another may be responsible in another concentration regime. A composite containing a significant volume fraction of well dispersed submicron size particles will have an extremely large matrix- particle interface area. In fact it has now become

widely accepted that the overall effect of forming the composite is to create a high-conducting path along the interface between the electrolyte matrix and the dispersed particles.

1.7 Statement of the Problem :

It is clear from the foregoing discussion that considerable work has been done on composite solid electrolytes since the effect was discovered by Liang in $LiI(Al_2O_3)$ composite system in 1973. The phenomenon has been shown to occur for both cationic and anionic conductors having either Schottky or Frenkel disorder. The mechanism of conduction has been proposed to be essentially the formation of high conducting space charge layer at the matrix / particle interface though the exact mechanism of formation and the characterization of the space charge layer are still subjects of intensive research.

The aim of this work was to investigate a series of composite solid electrolytes (CSEs) systematically and comprehensively with a view to :

(i) Contribute towards a better overall understanding of the ion transport mechanism in CSEs,

(ii) Test the various proposed models, especially the space charge theory, to explain the enhanced electrical conductivity in the CSEs, and

(iii) Develop new alkali (especially Na^+) ion-based CSEs for possible applications in high energy density batteries.

To achieve the aforesaid objectives, the following composite solid electrolyte systems were chosen for the investigation

(i) PbX_2-Al_2O_3 (X = Cl, Br, I), and

(ii) MCl-Al_2O_3 (M = Na, K, Rb and Cs)

The lead halides (PbX_2) were chosen because $PbCl_2$-Al_2O_3 is reported to show a decrease in the conductivity which is in sharp contrast to most other composite systems which show enhancement in the conductivity. Thus an investigation of the anomalous PbX_2-Al_2O_3 systems may provide some new insight into the conduction mechanism of composite solid electrolytes.

The alkali halides have been chosen because, even though the studies on CSEs are numerous and vigorous, surprisingly these, with the exception of lithium salts, have not been studied in any detail. As such the alkali halides are most suitable host materials to investigate the composite solid electrolyte effect because they (i) do not undergo any solid$\leftrightarrow$solid transformation at ambient pressure (cesium halides being the only exception), and thus provide a wider temperature range of study, (ii) are less hygroscopic (except lithium salts), and lastly but most importantly (iii) their defect and conduction mechanisms are reasonably well understood.

It may be pointed out that CsCl is different from the rest of the alkali metal chlorides (MCl) in that it undergoes a B1 (rock salt) $\longleftrightarrow$ B2 (CsCl) structural transformation at ~ $470^{o}C$ at atmospheric pressure, and that both its phases are normal ionic conductors. Thus the studies on CsCl-Al_2O_3 system offer additional opportunity to examine the effect of dispersion on the phase transition behavior. For this reason, the results on CsCl-Al_2O_3 system are discussed separately in Chapter 6 while those on MCl-Al_2O_3 (M=Na, K, Rb) in Chapter 5.

CHAPTER 2

THEORETICAL ASPECTS

2.1 Complex Impedance Analysis :

The electrochemical processes in galvanic cells cannot be represented by a simple combination of ideal resistances alone. Simple dc measurements cannot yield the dc resistance of the samples because of the choice of electrodes and the polarization at the electrode/electrolyte interface. The processes, however, can be represented by an equivalent circuit involving resistors, capacitors, inductors etc.(Randles, 1947). An equivalent circuit represents the way in which various current carrying elements in a galvanic cell are arranged.

The complex impedance spectroscopy is a technique to separate the contributions from various processes such as electrode reactions at the electrode/electrolyte interface, and the migration of charge carrying species through the grains and across the grain boundaries. AC complex impedance spectroscopy was first applied to solid electrolytes by Bauerle (1969). With the development of both electrode and electrolyte materials for solid state electrochemical devices such as batteries, sensors, fuel cells and electrochromic devices, the impedance spectroscopy has become an inevitable part of the characterization process (Raistrick, 1986; Martin and Angell, 1986; Almond and West, 1983; Hodge et.al.,1976).

The technique involves applying a sinusoidal signal of low amplitude across a solid electrolyte cell. The output signal, which is also a sine wave (Hooper, 1985; Badwal,1988), is compared with the input signal to determine the impedance modulus and phase shift corresponding to the equivalent circuit which represents the cell assembly, i.e., electrode/electrolyte/electrode. The complex impedance $Z(\omega)$ at an applied frequency ω can be written as :

$$Z(\omega) = Z_R(\omega) + jZ_I(\omega) \qquad (2.1)$$

where Z_R is the real and Z_I is the imaginary part of the complex impedance. The magnitude of the complex impedance is $Z = \sqrt{(Z_R^2 + Z_I^2)}$ and the phase angle is $\theta = \tan^{-1}(Z_I/Z_R)$.

For a resistance (R) and a capacitance (C) in parallel, the complex impedance $Z(\omega)$ is given by :

$$Z(\omega) = \frac{R\left(\frac{1}{j\omega C}\right)}{\left(R + \frac{1}{j\omega C}\right)} \qquad (2.2)$$

$$\text{or,} \quad Z(\omega) = \frac{R}{1 + \omega^2 C^2 R^2} + j\,\frac{-R^2\omega\, C}{1 + \omega^2 C^2 R^2} \qquad (2.3)$$

Thus, the real and imaginary parts of $Z(\omega)$ are :

$$Z_R = \frac{R}{1 + \omega^2 C^2 R^2} \qquad (2.4)$$

and, $$Z_I = \frac{-R^2\omega C}{1 + \omega^2 C^2 R^2} \qquad (2.5)$$

Elimination of ω from Eqs.(2.4) and (2.5) yields :

$$(Z_R - \frac{R}{2})^2 + Z_I^2 = \frac{R^2}{4} \qquad (2.6)$$

which is the equation of a circle of radius R/2, with its centre at (R/2,0).

Fig.2.1 shows the various impedance behaviors observed in the solid electrolytes. A cell system consisting of an electrolyte which has only one mobile ionic species, and two non-blocking electrodes made up of the same material as the mobile species, has an equivalent circuit (Fig.2.1a) which is a parallel combination of a capacitor C_g, representing the geometrical capacitance of the cell, and a resistance R representing the bulk resistance of the electrolyte. The bulk resistance can be obtained from the intersection of the semicircle and the real axis of the complex spectra. However, it is often difficult to use non-blocking electrodes. For example, for fluoride ion conductors, fluorine is in gaseous form at ambient temperature. Moreover, the use of blocking electrodes has the advantage of making it possible to determine the electronic contribution to the electrical conductivity using dc polarization measurements. The equivalent circuit for an elementary cell with blocking electrodes is shown in Fig.2.1b. The geometrical capacitance C_g and the bulk

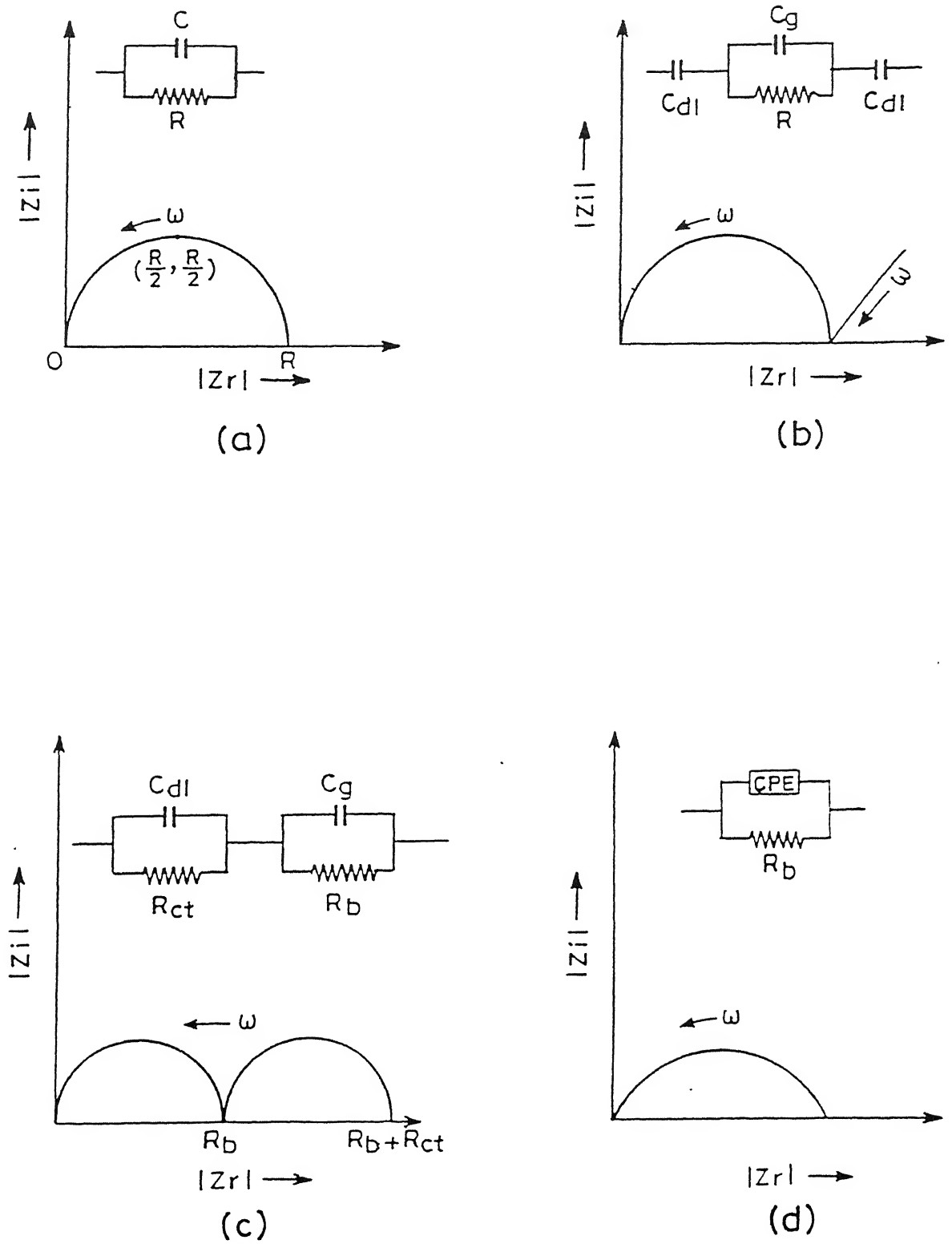

Fig.2.1 Various impedance behaviours observed in solid electrolytes.

resistance R have been supplemented by a double layer capacitance C_{dl} which represents the capacitance at the electrode/electrolyte interface. In this case also the bulk resistance is obtained from the intersection of the semicircle with the real axis. However a 90^{o} line in addition to the semicircle is obtained for perfectly smooth surfaces. The slope of the line decreases with the increasing roughness (Archer and Armstrong, 1980). This type of frequency response can be represented by a constant phase element (Raistrick, 1986; Liu et.al.,1986; and Wang and Bates, 1986) which has an impedance $Z = A(j2\pi f)^{-n}$, where A is a constant and the exponent 'n' has a value between 0 and 1.

For a polycrystalline material there may be a contribution to the impedance due to the presence of grain boundaries. The grain boundaries may act as a hindrance to the ion transport. In some of these cases one may detect a second semicircle in the impedance plot representing the grain boundaries (Hooper,1977; Archer et. al.,1980). The bulk resistance in such cases is obtained from the intersection of the semicircle with the real axis in the higher frequency region. If we have an increased conductivity at the grain boundaries it will give an apparent resistance that is lower than the real bulk effect (Fig.2.1c). Thus, a study of the conductivity dependence on the grain size may help identify the mechanism of conduction.

For the PbX_2-Al_2O_3 (X = Cl, Br, I) samples investigated in this work, the complex impedance spectra consist of a single

semicircle in the frequency domain 1kHz to 10 MHz. Therefore, such cell arrangements are equivalent to the circuits shown in Fig. 2.1a. However, due to the existence of a double layer capacitance owing to the application of blocking Pt electrodes, the equivalent circuit is expected to be the one shown in Fig.2.1b which is not observed in case of $Pt|PbX_2\text{-}Al_2O_3|Pt$ cell systems. This could be due to the limitation of the Impedance Analyzer to measure the $|Z|$ and θ values correctly and reproducibly at lower frequencies (below 1kHz) for these systems. In any case, the diameter of the semicircular plots yields the dc resistance which has been used to calculate the dc conductivity of the samples. For alkali chloride-Al_2O_3 samples, the typical complex impedance spectra obtained in the frequency domain 1 kHz-10 MHz are as shown in Fig.2.1b. The resistance associated with the spectra in the high frequency region has been used to calculate the (dc) conductivity of the samples.

Another effect observed in the impedance plots is that the high frequency semicircular portion of the spectrum is depressed so that the centre of the circle is situated below the real axis (Fig.2.1d). It has been shown that in this case a constant phase element connected in parallel with the bulk resistance will result in such a spectrum with a depressed semicircle (Raistrick, 1986; Macdonald, 1984).

2.2 General Theory of Ionic Conductors :

The electrical conductivity of any material is given by,

$$\sigma = \sum_i n_i\, q_i\, \mu_i \qquad (2.7)$$

where n_i, q_i and μ_i are the concentration, the charge, and the mobility respectively of the 'i' th species. The summation is over all possible charge carriers (e.g., vacancies, interstitials, electrons and holes etc.). In most ionic solids the contributions of the holes and electrons to the overall conductivity is negligible compared to those of ions. Assuming that only one type of mobile species makes a significant contribution to the observed conductivity, the Eq.(2.7) becomes :

$$\sigma = n\, q\, \mu \qquad (2.8)$$

where q=ze (z is the valency of the mobile ion and e is the electronic charge).

In poor and moderate conductors the charge carriers are thermally induced interstitial ions (Frenkel defects) or vacancies (Schottky defects) in the crystal structure. The equilibrium concentration of either type of defects is given to a good approximation by :

$$n = B\, n_o \exp\left[\frac{-G_f}{2kT}\right] \qquad (2.9)$$

where G_f is the free energy of formation of a defect pair at the temperature T, n_o the concentration of normal lattice sites, and B is an entropy factor which depends upon the crystal structure and

the type of defect involved (Jacobs and Tompkins, 1952).

The variation of mobility with temperature for poor and moderate conductors may be expressed as :

$$\mu = A\frac{a^2 e\nu}{kT}\exp\left[\frac{-G_m}{kT}\right] \qquad (2.10)$$

where G_m is the free energy of migration of the mobile species through the lattice, ν the frequency of vibration, a the jump distance, and A a factor which accounts for the change in G_m with temperature (Jacobs and Tompkins, 1952).

Combining Eqs.(2.8), (2.9) and (2.10) one obtains a general expression for conductivity (σ) as follows :

$$\sigma = \frac{C}{T}\exp[\{(-G_f/2)-(G_m)/kT\}] \qquad (2.11)$$

In terms of the corresponding enthalpy (H) and entropy (S), viz.,

$$G_f = H_f - TS_f \qquad (2.12a)$$

and,
$$G_m = H_m - TS_m \qquad (2.12b)$$

Eq. (2.11) can be rewritten as :

$$\sigma = (\sigma_o/T)\exp[\{(-H_f/2)-H_m\}/kT] \qquad (2.13a)$$

$$\text{or,} \qquad \sigma T = \sigma_o \exp[-E'_a/kT] \qquad (2.13b)$$

where $E'_a = (H_f/2 + H_m)$ is the overall activation energy for conduction. Thus a plot of $\log(\sigma T)$ vs $1/T$ is linear whose slope yields the overall activation energy $E'_a = H_f/2 + H_m$. However since the variation of $\log(T)$ over the experimental temperature range (300 K to 900 K) is negligible in comparison to that of $\log\sigma$, a plot of $\log(\sigma)$ vs $1/T$ is also found to be linear and is preferred because of its obvious simplicity. However the activation energy (E_a) obtained from this plot is slightly lower than E'_a obtained from Eq.(2.13b) by an amount equal to the thermal energy (kT), i.e., $E_a = E'_a - kT$.

Generally a plot of log σ versus $1/T$ for a nominally pure ionic solid consists of two linear segments; a high temperature linear region which is an intrinsic property of the material, and a low temperature extrinsic region characterized by a lower slope (hence lower activation energy). The intrinsic region relates to the temperature range in which the dominant defects are those which are present due to thermodynamic considerations. In this case E_a is the sum of half the formation (H_f)energy of formation and migration (H_m) of defects. The extrinsic region relates to the temperature range in which dominant defects are those introduced by the addition of aliovalent impurities and are present due to charge neutrality conditions. Here E_a is simply the migration energy (H_m) alone. The position of extrinsic-intrinsic transition temperature is known as *knee* temperature, and is often used as a

measure of impurity level in the crystal. The complete conductivity curve ($\log\sigma$ vs $1/T$) is, therefore, generally a superposition of two line segments corresponding to :

1. $A_1 \exp(-E_1/kT)$ in the low temperature, extrinsic region.

2. $A_2 \exp(-E_2/kT)$ in the high temperature, intrinsic region.

The activation energy E_1 is less than E_2 (typically $E_1/E_2 = 1/2$), and A_1 is by far less than A_2. A_2 is independent of the purity of the material, while A_1 increases as the impurity of the specimen increases. Moreover, the knee temperature increases as the impurity concentration increases in the sample.

The conductivity data may be used to calculate the diffusion coefficient (D_q) for the mobile charge carrying species via the Nernst-Einstein relation :

$$\frac{\sigma}{D_q} = \frac{ne^2}{kT} \qquad (2.14)$$

The value of diffusion coefficient D_q in the Eq.(2.14) may not necessarily be equal to the diffusion coefficient D_τ as measured from the radioactive tracer technique. The ratio D_τ/D_q is known as the Haven ratio. A given mechanism or a combination of mechanisms leads to unique value of H_R. Thus experimental determinations of H_R can usefully lead to the identification of a particular transport mechanism. The neutral defects contribute to D_τ but not

to D_q and thus H_R will be larger in their absence. Moreover H_R is anomalously small in the presence of any electronic conductivity. In the case of very large defect concentrations H_R will be close to unity. The temperature dependence of the tracer diffusion coefficient also has the same form as the conductivity, viz.,

$$D_o = D_o \exp(-E_A/kT) \qquad (2.15)$$

where $E_A = E_a$, if the diffusion and conduction mechanisms are the same and the electronic conductivity is negligible.

2.3 Theory of Composite Solid Electrolytes :

The enhancement in conductivity of normal ionic conductors by dispersion of insulating particles such as Al_2O_3, SiO_2 etc. stands in *stark contrast* to the Maxwell's theory (1881), according to which the conductivity should decrease monotonically with the addition of insulating particles. The effect suggests that such dispersoids cannot act as essentially simple diluents of the conducting phase in a manner envisaged by Maxwell. Instead of that, by processes, yet to be firmly established, either each dispersoid induces changes in the charged defect concentrations in the surrounding matrix so that the conductivity of the host phase is enhanced (Jow and Wagner, 1979; Maier, 1984,1985,1986,1987), or that each particle acts as a carrier of some chemical species (e.g. water molecules) which interacts with the host to form a high conductivity coating surrounding each inclusion (Stoneham

et.al., 1979). Thus, by one (or both) of these means a potential mechanism is introduced to counteract the dilution effect, which alone, is incorporated by the Maxwell's theory.

On the assumption that via some process of charge transfer or interfacial point defect trapping, the spatial redistribution of defects is the dominant operative mechanism, Jow and Wagner (1979) have highlighted two specific alternatives. One is that the formation of a charged double layer, while occurring at or near the dispersoid surface, influences the conductivity predominantly via changes in the defect concentration far from each inclusion. The second possibility is that the major effect on the overall conductivity resides in the much greater enhancement in defect concentration in the double layer itself. Wagner (1972) discards this eventuality on the basis of the volume fraction occupied by each such inclusion. Jow and Wagner (1979), however, favored the second possibility over the first one on the basis of its apparent ability to reproduce certain experimentally observed features. Stoneham et.al.(1979) extended the Landauer (1973) effective medium model successfully for the LiI(Al_2O_3) composite system and the composition dependence of conductivity. Maier(1984, 1985,1986) treated the space charge region as a separate phase and considered the normally conducting, insulating and space charge layer as a network of parallel resistors. Maier (1985) formulated the defect concentration profiles in the space charge region at the matrix-particle interface and gave a semiquantitative theory to account for the enhancement in conductivity in composite solid

electrolytes.

Bunde, Dieterich and Roman (1985, 1986) examined the conductivity enhancement in composite solid electrolytes purely from the macroscopic point of view. The model assumes the existence of a high conducting interface between normally conducting matrix and non-conducting dispersed phase without going into the mechanism of its formation. The normally conducting, highly conducting and the non-conducting bonds are mapped on to the problem of random walk (Bunde et.al,1986) on a lattice with three types of bonds (hopping rates) and the diffusion coefficient is calculated by means of Monte-Carlo simulations. The numerically exact solution of the problem consists of two threshold concentrations of the insulating phase, viz., p_c' and p_c''. At $p=p_c'$ the onset of high conductivity occurs and at the concentration $p=p_c''$ a conductor-insulator transition takes place. The model gives a characteristic dependence of the overall conductivity on composition which is in remarkable agreement with experimental observations. Some of the important models are discussed in detail in the following sections.

2.3.1 Jow and Wagner (1979) *Model :*

The existence of space charge regions near the lattice discontinuities (free surfaces, dislocations and grain boundaries etc.) in an ionic crystal was first proposed by Frenkel (1946). The charge distribution profiles have been formulated by several researchers (Lehovec, 1953; Eshelby et.al., 1958; Kliewer and

copper ion vacancies (Wagner and Wagner, 1957). Following the Kliewer and Koehler's (1965) treatment in the case of CuCl, the concentration of copper interstitials, $n_i(x)$, and copper vacancies $n_v(x)$, in a crystal of finite length in x direction and infinite length in y and z direction is given as follows :

$$n_v(x) = N \exp[-\{F_v - e\phi(x)\}/kT] \qquad (2.16a)$$

$$n_i(x) = 2N \exp[-\{F_i + e\phi(x)\}/kT] \qquad (2.16b)$$

where N is the number of CuCl molecules per unit volume, F_v the free energy of formation of a copper ion vacancy and F_i that of a copper ion interstitial, and potential $\phi(x)$ is the solution of Poisson's equation :

$$\frac{d^2\phi(x)}{dx^2} = \frac{-4\pi\rho(x)}{\varepsilon} \qquad (2.17)$$

where $\rho(x) = e(n_i(x) - n_v(x))$, is the charge density and ε is the static dielectric constant. Substitution of the solution of $\phi(x)$ in Eqs.(2.16) gives the complete dependence of the defect concentration on position x. The space charge layer extends a distance roughly equal to λ which is expressed as (Kliewer,1966) :

$$\lambda = \left\{\frac{8\pi Ne^2}{\varepsilon kT} \exp[(e\phi_\infty - F_v)/kT]\right\}^{-\frac{1}{2}} \qquad (2.18)$$

where ϕ_∞ ,the potential difference between the surface and the bulk is given by :

$$\phi_{\infty} = \frac{1}{2e}(F_v - F_i + kT\ln 2) \qquad (2.19)$$

Thus, from Eqs.(2.18) and (2.19), λ can also be expressed as :

$$\lambda = \left(\frac{8\pi e^2}{\varepsilon kT} n_v(\infty)\right)^{-\frac{1}{2}} = \left(\frac{8\pi e^2}{\varepsilon kT} n_i(\infty)\right)^{-\frac{1}{2}} \qquad (2.20)$$

where $n_v(\infty)$ and $n_i(\infty)$ are the equilibrium defect concentrations of copper vacancies and copper interstitials in the bulk. Since the defect concentration near the surface of an ionic solid is different from that in the bulk, the conductivity near the surface differs from that in the bulk as well (Lehovec,1953). Considering the conduction in a volume of $(4\pi/3)r_2^3$ containing one dispersed particle of radius r_1 as shown in Fig.2.2a, the total conductivity of the system can be written as :

$$\sigma = \sigma_o + \Delta\sigma \qquad (2.21)$$

where σ_o is the conductivity of the bulk, and $\Delta\sigma$ is the contribution due to space charge layer between r_1 and r_2. In the spherical polar coordinates, $\Delta\sigma$ will amount to :

$$\Delta\sigma = \sum_i e\,\mu_i \left[\frac{\int_{r_1}^{r_2}\int_0^{\frac{\pi}{2}}\int_0^{2\pi} [n_i(r) - n_i(\infty)]r^2 dr\,\sin\theta\, d\theta\, d\phi}{\int_{r_1}^{r_2}\int_0^{\frac{\pi}{2}}\int_0^{2\pi} r^2\, dr\,\sin\theta\, d\theta\, d\phi} \right] \qquad (2.22)$$

where μ_i is the mobility of the 'i' th defect species which is

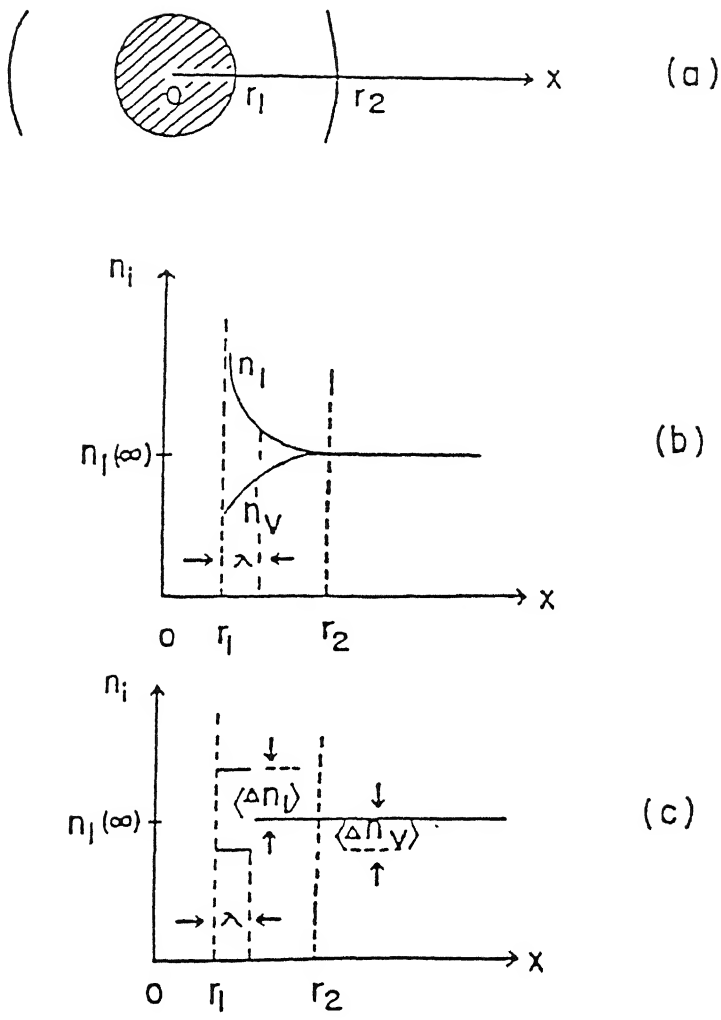

Fig.2.2 (a) Schematic cross sectional view, (b) defect concentration profile and, (c) average excess charge density in space charge layer for a single Al_2O_3 particle dispersed in a matrix.

assumed to be independent of the position, $n_i(r)$ and $n_i(\infty)$ are the defect concentrations at a point r and in the bulk, respectively. The defect concentration profile, along the x direction from the surface of the particle into the bulk of the crystal, is shown in Fig.2.2b. Assuming that the thickness of the space charge layer is smaller than the radius of the dispersed particle, i.e. $\lambda \ll r_1$, the excess defect concentration can be taken to be the arithmetic mean, $\langle \Delta n_i \rangle$, of the defect concentrations immediately at the surface and in the bulk as shown in Fig. 2.2c. Thus, Eq.(2.22) can be solved to yield :

$$\Delta\sigma \cong \sum_i e\,\mu_i \langle \Delta n_i \rangle \left[\frac{4\pi r_1^2\,\lambda}{\frac{4\pi}{3}(r_2^3 - r_1^3)} \right] \qquad (2.23)$$

The ratio r_1/r_2 is a function of volume fraction of the dispersed second phase. Assuming $r_1 \ll r_2$, $(r_1/r_2)^3 \simeq V_f$, the Eq.(2.23) can be rewritten as :

$$\Delta\sigma \cong 3 \sum_i e\mu_i \langle \Delta n_i \rangle (\lambda/r_1) \left[\frac{V_f}{1 - V_f} \right] \qquad (2.24)$$

where μ_i, $\langle \Delta n_i \rangle$ and λ are the functions of temperature.

Eq.(2.24) provides a qualitative explanation for the temperature dependence of the conductivity in the composite solid electrolytes. The experimentally observed fact that the ionic conductivity of the composites in relation to the pure hosts are larger at low temperatures than those at higher temperatures is

reflected in Eq.(2.20). As the temperature increases the Debye length, λ, decreases because the defect concentration is a stronger (exponential) function of temperature. Eq.(2.24) also accounts for the decrease in the conductivity with increase in the size of the dispersed particles. The model, however, fails to explain the observed maximum in the conductivity at a particular concentration of the dispersoid and also the mechanism leading to the enrichment of the defect concentration in the space charge region of various composite solid electrolytes.

2.3.2 Maier's Theory of Heterogeneous Doping :

Maier(1984,1985,1986) considered how exactly the surface charge layer is formed on account of possible surface interactions of the mobile defects in the matrix phase with the dispersed second phase allowing a complete and quantitative description of the effect.

For a composite system of a Frenkel disordered ionic conductor (MX) in contact with a chemically inert second phase (A), the Frenkel disorder reaction at the interface can be split into the separate formation reactions of the vacancies (V'_M) and interstitials ($M^{\cdot}_i$) :

$$M_M + V_A \Leftrightarrow M^{\cdot}_A + V'_M \qquad (2.25a)$$

$$M^{\cdot}_A + V_i \Leftrightarrow M^{\cdot}_i + V_A \qquad (2.25b)$$

where the Kröger-Vink notation is used; the subscripts M, i and A

indicate a regular cation (M^+) site, an interstitial site and an interface site respectively, and the superscripts (.) and (') indicate an excess positive and negative charge.

Due to the requirement of the local electroneutrality, in thermodynamic equilibrium the concentrations of interstitials and vacancies are identical in the bulk of a crystal. Near the surface, and/or equivalently near every heterogeneity such as matrix-particle interface, however, these concentrations may deviate from each other (Fig.2.3). If the free energy of the reaction Eq.(2.25a) ($\Delta_{vA}G^o$) is exceeded by the free energy for reaction Eq.(2.25b) ($\Delta_{iA}G^o$), then the surface will be enriched with the cations. Such an energetic interaction, if high enough to overcompensate entropic effects, lowers the free energy of formation of a vacancy and enlarges the free energy of formation of an interstitial compared to the intrinsic values. As a result the vacancy concentration (N_v) will be enlarged with respect to the bulk concentration (N_∞), i.e., the boundary regions will be depleted of cations. On the other hand, if the free energy change of Eq.(2.25b) exceeds that of the reaction Eq.(2.25a), the cations will be driven into the space charge region and the concentration of interstitials will be larger than the bulk concentration N_∞. In equilibrium this locally realized space charge ($N_v \neq N_i$) is fixed and the resultant electric field in its energetic influence is compensated by the variation of the chemical potential.

The criterion for a charge carrier rich boundary region is :

$$|\Delta_{vA}G^{o} - \Delta_{iA}G^{o}| = 2|\Delta_{vA}G^{o} - \Delta_{F}G^{o}/2| = 2kT\ |\ln(N_{vo}/N_{\infty})| \gg kT \qquad (2.26)$$

where $\Delta_{F}G^{o} = \Delta_{vA}G^{o} + \Delta_{iA}G^{o}$, is the Gibbs free energy of the Frenkel reaction, N_{vo} the concentration of vacancies at the interface and N_{∞} is the bulk concentration of vacancies (and of interstitials). The concentration of vacancies (or interstitials) N_{∞} in the bulk of a crystal is given by the law of mass action as follows :

$$N_{i\infty} = N_{v\infty} = N_{\infty} = \sqrt{K_{F}} = \exp[-\Delta_{F}G^{o}/2kT] \qquad (2.27)$$

where K_{F} is the Frenkel constant. From the law of mass action it follows :

$$N_{v}\ N_{i} = N_{\infty}^{2} = K_{F} \qquad (2.28)$$

The concentration profiles of the charge carriers in the surface charge layer can be obtained from the constancy of the electrochemical potential, the Poisson's equation, and the boundary condition that the electric field ($-\frac{\partial \phi}{\partial x}$) vanishes in the interior of the crystal. Following the Kliewer's (1966) treatment the concentration profiles of N_{v} and N_{i} in the space charge layer are given as :

$$N_{v} = N_{v\infty}\ \exp(z) \qquad (2.29a)$$

$$N_{i} = N_{i\infty}\ \exp(-z), \qquad (2.29b)$$

where $$z = 4 \tanh^{-1}\{e^{(-x/\lambda)} \tanh(z_o/4)\}, \quad (2.30)$$

with $$z_o = z(x=0) = -(\Delta_{vA}G^o - \Delta_{iA}G^o)/(2kT), \quad (2.31)$$

and λ is the Debye length which characterizes the effective thickness of the space charge layer and is given by :

$$\lambda = \left(\frac{\varepsilon\varepsilon_o kT}{2e^2 N_\infty} \right)^{\frac{1}{2}}, \quad (2.32)$$

where $\varepsilon\varepsilon_o$ is the absolute dielectric constant, e the electronic charge and N_∞ is the density of the defects in the interior of the crystal.

Defining the normalized concentration (ζ) and normalized space coordinate (ξ) :

$$\zeta_v = \frac{N_v}{N_\infty} \quad \text{and} \quad \zeta_i = \frac{N_i}{N_\infty} \quad (2.33a)$$

and, $$\xi = \frac{x}{\lambda} \quad (2.33b)$$

Using Eqs.(2.33), the concentration profiles N_v and N_i Eqs.(2.29) can be rewritten in a more appropriate form :

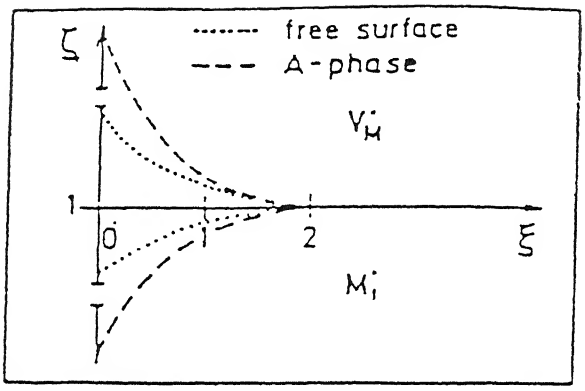

Fig.2.3 Concentration profiles for cation vacancies and interstitials in a Frenkel disordered material from the free surface and, surface in contact with a second phase 'A' into the interior of the crystal.

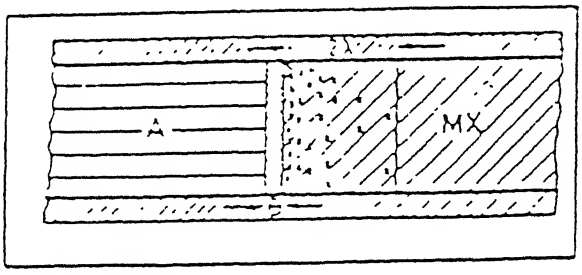

Fig.2.4 A crystal MX in contact with a second phase 'A'.

$$\zeta_v(\xi) = \frac{\left[1 + \exp(-\xi)\Theta_v \right]^2}{\left[1 - \exp(-\xi)\Theta_v \right]^2} \tag{2.34a}$$

with, $$\Theta_v = \frac{\left[\zeta_{vo}^{1/4} - \zeta_{vo}^{-1/4} \right]}{\left[\zeta_{vo}^{1/4} + \zeta_{vo}^{-1/4} \right]} \tag{2.34b}$$

and $$\zeta_i(\xi) = \frac{\left[1 + \exp(-\xi)\Theta_i \right]^2}{\left[1 - \exp(-\xi)\Theta_i \right]^2} \tag{2.35a}$$

with, $$\Theta_i = \frac{\left[\zeta_{io}^{1/4} - \zeta_{io}^{-1/4} \right]}{\left[\zeta_{io}^{1/4} + \zeta_{io}^{-1/4} \right]} \tag{2.35b}$$

The contribution of the space charge layer to the conductance can be calculated by imagining a system of parallel layers of crystal MX and phase A, and measuring the resistance parallel to the interface as shown in Fig.2.4. The electrodes are fixed perpendicular to the interface. The total conductance of the system, for the sake of simplicity being freed of unimportant geometric parameters in y and z directions, is

$$G = G_A + G_o + \Delta G \tag{2.36}$$

where G_A is the conductance of the second phase including possible contributions of the interaction layer and G_o is the conductance

of MX phase due to bulk defect concentrations. ΔG is the space charge contribution to conductance due to excess defects in the space charge region and is the sum of the contributions from the vacancies $(\Delta G)_v$, and the interstitials $(\Delta G)_i$. Assuming the changes in the dielectric constant, the mole volume V^m and the mobilities (μ_v and μ_i) to be negligible and the size of the MX crystal in the x direction being large compared to the Debye length λ, ΔG can be obtained as follows :

$$(\Delta G)_{v,i} = e \int_o^\infty \mu_{v,i} [N_{v,i}(x) - N_\infty] dx \qquad (2.37)$$

Using Eqs.(2.33), Eq.(2.37) can be written as :

$$(G)_{v,i} = e\, \mu_{v,i}\, N_\infty\, \lambda \int_o^\infty [\zeta_{v,i}(\xi) - 1] d\xi \qquad (2.38)$$

Inserting $\zeta_{v,i}(\xi)$ from Eqs.(2.34a) and (2.35a) into Eq.(2.38) and integrating we obtain :

$$(\Delta G)_{v,i} = 4\, \lambda\, u_{v.i} \left[\frac{\Theta_{v.i}}{1 - \Theta_{v,i}} N_\infty \right] \qquad (2.39)$$

It is assumed that the M ion is stabilized at the interface, so that the vacancy concentration is increased in the space charge region and the contribution to conductance due to the interstitials $(\Delta G)_{v,i}$ is negligible. Using Eqs.(2.34b) and (2.35b) the Eq.(2.39) simplifies to :

$$(\Delta G)_v \cong e(2\lambda)\mu_v \sqrt{N_o}\, N_{v\infty} \qquad (2.40)$$

and, $$(\Delta G)_i \cong - e(2\lambda)\mu_i N_\infty \qquad (2.41)$$

In all practically important cases, one species of the charge carriers (either interstitials or vacancies) dominates the conduction. In the case of cations being stabilized at the interface, i.e. $\Delta_{vA}G^o < \Delta_{iA}G^o$ and hence $N_{vo} \gg N_\infty \gg N_{io}$, the extra layer conductance ΔG is dominated by $(\Delta G)_v$, whereas $(\Delta G)_i$ is a negligible and negative quantity and as such physically unacceptable. Eqs.(2.40) and (2.41) are very fascinating results which suggest that the conductance of the space charge region can be obtained simply by assuming a resistor of effective thickness 2λ, and the geometric mean of the concentrations in the bulk and immediately below the interface as the effective concentration.

In case of a dispersed system, however, the insulating phase A is randomly distributed and the total conductivity of the composite depends on the distribution topology of the two phases. A parallel switching of the resistivities is, however, exactly valid only for the case of parallel layers of A and MX, and it can be regarded as an upper limit. However, the parallel switching treatment can be retained by simply introducing a correction factor β_α which depends on the distribution topology of phase A into the matrix MX and is a measure of deviation from an ideal parallel switching ($\beta_\alpha = 1$). The correction factor β_α is given by the ratio of effective phase volume, which can be considered as being affected by the parallel switching to the whole phase volume.

The total conductivity (σ) of the composite may be expressed as :

$$\sigma = \Sigma_{\alpha} \beta_{\alpha} \varphi_{\alpha} \sigma_{\alpha} \qquad (2.42)$$

where α = A (the second phase including the interaction layer); α = L (the space charge region); α = o (the bulk phase; as $x \rightarrow \infty$). Assuming spheres of a phase A embedded in a crystal MX as shown in (Fig. 2.5a), and $\lambda \ll r_A$, the volume fraction of the space charge layer (α = L) is :

$$\varphi_L = 3 \frac{2\lambda}{r_A} \varphi_A \qquad (2.43)$$

Fig.2.5b represents a realistic distribution of particles in the matrix MX. Here spheres of the insulating phase A form coherent chains in the areas between the MX grains. Assuming the conductivity of phase A to be zero, the total conductivity of the composite from Eqs.(2.40) and (2.42) can be written as :

$$\sigma = (1-\varphi_A)\sigma_o + 3\, e\, \beta_L\, (2\lambda/r_A)\, \varphi_A\, \mu_v \sqrt{N_{vo} N_{v\infty}} \qquad (2.44)$$

Substituting for Debye length λ from Eq.(2.32) and for φ_L from Eq.(2.43) in the Eq.(2.44), the expression for the conductivity of the composite can be written as :

$$\sigma = (1-\varphi_A)\sigma_o + (3\sqrt{2})\, \beta_L\, (\varphi_A/r_A) \sqrt{(\varepsilon\varepsilon_o RT/V^m)}\, \mu_v \qquad (2.45)$$

The problem of the overall conductivity (σ) of a dispersed

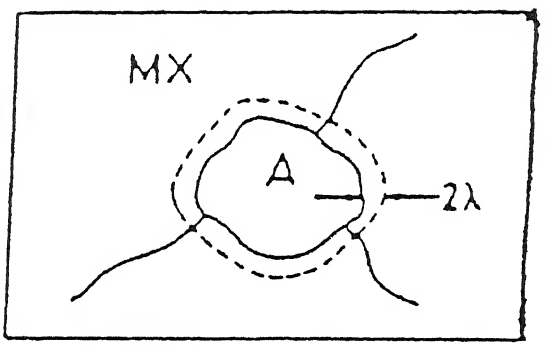

(a)

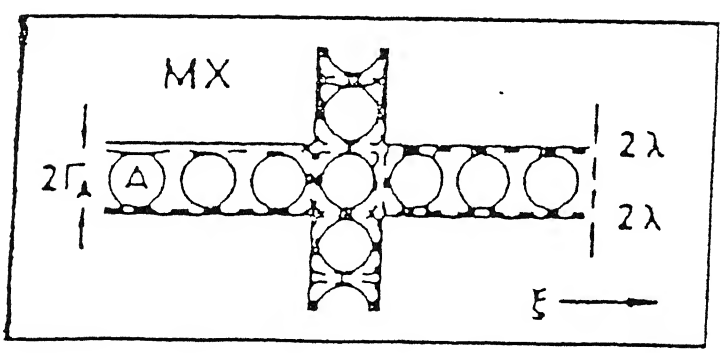

(b)

Fig.2.5 (a) Particle of a second phase 'A' embedded in a crystal MX surrounded by a space charge layer and (b) coherent spheres of phase 'A' forming cross chains.

system is very complex and quite sensitive to the distribution topology of the second phase particles. Thus, not only the exact problem is analytically intractable, but a precise numerical solution depends much on the individual situation to be of general interest. For these reasons simplified topologies, still representative enough, have been used to arrive at a general conclusion Eq.(2.45). Beyond the mathematical simplicity, this model corresponds to the most favorable topology and quite well fulfills the realistic experimental observations made for a variety of composite systems reported in the literature. Eq.(2.45) explains the linear dependence of σ on φ_A in the low concentration region. For higher volume fractions the blocking effect of alumina becomes important. For very low concentrations, a linear relationship cannot be expected because the particles are totally isolated.

2.3.3 Random Resistor Network (Percolation) Model :

The percolation model, which is also called the Random Resistor Network (RRN) model (Bunde, Dieterich and Roman, 1985), considers the problem of conductivity enhancement in composite solid electrolytes from the macroscopic point of view. It basically assumes that the enhancement results from the formation of a space charge layer along the interface between the two phases. In their model Bunde, Dieterich and Roman (1985) started from a square lattice in two dimensions and from a cubic lattice in three dimensions. In two dimensions the square lattice has randomly occupied squares with probability p (Fig.2.6a) and in

three dimensions unit cubes occupy the simple cubic lattice with probability p (Fig.2.6b). Physically the occupied space for both the cases represent the dispersed insulating material. The bonds connecting the two neighboring sites are regarded as electrical resistors. Three types of bonds could be distinguished, (a) highly conducting bonds with interface conductance σ_A, (b) normally conducting bonds with interface conductance σ_B and (c) insulating bonds with conductance σ_C which is zero. For the square lattice the bonds are highly conducting if they belong to one occupied square, insulating if they correspond to two occupied squares, and normally conducting if both the squares are empty. In the case of cubic lattice the bonds are highly conducting if they belong to either one, two or three occupied cubes and insulating if they belong to four occupied cubes, and normally conducting if all four cubes are empty. The fractions f_A, f_B and f_C of highly conducting, normally conducting, and insulating bonds depend on the concentration p of the dispersoid. For a square lattice the corresponding fractions can be written as :

$$f_C = p^2 \tag{2.46a}$$

$$f_B = (1-p)^2 \tag{2.46b}$$

$$f_A = 1 - f_B - f_C$$

$$= 1-p^2-(1-p)^2 = 2p(1-p) \tag{2.46c}$$

In case of a cubic lattice, four neighboring cubes should be occupied to generate an insulating bond and four neighboring cubes

should be empty to generate a normally conducting bond. Thus the fractions of the corresponding bonds become :

$$f_C = p^4 \tag{2.47a}$$

$$f_B = (1-p)^4 \tag{2.47b}$$

$$f_A = 1-p^4-(1-p)^4$$

$$= 2p(1-p)\{2-p(1-p)\} \tag{2.47c}$$

In order to determine quantitatively the total conductivity of the composite material, the three types of bonds are mapped onto the problem of random walk on a lattice. The three types of bonds are represented by three different jump rates τ_A^{-1}, τ_B^{-1} and $\tau_C^{-1}(=0)$, which are proportional to the corresponding conductances. The walker jumps between the sites which are the end points of the bonds. The following rules of the random walk are used.

(i) The probability Π_δ that a walker takes a jump from a given site to one of its nearest neighbors in the direction δ is proportional to the hopping rate τ_δ^{-1} in that direction.

$$\text{i.e.,} \qquad \Pi_\delta = \tau_\delta^{-1} / \sum_{\delta=1}^{z} \tau_\delta^{-1} \tag{2.48}$$

since $\sum_{\delta=1}^{z} \tau_\delta^{-1} = 1.$

(ii) The total elapsed time t after N_A steps along highly conducting bonds and N_B steps along normally conducting bonds is :

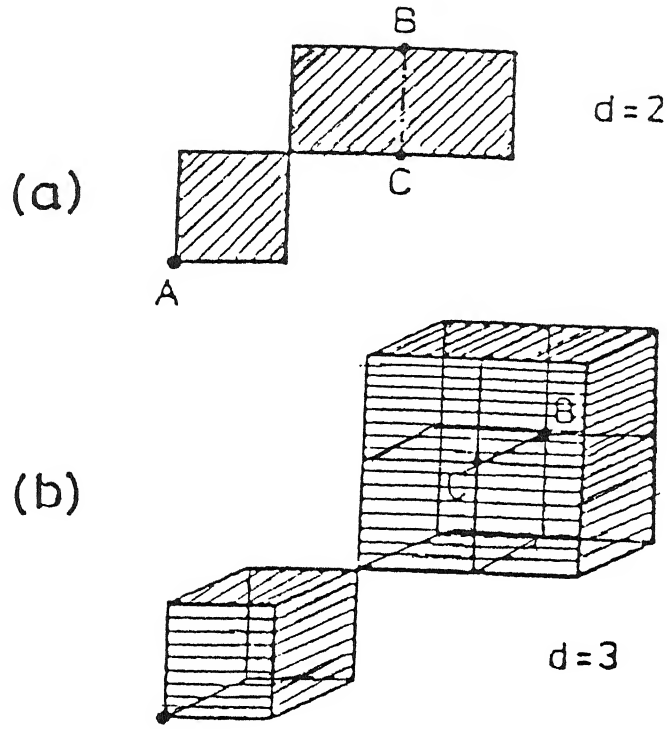

Fig. 2.6 Insulating material embedded in a poor conductor (a) for a square and, (b) for a simple cubic lattice.

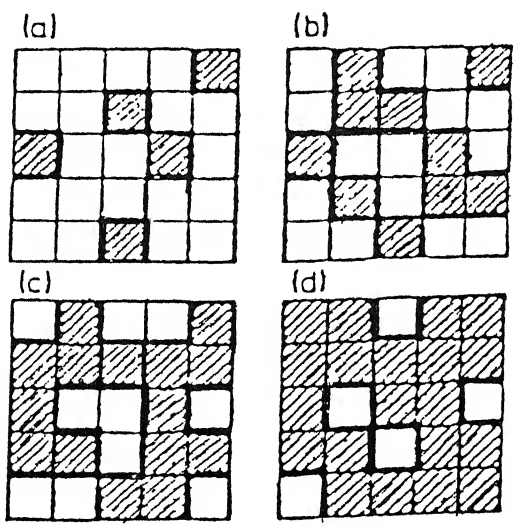

Fig. 2.7 The two phase mixture on a square lattice for different concentration p of insulating material (a) $p < p'_c$, (b) $p = p'_c$, (c) $p = p''_c$ and, (d) $p > p''_c$.

$$t = N_A.\tau_A + N_B.\tau_B \qquad (2.49)$$

as there are no jumps along the insulating bonds, i.e., $N_C = 0$.

(iii) For large times t, the mean-square displacement of the walker $\langle r^2(t)\rangle$ is proportional to $D(p)t$. $D(p)$ is the diffusion constant which is proportional to the conductivity in accordance with Nernst-Einstein relation. The problem is solved by Monte-Carlo simulations. From the asymptotic behavior of $\langle r^2(t)\rangle$ one can determine the total conductivity of the system.

The solution of the problem gives two critical concentrations of the insulating bonds, namely, p_c' and p_c''. p_c' is related to the onset of the enhanced conductivity and defines the lowest concentration of the insulating bonds where an infinite network of highly conducting bonds is formed (interface percolation). p_c'' corresponds to the percolation threshold when all interface bonds get disrupted. For simple square and cubic lattice types considered here p_c' and p_c'' are connected by the relation $p_c' = 1 - p_c''$.

Fig.2.7 shows the two phase mixture on a square lattice, for different concentrations (p) of the insulating material which is represented by the shaded region. For $p \ll p_c'$ (Fig.2.7a), a certain enhancement of conductivity is expected due to the increment of the current flow along σ_A bonds. This enhancement, however, will saturate to a finite value even in the limit $\eta \to \infty$ ($\eta = \sigma_A/\sigma_B$,

is a measure of enhanced interface conductance relative to the bulk value), since the σ_A bonds form only isolated clusters. At concentrations $p=p_c'$, the interface percolation starts and the conductivity will increase indefinitely as $\eta \to \infty$ (Fig.2.7b). By further increasing p, the conductivity for a given finite η will first pass through a maximum (which is a consequence of the maximum at p = 0.5 in f_A, Eq.(2.46c)) and then drops suddenly at p_c'' where all the conduction paths get disrupted (Fig.2.7c). For $p_c' > p_c''$, the conducting material is completely immersed in the insulator (Fig.2.7d) and the conductivity vanishes. Comparing Figs.2.7a to 2.7d, it is observed that the role of conducting and insulating phases are interchangeable leading to the relation $p_c'= 1-p_c''$ for simple square and cubic lattices considered above.

Fig.2.8 shows the normalized conductivity versus concentration curves for simple two and three dimensional (2-d and 3-d) lattices considered above. Since the value of p_c' for 2-d lattice is larger than that for 3-d lattice, the difference $1- p_c' = p_c''$ is correspondingly smaller. Therefore, the conductivity versus composition curves are broader for 3-d lattice case as compared to the 2-d case as shown in Fig.2.8. In principle these predictions are experimentally observed for a variety of systems. The values for p_c' and p_c'' depend upon the type of lattice or the size of the dispersed particles.

Roman and Yussouff (1987) generalized this model to incorporate the particle size effect on the threshold

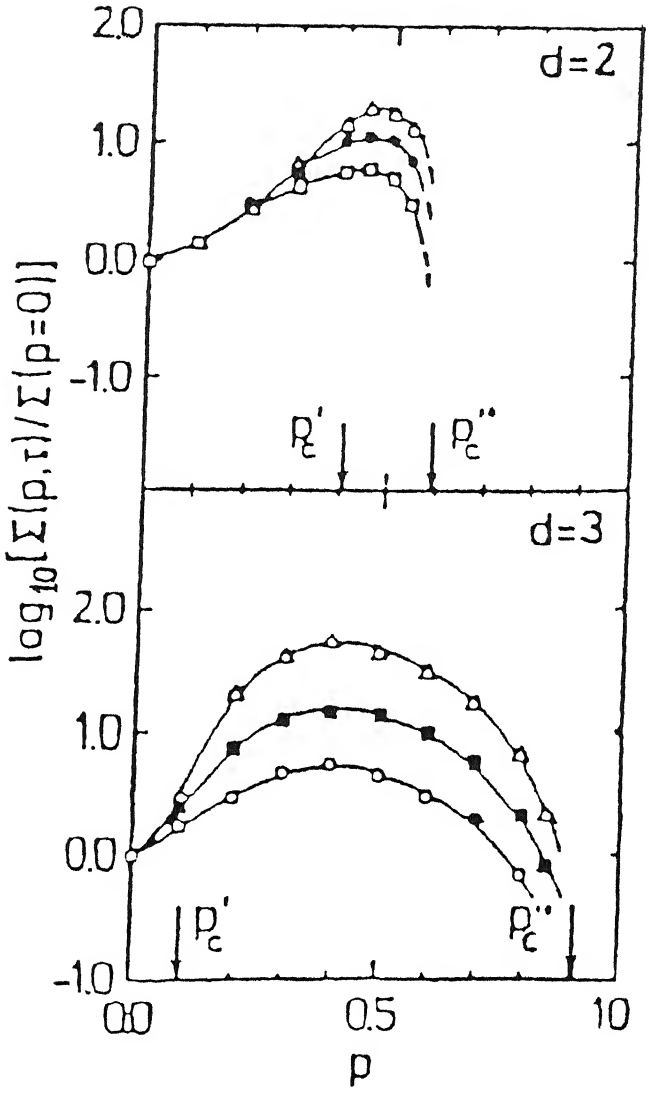

Fig.2.8 The normalized conductivity as a function of concentration (p) for different hopping rates (τ) = 20(□), 50(∘) and 100(Δ) for 2-d lattice and, for τ = 10(∘),30(□) and 100(Δ) for 3-d lattice.

concentrations p_c' and p_c''. They introduced a new parameter 's' called the particle size parameter in the model. Fig.2.9 shows the generalized random resistor network model for the concentration p = 0.375 with three different particle sizes, (a) s = 1, (b) s = 2 and, (c) s = 4. The area of the particles is proportional to s^2. The concentration of particle in terms of s is

$$p = ns^2/L^2 \tag{2.50}$$

where n is the total number of insulating particles and L is the length of the lattice.

Though the concentration of the insulating particle remains same in all the three cases, the concentrations of various kinds of bonds are different for the three different cases. The diffusion coefficient is calculated by Monte-Carlo simulations in the similar way. Fig. 2.10 shows the diffusion coefficient, D(p), as a function of concentration p for different values of η. As the particle size increases from s = 1 (Fig.2.9a) to s = 4 (Fig.2.9c), the peak value of D(p) for a constant η decreases and the peak position shifts to higher concentration. The fact that D(p), for a fixed p, decreases with increasing s, can be understood by noting that the corresponding fraction of highly conducting bonds decreases with the increase in the particle size. One also expects a shift in the position of maximum since the threshold for interface percolation p_c' occurs at higher concentration for larger particle size while the second threshold

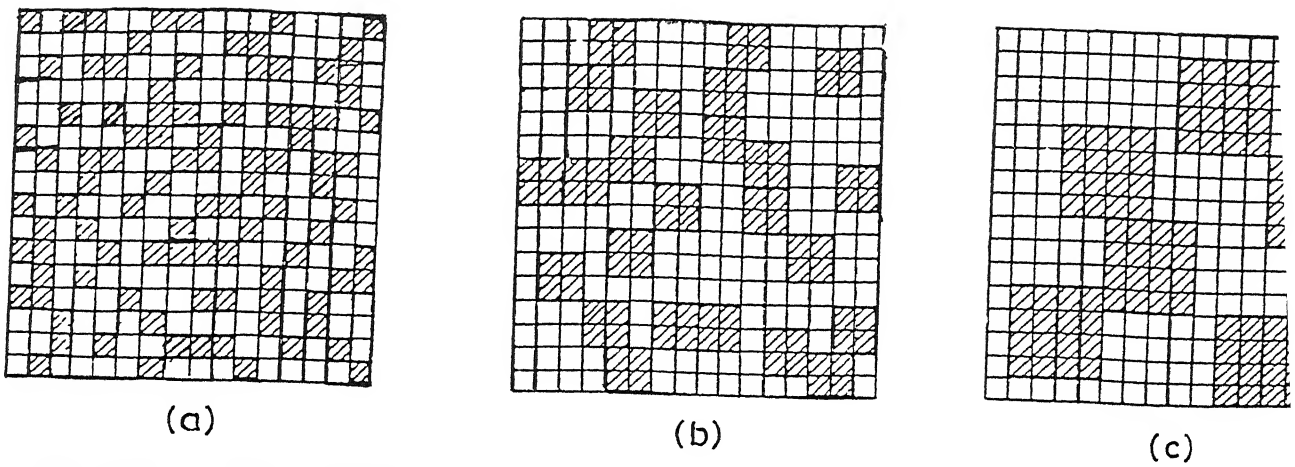

Fig.2.9 The random resistor network model for concentration p = 0.375 for different particle sizes (a) s = 1, (b) s = 2 and, (c) s = 4.

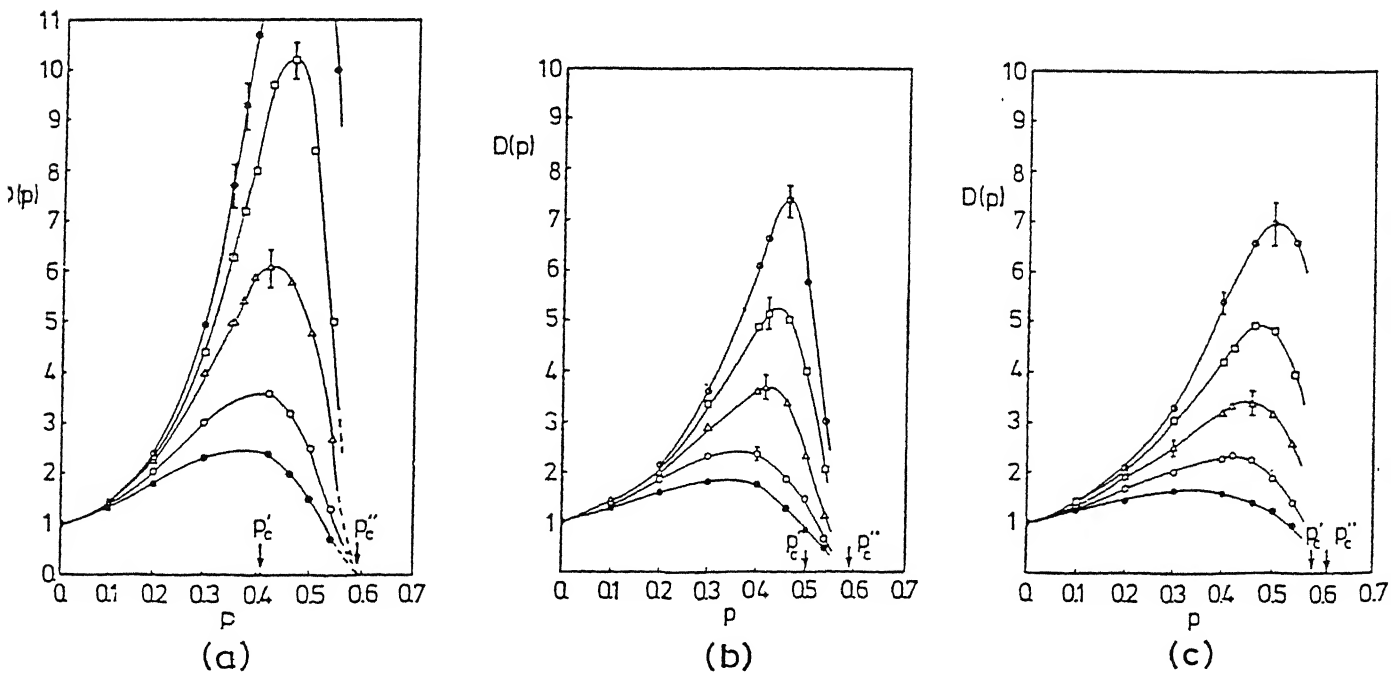

Fig.2.10 Diffusion coefficient as a function of concentration (p) for different hopping rates (τ) with different

remains almost unchanged by increasing the particle size, *s*.

Though the random resistor network model does not seem to be a realistic one, as serious approximations such as a special shape of the second phase particles and a constant interface conductivity, are involved. However, from a rigorous point of view the random distribution theory is appropriate to solve superposition problems in heterogeneous media such as the composite systems since the simulated results can be used to mark off the range of validity of realistic models such as those given by Maier (1985), and Jow and Wagner (1979).

CHAPTER 3

EXPERIMENTAL DETAILS

3.1 Starting Materials :

The high purity alkali halides were obtained from Aldrich Chemicals Inc.(USA) and high purity lead halides were obtained from Alfa Products (USA) and MERCK-Schuchardt (Germany). The deagglomerated Al_2O_3 powder of three different particle sizes (0.05,0.3 and 1.0 μm) was obtained from Buehler Micropolish II (USA). The purity of the chemicals and their other details are given in Table 3.1. The as-received Al_2O_3 powder was milled thoroughly in acetone medium in a ball mill (Fritsch Puloeriette Type.05.202, Germany) for 6-8 hrs to ensure the deagglomeration of Al_2O_3 particles. The materials synthesis and processing, such as melting, grinding and pelletization etc., of the hygroscopic samples were carried out in a controlled atmosphere glove box (model GB-80, Mecaplex, Switzerland).

3.2 Sample preparation :

Various composite samples have been prepared by two different methods; (i) The conventional and, (ii) The solution casting methods. Mettler *AE 160* balance was used to weigh the desired amount of the constituents.

Table 3.1

Details of the chemicals used in this work

compound	manufacturer	purity (%)	melting point (^{o}C)	density (gm/cm^{3})
$PbCl_2$	Aldrich Chemicals (USA)	99.99	501	5.85
$PbBr_2$	MERCK-Schuchardt (Germany)	99+	373	6.66
PbI_2	Alfa Products (USA)	98.5	402	6.16
NaCl	Aldrich Chemicals	99+	801	2.165
KCl	Aldrich Chemicals	99+	770	1.984
RbCl	Aldrich Chemicals	99+	717	2.8
CsCl	Aldrich Chemicals	99.9	636	3.988
α-Al_2O_3	Buehler Micropolish II (USA) Particle sizes 0.3 and 1.0 μm	-	2050	3.965
γ-Al_2O_3	Buehler Micropolish II (USA) 0.05 μm	-	2050	3.97

3.2.1 Conventional method :

In this method, the sample preparation involves the following steps :

(i) The appropriate amounts of salt and Al_2O_3 were weighed and ball-milled thoroughly in an acetone medium.

(ii) The mixture so obtained was heated above the melting point of the salt (method-II) in a porcelain crucible to promote the bonding of the two phases. In the case of method-I, however, this step is left out.

(iii) The fused solid chunk was thoroughly ground in a pestle and mortar to distribute the particles more homogeneously.

(iv) The fine powder was pelletized in a 9mm diameter steel die at a pressure of 5 to 6 ton/cm^2.

(v) The pellets were generally sintered at a temperature 50^{o}C below the melting point of the salt, before being used for any measurements.

(vi) The sintered pellets were electroded with platinum paint followed by curing at 160^{o}C for 1 h.

3.2.2 Solution casting method :

This method comprises the following steps :

(i) The salt (matrix) is first ionized in distilled water.

(ii) An appropriate amount of Al_2O_3 is added in the solution containing the ionized salt.

(iii) This solution is magnetically stirred and simultaneously evaporated by heating.

(iv) The solid chunk so obtained is processed as in case of the conventional method involving the steps from (iii) to (vi) described in the preceding section.

3.3 Furnace and Temperature Controller :

An electrical resistance heating furnace comprising of a mullite tube (dia. ~ 1.5') over which Kanthal wire of 22 gauge was wound inductively and uniformly has been used. The resistance of heating element was ~ 43 Ω. A high temperature cement was applied over the Kanthal windings to fix them in place. The mullite tube with cemented Kanthal wiring was enveloped with a cylindrical stainless steel container, and the space between the two shells was filled with MgO powder to minimize the heat loss. The two (top and bottom) ends were covered by fixing circular asbestos followed by steel plates.

A PID type temperature controller (Indotherm, Model 401D) and a chromel-alumel thermocouple were used to control and measure the furnace temperature respectively. The temperature was controlled to within $\pm 1^{\circ}C$.

3.4 Sample holder :

A versatile sample holder which can be used for electrical conductivity measurements up to $700^{\circ}C$ has been employed in the present work. Figure 3.1 shows the schematic diagram of the sample holder. It consists of three identical lava discs (dia.~ 2.5 cm and thickness 1 ~ cm), each having a central hole and four symmetrically located holes near the periphery. A pair of stainless steel rods are passed through the two diametrically opposite holes to provide support to the sample holder. The spring which is so located that it remains outside the furnace, applies

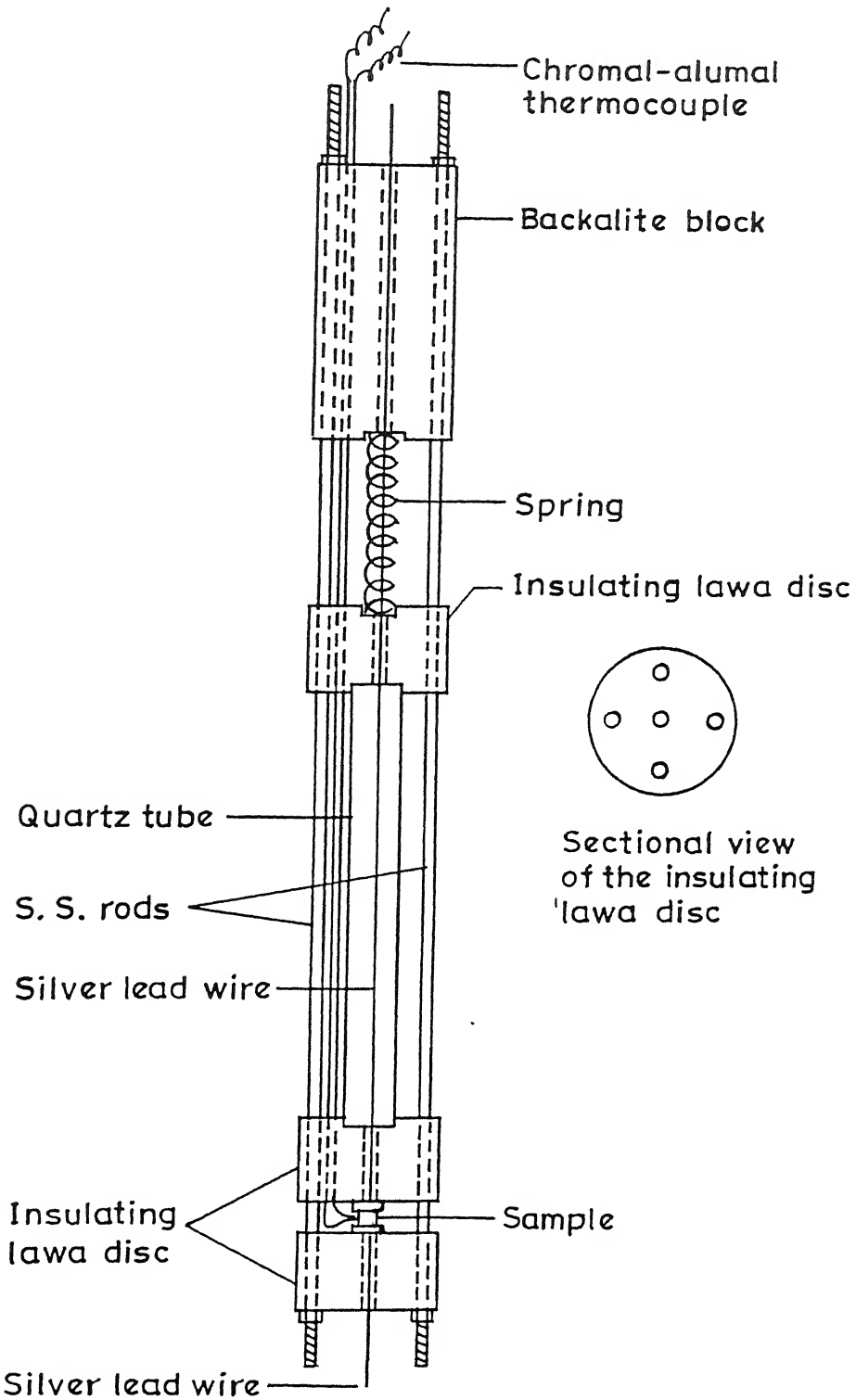

Fig. 3.1 Sample holder for electrical conductivity measurement.

uniform pressure due to spring action to ensure a firm contact between the electrodes and the sample. A quartz tube is used to provide the body to the sample holder. Thin stainless steel foils (dia. ~ 11 mm, thickness ~ 1 mm) were spot-welded with silver wires between which the platinum coated samples were sandwiched for conductivity measurements.

3.5 Impedance Analyzer :

Fig.3.2a shows the set-up for conductivity measurements used in this work. HP 4192A Low Frequency Impedance Analyzer along with HP 16047A test fixture has been employed for the complex impedance (modulus z and phase angle θ) measurements. The equipment is an auto balancing bridge with test signal level from 5 mV to 1.1 V with 1 mV resolution. It has a built-in frequency synthesizer which has frequency range 5 Hz to 13 M Hz with 1 m Hz frequency resolution. There are two display sections, namely Display A and Display B, which provide direct readout of the selected measurement parameters.

The impedance measurements were carried out generally in the cooling cycle at a temperature interval of around 25^{o}C. Sufficient time (about 1 h) was allowed at each temperature for thermal equilibration and reproducibility of the data.

Fig. 3.2b shows the conductivity set-up (Fig.3.2a), and the block diagram of the impedance measurement set-up (Fig.3.2b). The dc resistance of the samples were obtained from the complex

(a)

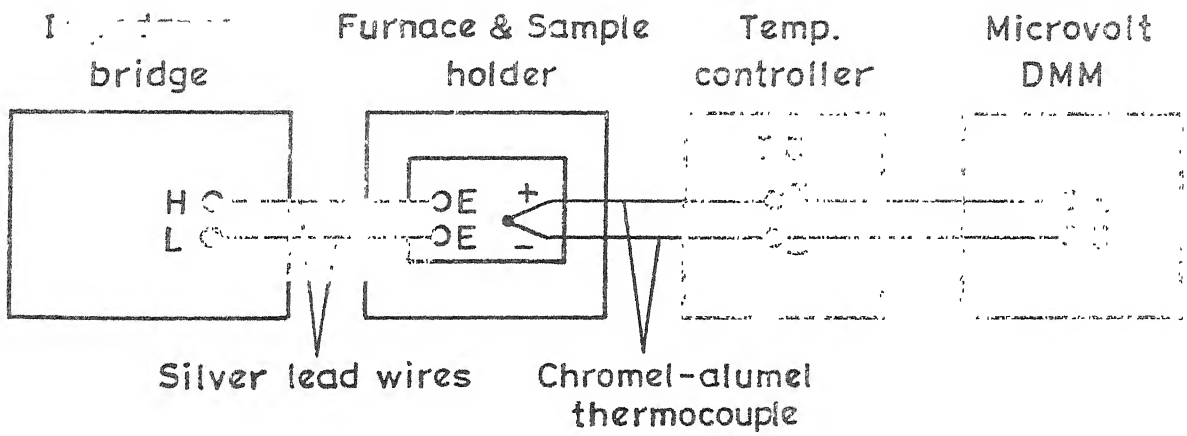

(b)

Fig. 3.2 (a) Experimental set-up and, (b) block diagram for conductivity measurements.

impedance analysis. The electrical conductivity was subsequently obtained from :

$$\sigma = (1/R_{dc})L/A \qquad (3.1)$$

where L is the thickness and A is the area of cross section of the pellet.

3.6 Differential Thermal Analysis (DTA) :

The differential thermal analysis involves the heating/cooling of the test sample at a constant rate alongwith a reference sample which does not undergo any phase transformation in the temperature range of investigation. Any phase change or chemical reaction accompanied by absorption or evolution of heat can be readily detected by DTA. The phase transformation temperature can be determined by this method and hence the presence or absence of the phase can be known.

In order to confirm that Al_2O_3 does not form any solid solution or a new phase with the matrix material, almost all the samples have been investigated by DTA. A mini DTA equipment (Linseis L62, Fig.3.3) has been employed to carry out the DTA measurements. The equipment employs a helics-shaped SiC heating element of very small heat capacity which permits a fast and efficient heating/cooling rate over a wide temperature range (room temperature to 1500^{o}C). Pt/Pt-13% Rh thermocouple was used to measure the temperatures of the test (T_{test}) and the reference

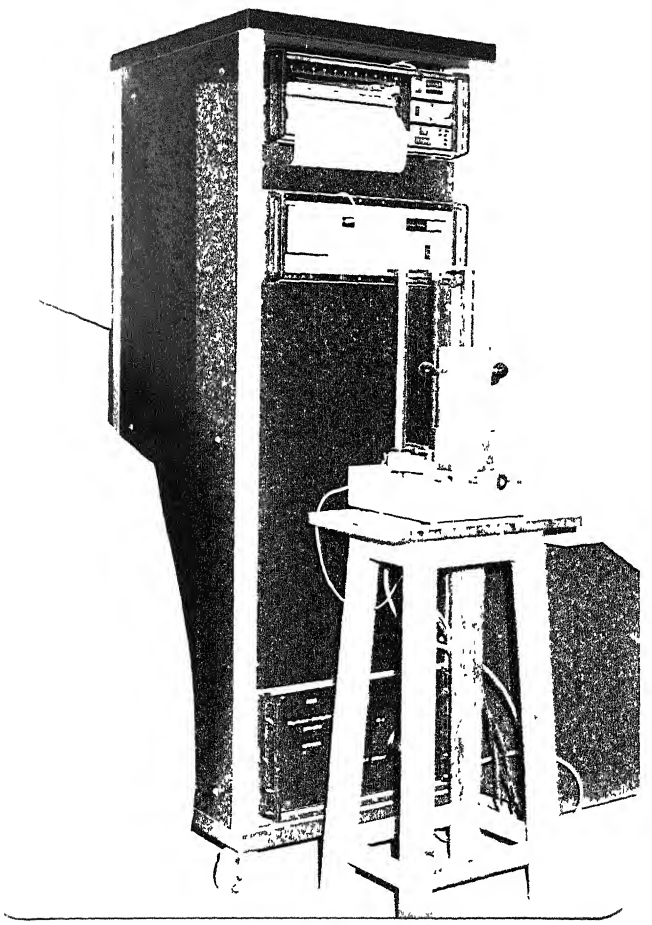

Fig. 3.3 Differential Thermal Analyzer set-up (Linseis model L62).

(T_{ref}) samples. Al_2O_3 powder was invariably used as the reference material. A heating/cooling rate of has been kept ~ 5^oC per minute was generally employed un this work.

3.7 X-ray Diffraction (XRD) :

The X-ray diffraction patterns give the information about the constituent phases present in the test sample and the formation of compound, if any, as a result of reaction between the constituents. X-ray diffraction (XRD) patterns for various composites have been recorded using the Rich-Seifert (Iso-Debyeflex 2002D) counter diffractogram employing a filtered Cu K_α radiation (λ= 1.5418 A^o). The generator was operated at 30 kV and 20 mA, the chart speed was fixed at 1.5 cm/min and the scanning speed was fixed at 1.2 ^{o}/min. in 2θ.

The observed XRD patterns of multiphase mixtures are expected to differ from those of the individual phases present in the mixture due to superposition of lines common to two or more phases. In general, the XRD patterns recorded at room temperature for a composite mixture, without heat-treatment (method-I) and after heating the mixture above the melting point of the matrix (method-II) or to a reasonably high temperature, showed no discernible difference signifying no evidence of any chemical reaction or solid solution formation between Al_2O_3 and the matrix material.

3.8 Scanning electron microscopy (SEM) :

The SEM studies were carried out using Jeol model *JSM-840A*, scanning electron microscope to examine the size and the distribution pattern of Al_2O_3 particles in the matrix material. The equipment has a range of magnification from 10x to 300000x. The surface of each sample was polished on very fine emery paper and cleaned with acetone. Each specimen was gold/silver coated using a sputtering unit (International Scientific Instruments PS-2 coating unit) before taking the micrographs. The micrographs were taken at 10^{-11}A probe current and 15 kV accelerating voltage. The magnification was fixed according to the need from 5000x to 7500x.

CHAPTER 4

PbX_2 - Al_2O_3 (X = Cl, Br, I) SYSTEMS

The dispersion of fine insulating particles such as Al_2O_3, SiO_2 etc. (heterogeneous doping) is a well known method to enhance the ionic conductivity of normal cationic conductors such as alkali, silver and copper halides (Liang, 1973; Jow and Wagner, 1979; Shahi and Wagner, 1981; Maier,1984,1985,1986) and of anionic conductors such as CaF_2, BaF_2, $SrCl_2$ and HgI_2 (Fijitsu et.al, 1985, 1986; Pack, 1979; Vaidehi et.al., 1986). However, Brune and Wagner (1987) reported a lowering of conductivity in $PbCl_2$ containing dispersion of Al_2O_3 particles. This result is in stark *contrast* to the reported results on most composite solid electrolyte systems where enhancement in conductivity is generally observed. The aim of this part of study is to (i) investigate the lead halide-alumina (PbX_2-Al_2O_3; X = Cl, Br, I) systems systematically and (ii) examine if the data on these anomalous systems lead to any new insight into the mechanism of enhanced ionic conduction.

PbX_2-Al_2O_3 (X = Cl, Br, I) composite systems of various compositions have been prepared in two slightly different ways as described in Chapter 3 (Section 3.2.1). In the first case, the appropriate amounts of the constituents are mixed, milled and ground followed by pelletization (method-I). In the second method the mixture obtained after regrinding was heated above the respective melting point of the lead salt before pelletization to

ensure a homogeneous dispersion of Al_2O_3 particles in the matrix phase (method -II). The pressed pellets of $PbCl_2$-Al_2O_3 are sintered at 450°C, $PbBr_2$-Al_2O_3 at 300°C and PbI_2-Al_2O_3 at 320°C for ~ 20-24 hrs.

Most of the composite samples have been investigated by XRD and DTA for phase characterization and to find out the solubility (if any) of Al_2O_3 in the matrix phase, and also by SEM to examine the distribution of Al_2O_3 particles in the matrix phase. The dc electrical conductivity of various samples has been obtained at each temperature from the complex impedance analysis described in Chapter 2 (section 2.1). The resistance obtained from the high frequency semicircular portion of the complex spectra has been used to calculate the dc conductivity of each sample. The results of various studies on $PbCl_2$-Al_2O_3 are presented below followed, by those on $PbBr_2$-Al_2O_3 and PbI_2-Al_2O_3 systems.

4.1 $PbCl_2$ - Al_2O_3 System :

4.1.1 Differential Thermal Analysis :

The DTA results for pure $PbCl_2$ and $PbCl_2$-30 m/o Al_2O_3 samples prepared by methods I and II are shown in Fig.4.1. In each case only one endothermic peak corresponding to the melting of $PbCl_2$ is observed leading to the obvious conclusion that Al_2O_3 remains as a separate phase in $PbCl_2$ - Al_2O_3 composites prepared by both the methods and that no chemical reaction takes place between the two components. The decreased peak-heights and peak-areas for $PbCl_2$-30 m/o Al_2O_3 composites (curves b and c in

Fig. 4.1) are merely due to lower concentration of $PbCl_2$ in the composites compared to the pure salt (curve a).

4.1.2 X - ray Diffraction :

Fig.4.2 shows the XRD patterns for $PbCl_2$-30 m/o Al_2O_3 composites prepared by the methods I and II. These results show that the heat treatment (method II; curve b) does not affect the X-ray diffraction patterns which signifies that no chemical reaction or solid solution formation takes place between $PbCl_2$ and Al_2O_3 even after the heat treatment. However, since the XRD patterns were recorded at room temperature, it is possible that some new phase or solid solution formation occurs at higher temperature but at room temperature the two parent phases (viz., $PbCl_2$ and Al_2O_3) separate out. This possibility is, however, ruled out by the DTA studies reported above.

4.1.3 Scanning Electron Microscopy :

Figs.4.3a and 4.3b are the SEM micrographs of well polished samples of polycrystalline $PbCl_2$ and $PbCl_2$-30 m/o Al_2O_3 respectively. The samples were presintered at 450°C for ~ 20 hrs. It is observed (Fig.4.3b) that Al_2O_3 particles are dispersed in $PbCl_2$ grains. Thus Al_2O_3 remains as a separate phase and the $PbCl_2$-Al_2O_3 system forms a two-phase composite.

4.1.4 Conductivity versus Composition :

The conductivity isotherms for $PbCl_2$-Al_2O_3 composites at three different temperatures, viz. 100, 200 and 300°C, are shown in Fig. 4.4. It is found that as the concentration of Al_2O_3

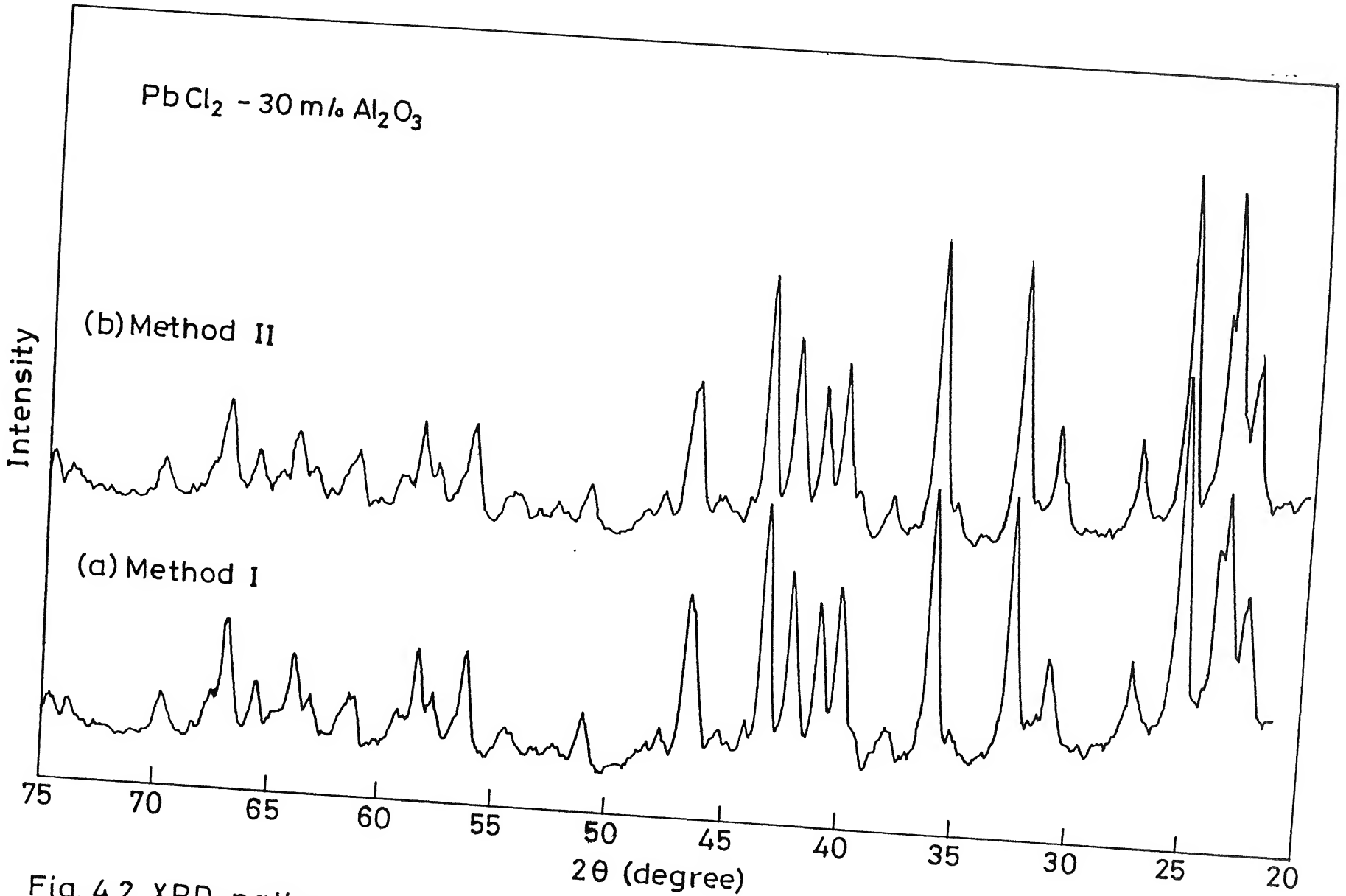

Fig. 4.2 XRD patterns for $PbCl_2$ - 30 m/o Al_2O_3 samples prepared by method I & II.

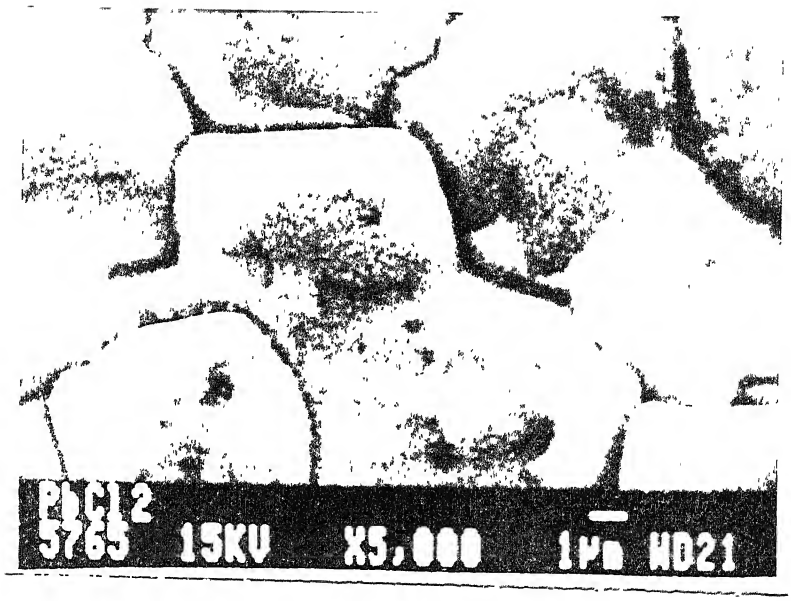

(a)

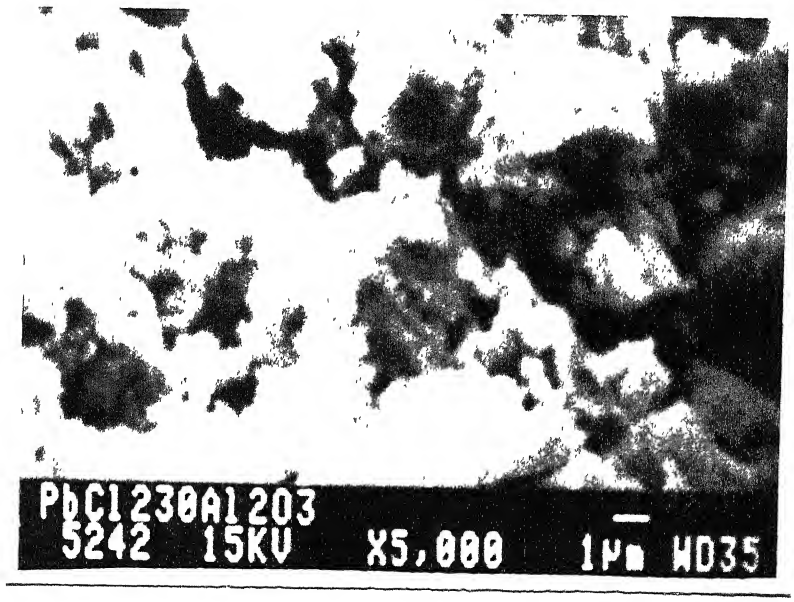

(b)

Fig. 4.3 SEM micrographs for (a) $PbCl_2$ and, (b) $PbCl_2$-30 m/o Al_2O_3 composite sintered at 450°C.

increases the conductivity decreases monotonically. This behavior is in *stark contrast* to most of the reported results on composite solid electrolytes which show substantial enhancement in the conductivity instead. It appears that in $PbCl_2$-Al_2O_3 composites a high-conducting layer does not form and the addition of an insulator results in dilution of the conductivity. Table 4.1 compares the normalized conductivity, the ratio of conductivity of the composite to that of pure salt (σ/σ_o),for the $PbCl_2$-Al_2O_3 composites at three different temperatures. It is observed that the decrease in the conductivity is higher at lower temperatures.

Table 4.1

Normalized conductivity (σ/σ_o) for $PbCl_2$-Al_2O_3 composites of various compositions at three different temperatures

composition (Al_2O_3)*		σ/σ_o		
(m/o)	(v/o)	300°C	200°C	100°C
0	0	1	1	1
10	6	0.63	0.41	0.22
20	12	0.40	0.17	0.05
30	19	0.16	0.05	7.2×10^{-3}

*The particle size of Al_2O_3 used in this work is *0.05 μm* unless otherwise specified.

$PbCl_2$ is known to be an anionic conductor (Tubandt, 1921, 1923). However, unlike PbF_2, it exhibits Schottky disorder owing to the larger size of chloride ions (Simkovich, 1963; De Vries and Van Santen,1963; Hoshino et.al.,1969) and the narrow free space around interstitial sites (Braekken, 1932). The cation and anion

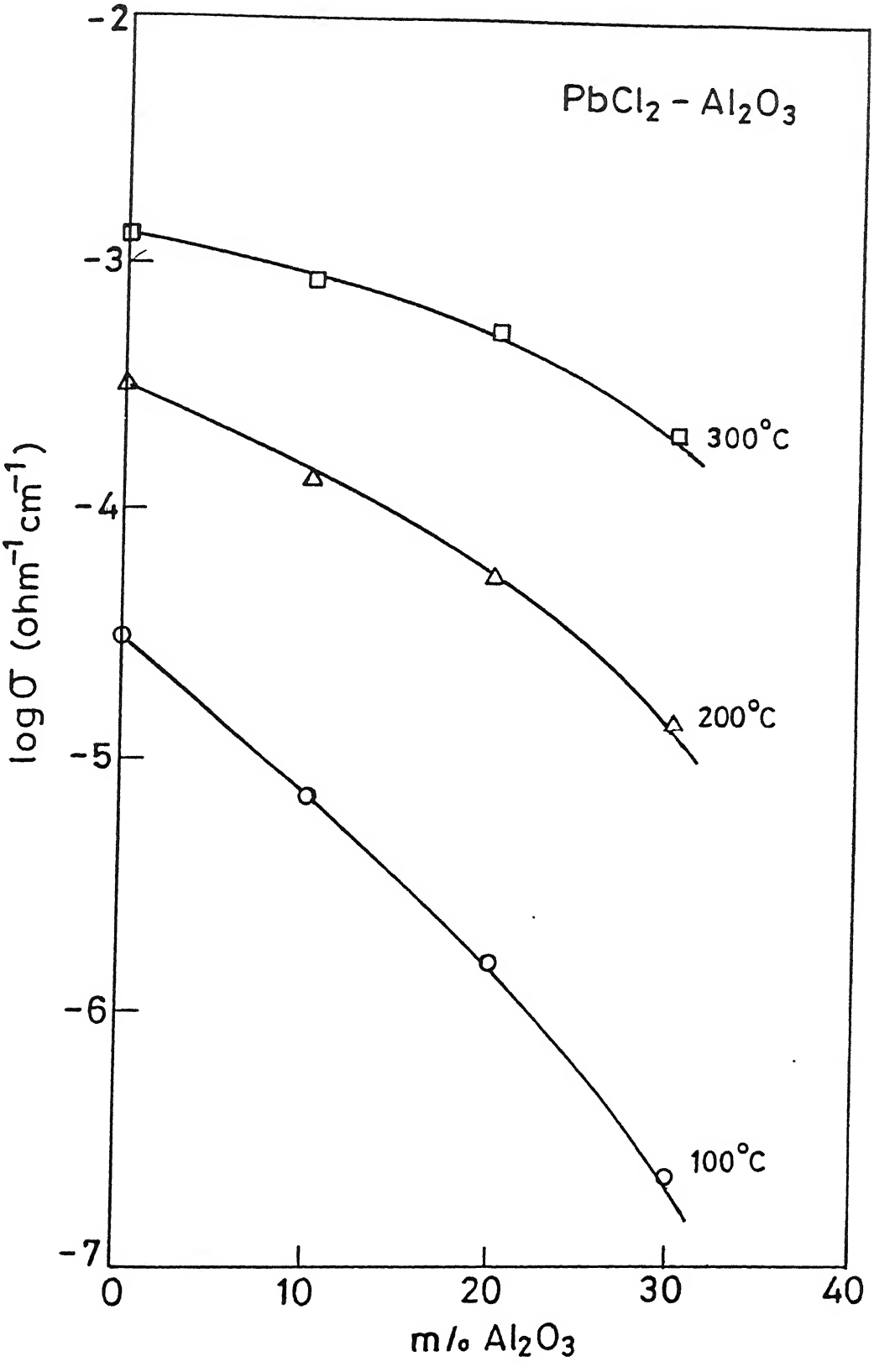

Fig. 4.4 log (σ) vs composition (m/o of Al_2O_3) for $PbCl_2 - Al_2O_3$ composites at three different temperatures.

vacancies (V''_{Pb} and $V^{\cdot}_{Cl}$) are formed according to the equation :

$$O \Leftrightarrow V''_{Pb} + 2V^{\cdot}_{Cl} \Leftrightarrow (V_{Pb}V_{Cl})' + V^{\cdot}_{Cl} \qquad (4.1)$$

One may be tempted to explain the observed decrease in the conductivity due to trace amounts of dissolved Al_2O_3 in the host matrix $PbCl_2$, as it is well established that the conductivity of ionic solids doped with *suitable* aliovalent impurities first decreases before increasing as the dopant concentration increases (Teltow, 1950; Lidiard, 1957; Friauf, 1972). The dissolution of Al_2O_3 in $PbCl_2$, using Kröger-Vink notation, may be described by the following relation :

$$Al_2O_3 \Leftrightarrow 2Al^{\cdot}_{Pb} + V^{\cdot}_{Cl} + 3O'_{Cl} \qquad (4.2)$$

Thus one molecule of dissolved Al_2O_3 produces one excess chloride ion vacancy which is also the *more mobile* charge carrier. Hence the conductivity should have increased due to addition of Al_2O_3, it decreases instead. The decrease in the conductivity could have occurred as a result of chemical reaction between the constituents and formation of a new compound with a lower conductivity. However, both DTA and XRD results rule out the formation of any new intermediate compound.

It would be appropriate to interpret the observed effect of dispersion of Al_2O_3 in $PbCl_2$ in terms of interaction between the nucleophilic groups on the dispersoid (Maier, 1984) and the anion vacancies which cause a depletion in the concentration of majority

charge carriers. When Al_2O_3 is added, the positively charged species (lead ions) are attracted towards the alumina surface. Brune and Wagner (1987) expected the dominant transport to change to via the negatively charged cation vacancies V''_{Pb}. However, the mobility ratio, μ_{Pb}/μ_{Cl}, in $PbCl_2$ at 200°C is 4.18×10^{-5} (Schwab and Eulitz, 1967), i.e. the mobility of negatively charged lead ion vacancies V''_{Pb} is too low to allow the cation vacancies to become the dominant ionic current carriers in the composite. Thus it would appear that in $PbCl_2$-Al_2O_3 composites Pb^{2+} ions are attracted towards the dispersoid resulting in an increased concentration of cation vacancies V''_{Pb} in the space charge layer which are relatively immobile. As the product of concentrations of cation and anion vacancies is fixed at a constant temperature by Schottky constant (Friauf, 1972), the concentration of Cl^- ion vacancies decreases resulting in decreased conductivity in the composites.

4.1.5 Conductivity versus Temperature :

Fig. 4.5 shows the $\log\sigma$ vs $10^3/T$ plots for pure $PbCl_2$ and various $PbCl_2$-Al_2O_3 composites. It is observed that the conductivity of $PbCl_2$-Al_2O_3 composite decreases monotonically as the concentration of Al_2O_3 increases, and that the processing has little effect on the conductivity as the results for $PbCl_2$-30 m/o Al_2O_3 composites prepared by both methods (I and II) are similar. Table 4.2a compares the ionic transport parameters, viz., the overall activation energy E_a and the preexponential factor σ_o for pure $PbCl_2$ reported by different investigators. The E_a value found in this work agrees, within the experimental error, with those

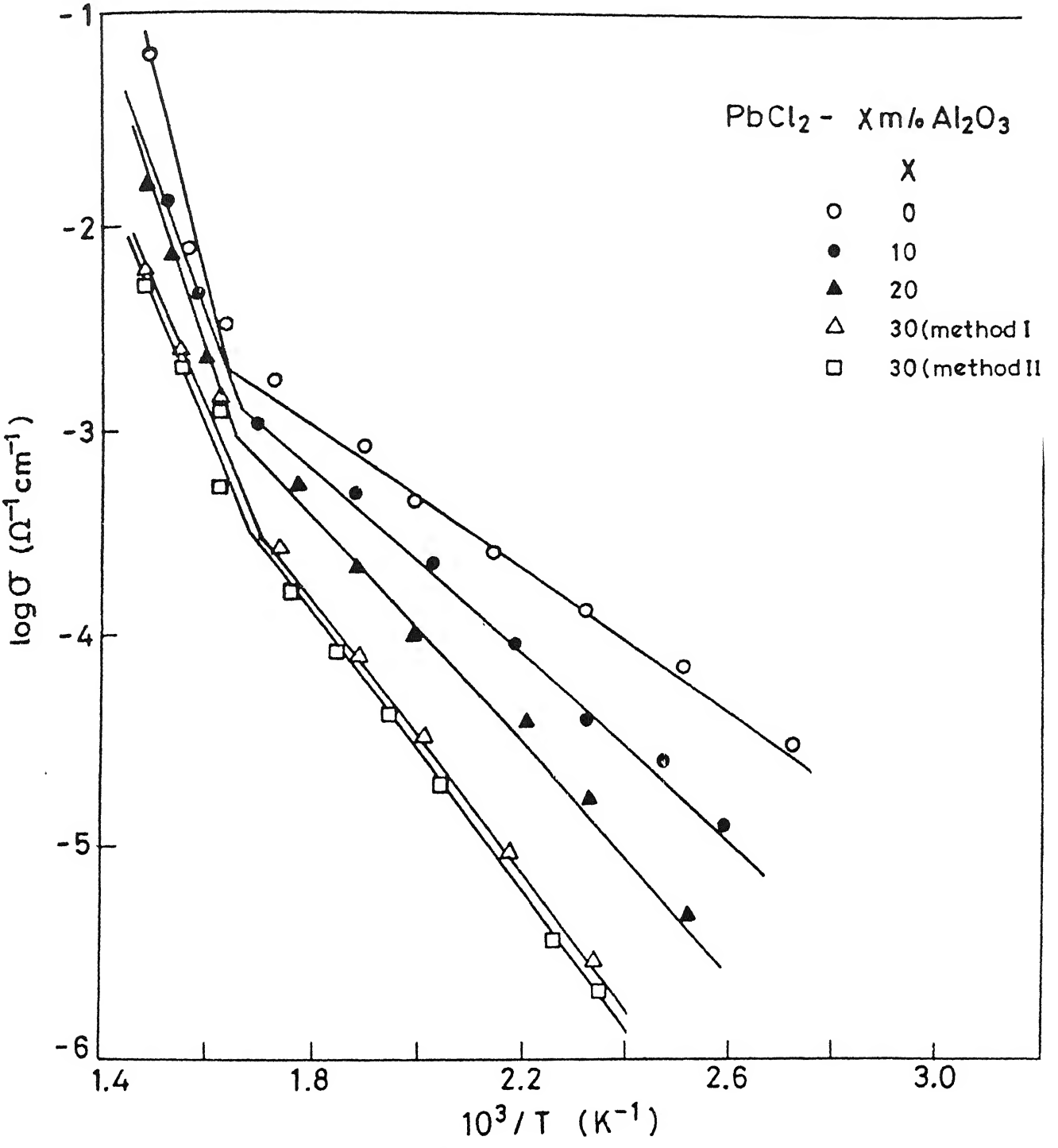

Fig. 4.5 log(σ) vs $10^3/T$ for various $PbCl_2$-Al_2O_3 composites

reported by a majority of investigators.

Table 4.2(a)

Ionic transport parameters, the activation energy (E_a) and the preexponential factor (σ_o) in $PbCl_2$

E_a(eV)	σ_o(ohm cm)$^{-1}$	reference
0.34	1.3	This work
0.39	-	Gyuali (1931)
0.40	8.7	Simkovich (1963)
0.30	-	De-Vries and Van Santen (1963)
0.22	-	Toshima et.al.(1968)
0.20	-	Hoshino et.al.(1969)
0.35	-	Van Den Brom et.al. (1972)
0.33	-	Pansare and Patankar (1974)
0.30	-	Melo et.al.(1979)
0.32	1.7	Oberschmidt and Lazarus (1980)

The ionic transport parameters E_a and σ_o for various $PbCl_2$-Al_2O_3 composites are listed in Table 4.2b. It is noticed that the E_a value increases systematically as the concentration of the dispersed phase (Al_2O_3) increases in the composite material. It would appear that with increasing Al_2O_3 content in $PbCl_2$, the concentration of lead ion vacancies increases which have a higher activation energy.

Table 4.2(b)

Ionic transport parameters, the activation energy (E_a) and the preexponential factor (σ_o), for various $PbCl_2$-Al_2O_3 composites in the temperature range 100-300°C

composition (Al_2O_3) (m/o)	(Al_2O_3) (v/o)	E_a(eV)	σ_o(ohm-cm)$^{-1}$
0	0	0.34	1.3
10	6	0.43	6.3
20	12	0.54	31
30 (method-I)	19	0.63	70
30 (method-II)	19	0.64	79

4.2 $PbBr_2$ - Al_2O_3 System :

4.2.1 Differential Thermal Analysis :

Fig.4.6 shows the DTA curves for $PbBr_2$ (curve a) and $PbBr_2$-30 m/o Al_2O_3 composite system (curve b). Both samples are found to exhibit one and only one thermal event at about the same temperature which corresponds to the melting temperature of the host matrix ($PbCl_2$). These results suggest that no chemical reaction or solid solution formation takes place between the two constituents and that the $PbBr_2$ and Al_2O_3 remain as separate phases in the composite.

4.2.2 X-ray Diffraction :

Fig.4.7 shows the XRD patterns at room temperature for $PbBr_2$-30 m/o Al_2O_3 with (Fig.4.7a) and without (Fig.4.7b) heat-treatment of the mixture at 300°C. The observed XRD peaks in

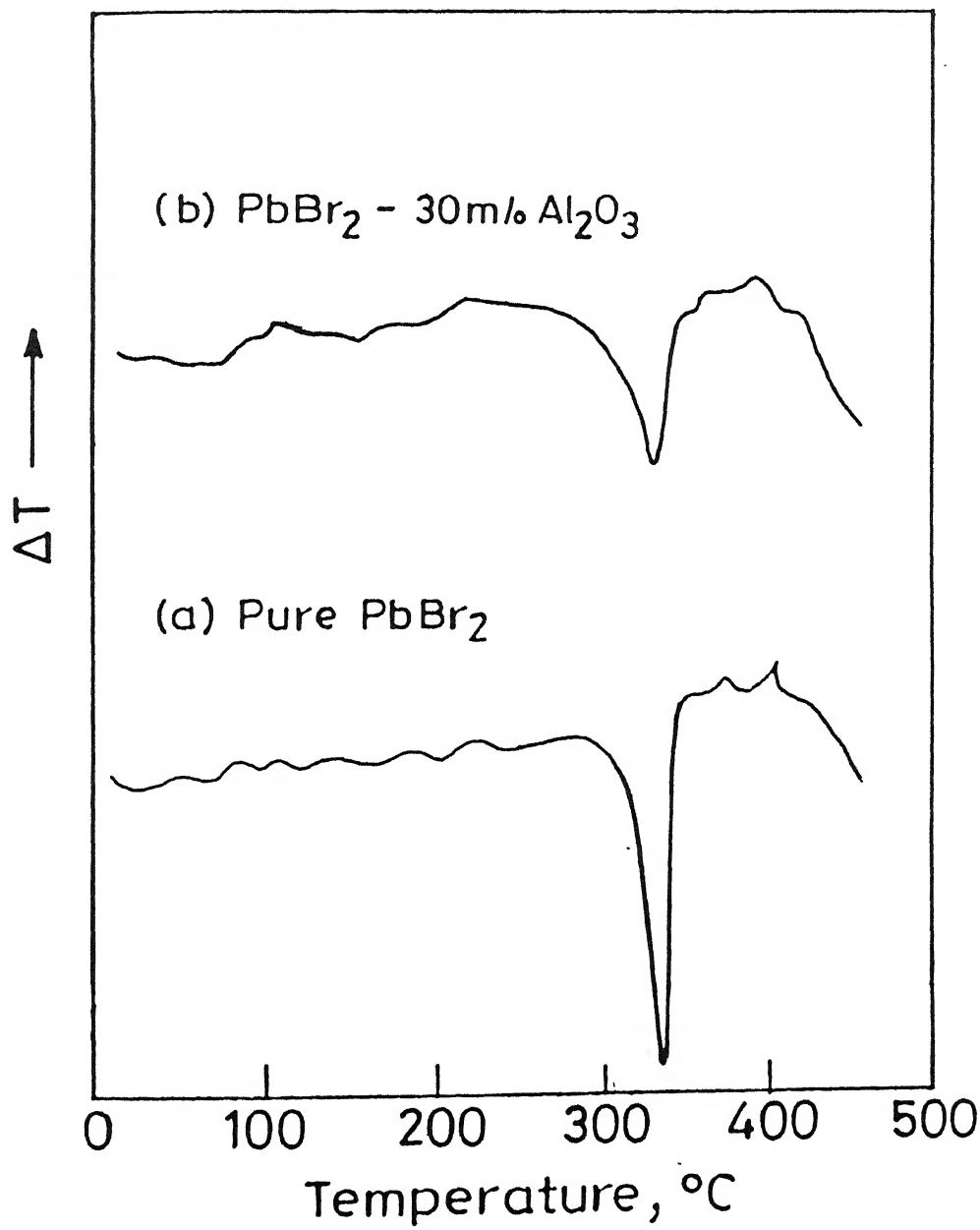

Fig. 4.6 DTA curves for $PbBr_2$ (a), and $PbBr_2$ - 30m/o Al_2O_3 composite (b).

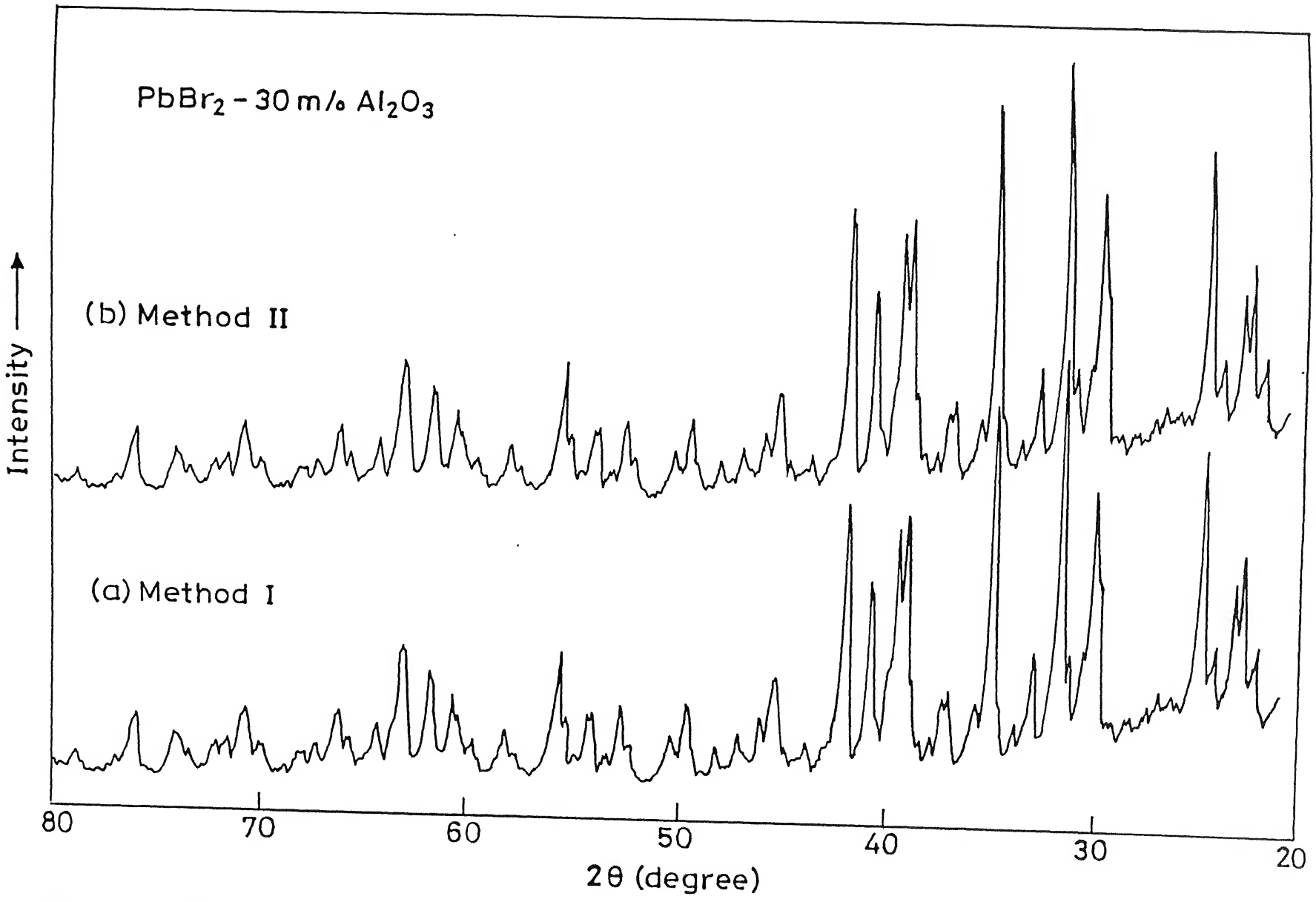

Fig. 4.7 XRD patterns for $PbBr_2$ - 30 m/o Al_2O_3 samples prepared by method I and method II.

the two cases (curves a and b) are almost identical, and could either be attributed to $PbBr_2$ or to Al_2O_3. Thus the combined DTA and XRD results rule out the possibility of any chemical reaction or formation of any new phase between the two constituents.

4.2.3 Scanning Electron Microscopy :

Fig.4.8 shows the scanning electron micrographs for polycrystalline $PbBr_2$ and $PbBr_2$-30 m/o Al_2O_3 samples sintered at 300°C. Fig.4.8b shows a two phase microstructure of Al_2O_3 and $PbBr_2$. These results therefore suggest that $PbBr_2$-Al_2O_3 system is a composite wherein Al_2O_3 particles are dispersed in $PbBr_2$ grains.

4.2.4 Conductivity versus Composition :

The variation of conductivity as a function of concentration (m/o) of Al_2O_3 in $PbBr_2$ at 100, 150 and 200°C, is shown in Fig.4.9. Table 4.3 compares the normalized conductivity, σ(composite)/σ_o(host) of $PbBr_2$-Al_2O_3 composites at the three temperatures. It is observed that the conductivity decreases monotonically as the concentration of Al_2O_3 in $PbBr_2$ increases and that the rate of decrease in the conductivity is faster at lower temperatures.

Like $PbCl_2$, $PbBr_2$ is a predominantly anionic conductor (Tubandt and Eggert, 1920). It exhibits Schottky disorder and the cation and anion vacancies are formed according to the following equation (Schoonman and Verwey, 1968):

$$0 \Leftrightarrow V''_{Pb} + 2V^{\cdot}_{Br} \qquad (4.3)$$

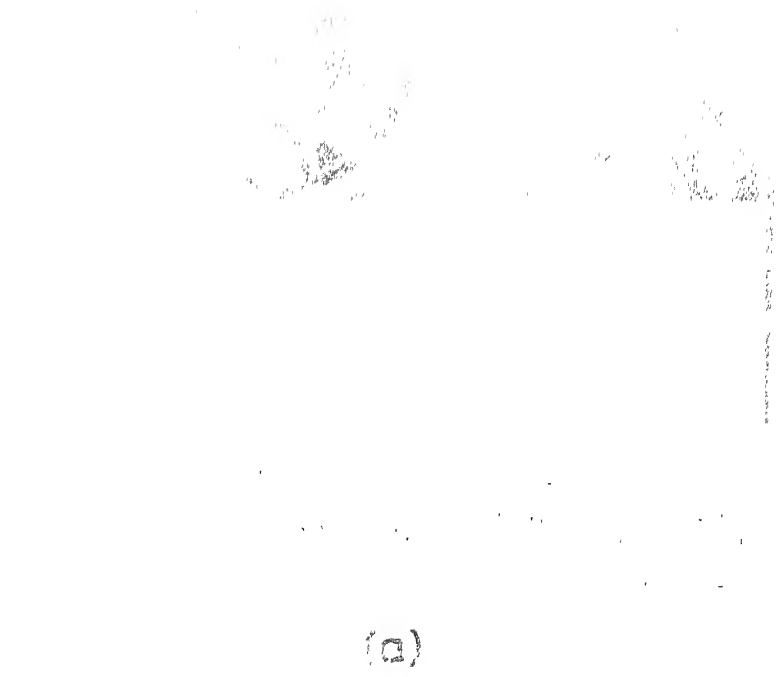

(a)

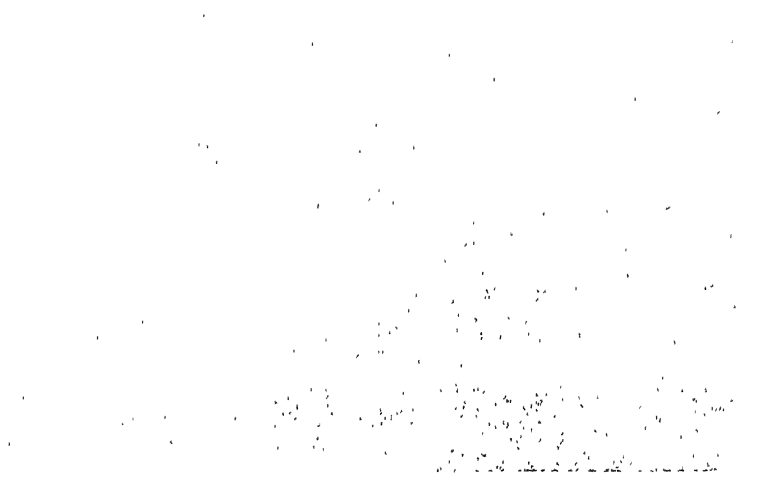

(b)

Fig. 4.8 SEM micrographs for (a) $PbBr_2$ and (b) $PbBr_2$ - 30 m/o Al_2O_3 composite sintered at 350°C.

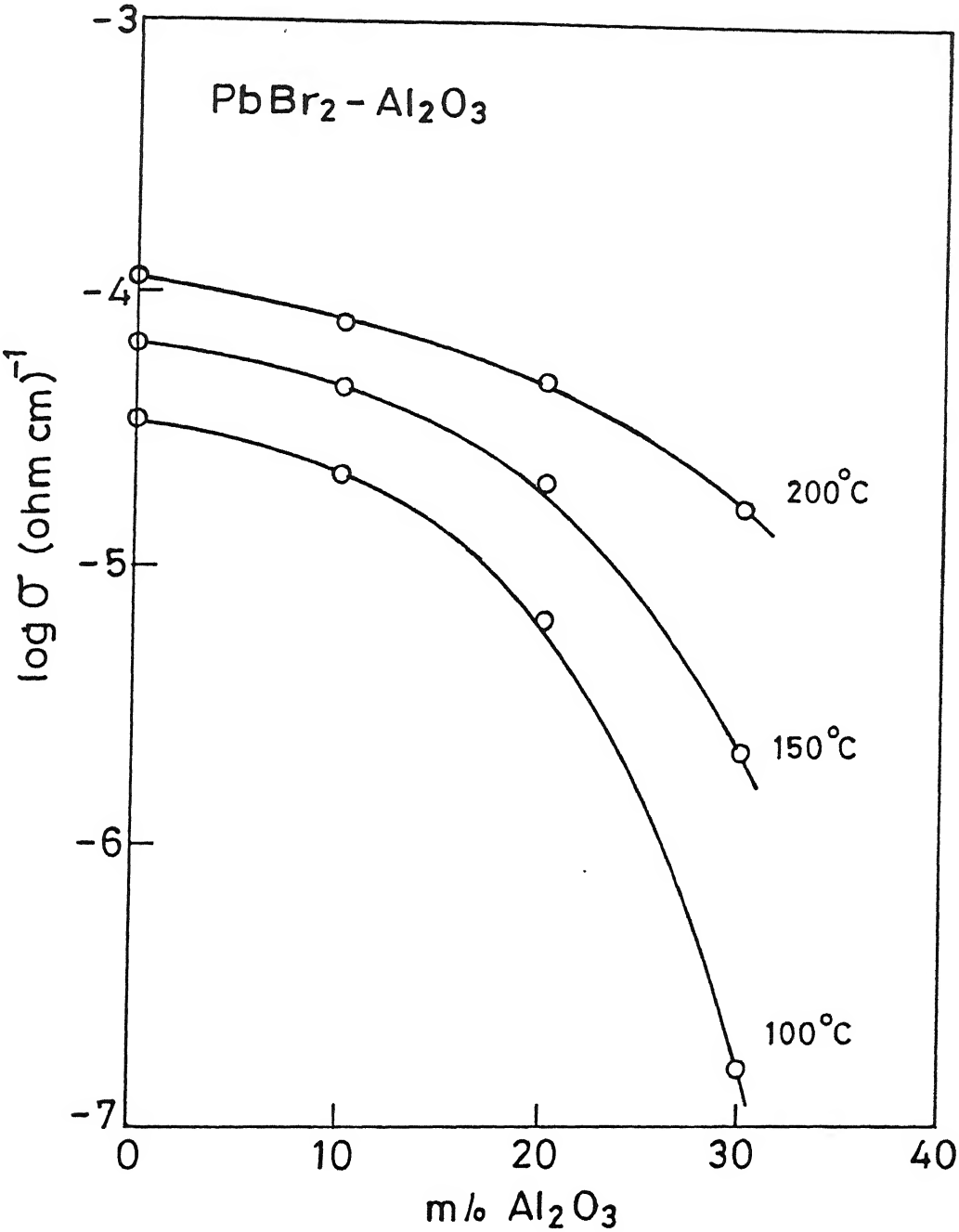

Fig. 4.9 Conductivity vs composition (m/o of Al_2O_3) for $PbBr_2$-Al_2O_3 system at three different temperatures.

The classical doping mechanism can be ruled out as a factor responsible for the decrease in the σ of $PbBr_2$-Al_2O_3 composites, on a similar basis as for $PbCl_2$-Al_2O_3 system.

The decrease in the conductivity of $PbBr_2$ due to dispersion of Al_2O_3 can be explained, as in case of $PbCl_2$-Al_2O_3, if we assume that the positively charged lead ions are attracted towards the nucleophilic groups at the alumina surface and thereby cause an

Table 4.3

Normalized conductivity (σ/σ_o) for various $PbBr_2$-Al_2O_3 composites at three different temperatures

composition (Al_2O_3) (m/o)	(v/o)	σ/σ_o 200°C	150°C	100°C
0	0	1	1	1
10	5	0.72	0.69	0.63
20	10	0.44	0.32	0.19
30	17	0.15	3.3×10^{-2}	4.8×10^{-3}

increased concentration of lead ion vacancies, and hence a decreased concentration of bromide ion vacancies in the space charge layer. However, the lead ion vacancies are far less mobile ($\mu_{Pb}/\mu_{Br} \simeq 10^{-6}$ at 200°C) to become the dominant ionic charge carriers in $PbBr_2$-Al_2O_3 composites. Therefore the space charge regions around the Al_2O_3 particles do not control the electrical conductivity of $PbBr_2$-Al_2O_3 composites and Al_2O_3 dispersion results in the dilution of conductivity in the composites.

4.2.5 Conductivity versus Temperature :

Fig.4.10 shows the logσ versus $10^3/T$ plots for $PbBr_2$ and $PbBr_2$ containing dispersions of 10, 20 and 30 m/o Al_2O_3. These results reveal that the dispersion of Al_2O_3 results in a decreased conductivity over that of pure $PbBr_2$. Tables 4.4a and 4.4b list the Arrhenius activation energy (E_a) and the preexponential factor (σ_o) for $PbBr_2$and various $PbBr_2$-Al_2O_3 composites respectively. The E_a value for pure $PbBr_2$ obtained in this work is comparable, within the experimental error, with those reported by Schoonman and Verwey (1968) and Hoshino et.al.(1973). Others have reported

Table 4.4(a)

Activation energy (E_a) for conduction in $PbBr_2$

E_a(eV)	reference
0.20	This work
0.28	Smakula(1965)
0.29	Verwey and Schoonman (1967)
0.29	Schoonman and Verwey (1968)
0.25	Van Den Brom et.al. (1972)
0.23	Hoshino et.al.(1973)
0.30	Oberschmidt and Lazarus (1980)

somewhat higher values. As for the $PbBr_2$-Al_2O_3 composite, the E_a value keeps increasing as the concentration of Al_2O_3 in $PbBr_2$ increases, just as in case of $PbCl_2$-Al_2O_3 composite system.

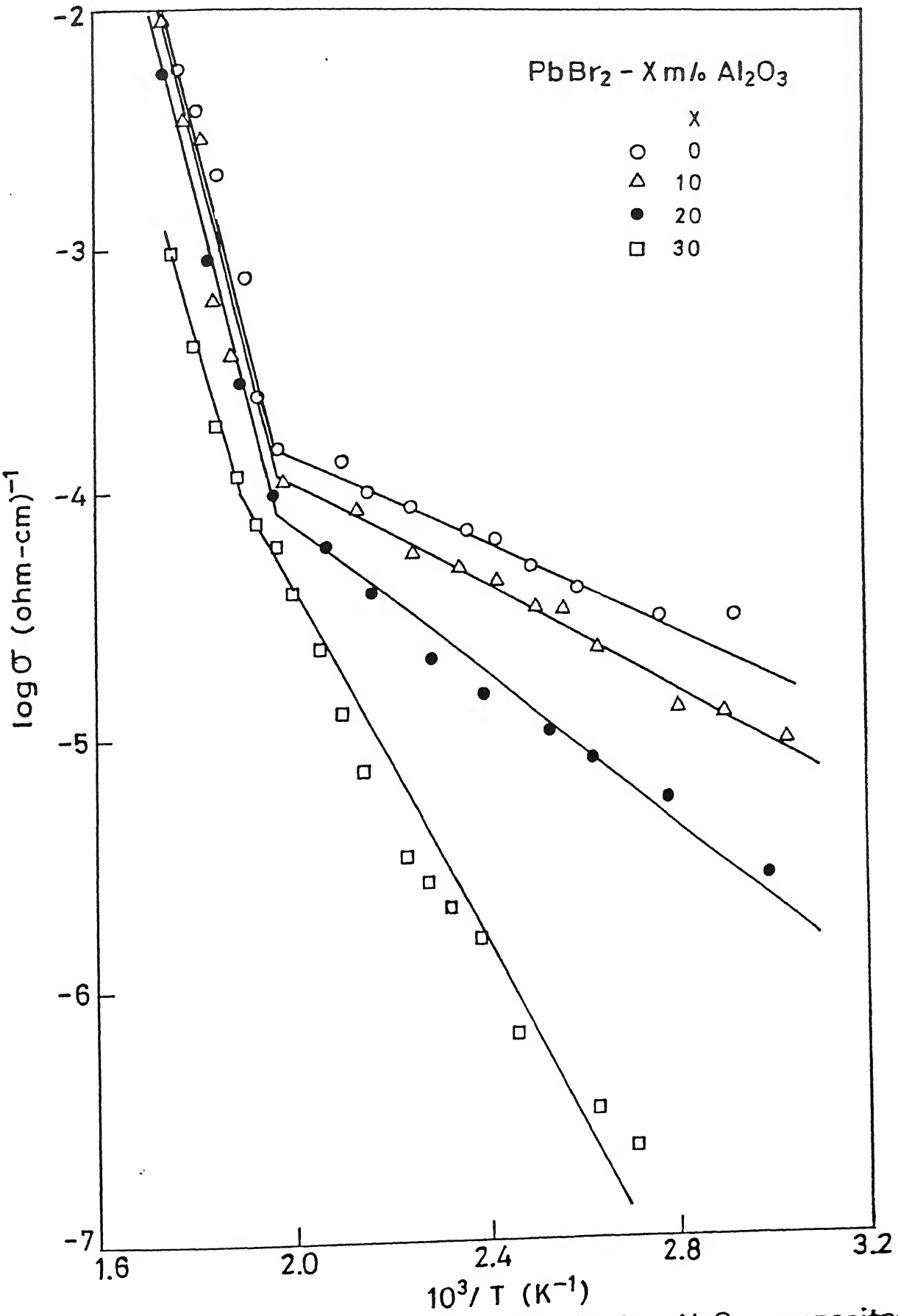

Fig. 4.10 log (σ) vs $10^3/T$ for various $PbBr_2$-Al_2O_3 composites.

Table 4.4(b)

The ionic transport parameters, the activation energy (E_a) and the preexponential factor (σ_o), for various $PbBr_2$-Al_2O_3 composites in the temperature range 100-250°C

composition(Al_2O_3) (m/o)	(v/o)	E_a (eV)	σ_o $(ohm\text{-}cm)^{-1}$
0	0	0.20	8.8×10^{-3}
10	5	0.24	3.3×10^{-2}
20	10	0.30	7.0×10^{-2}
30	17	0.44	2.3×10^{-1}

4.3 PbI_2 - Al_2O_3 System :

4.3.1 Differential Thermal Analysis :

Fig. 4.11 shows the DTA curves for pure PbI_2 and PbI_2-30 m/o Al_2O_3 composites prepared by methods I and II as described in Chapter 3. The lone peak appearing in case of PbI_2 (curve a) is due to the melting of PbI_2. The DTA curve for the PbI_2-30 m/o Al_2O_3 sample (curve b) prepared by method-I also exhibits a peak corresponding to the melting of pure PbI_2 which implies that the PbI_2 in the composite remains as a separate phase at least upto the melting point of PbI_2. However, an additional (though minor) exothermic peak appears at ~ 450°C which may be due to (i) decomposition of PbI_2, (ii) release of adsorbed water molecules on Al_2O_3 surface or (iii) some chemical reaction between the constituents. The DTA curve of the sample prepared by method II does not show any thermal event (peak) in the investigated temperature range, which suggests that PbI_2 is no more there in

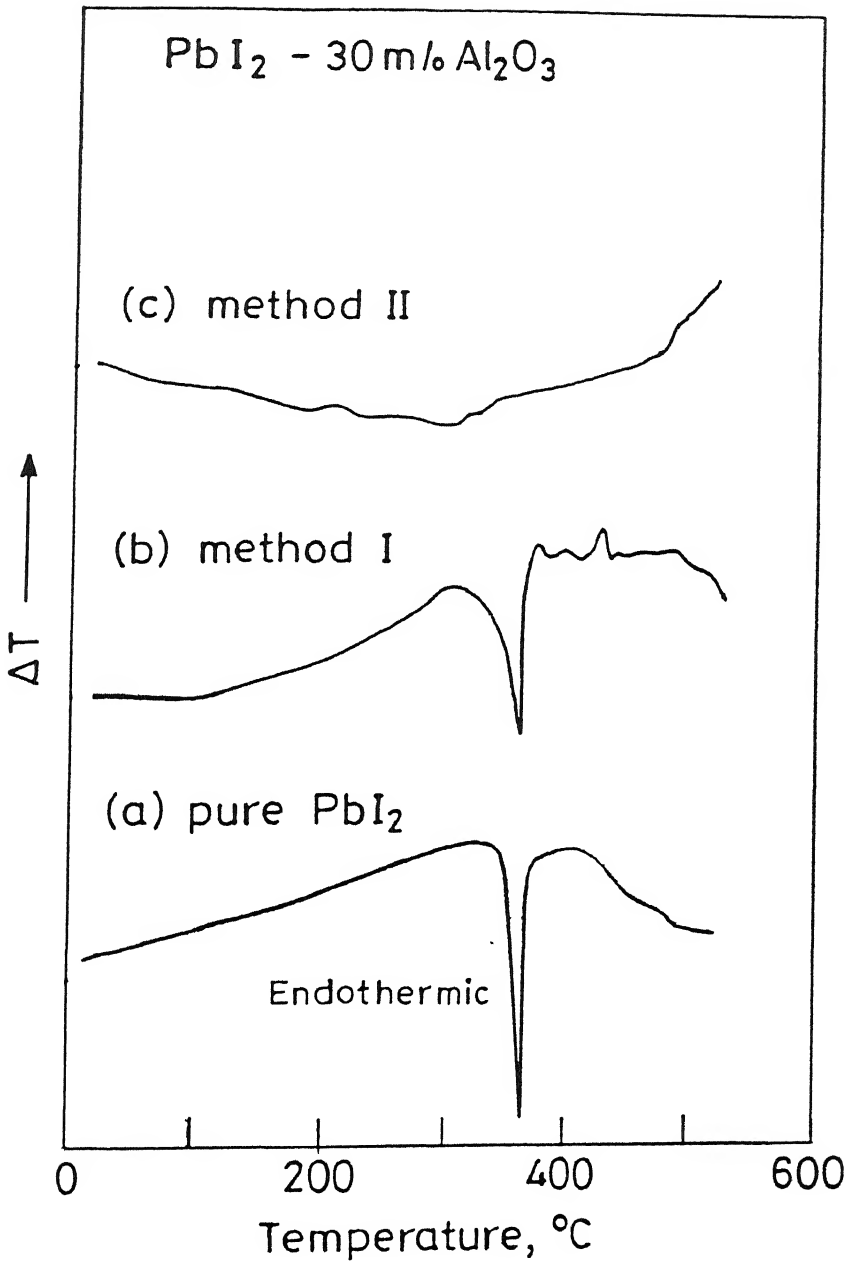

Fig. 4.11 DTA curves for PbI_2 (a), PbI_2 – 30 m/o Al_2O_3 prepared by method I (b), and method II (c).

the composite, and that the sample is a chemically different material. The observed change of color of the sample also suggested that a chemical change takes place in the samples prepared by the method II. It is thus inferred that the samples prepared by the method I are two-phase (PbI_2-Al_2O_3) composites and those prepared by the method II, wherein the constituents are heat-treated above the melting point of PbI_2, are not two-phase composites.

4.3.2 X-ray Diffraction :

Fig.4.12 shows the X-ray diffraction patterns at room temperature for PbI_2-30 m/o Al_2O_3 composites prepared by the methods I and II. The XRD pattern for the sample prepared by the method II (curve b) does not contain even the prominent peaks present in the curve (a). Moreover, it contains several major peaks, which are not at all present in the curve(a). These together with the DTA results clearly suggest that the sample prepared by method II is a chemically different material, and not a two-phase composite of PbI_2 and Al_2O_3.

4.3.3 Scanning Electron Microscopy :

Fig.4.13 shows the SEM micrographs of well polished samples of polycrystalline PbI_2 and PbI_2-30 m/o Al_2O_3 composite prepared by method I. The samples were presintered at 320^{o}C, well below the melting point of PbI_2 (402^{o}C). The microstructure of the composite (Fig.4.13b) shows that the Al_2O_3 particles are well dispersed in the PbI_2 matrix. Thus the samples prepared by the method-I form a two-phase composite.

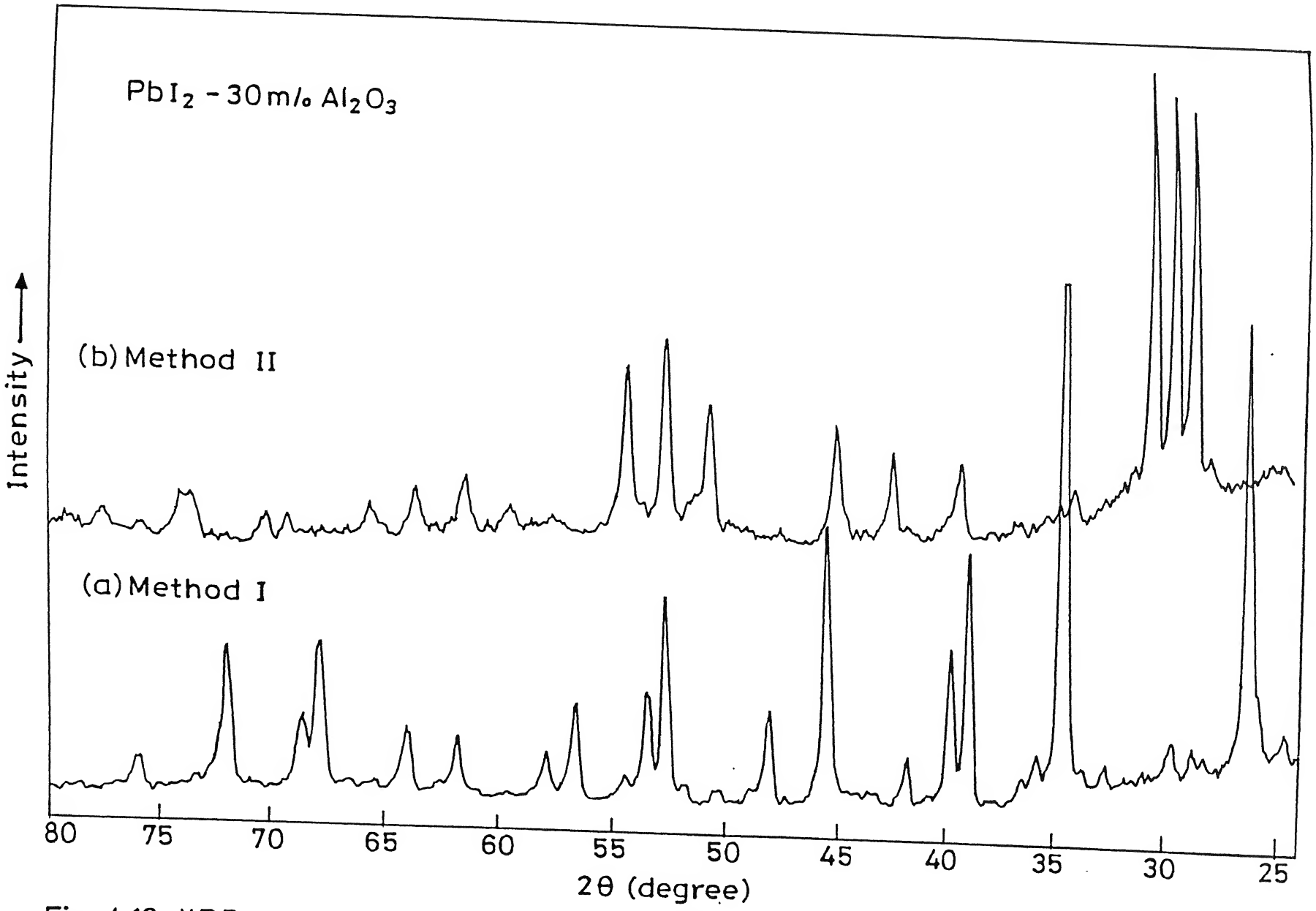

Fig. 4.12 XRD patterns for PbI_2 - 30m/o Al_2O_3 samples prepared by method I & II.

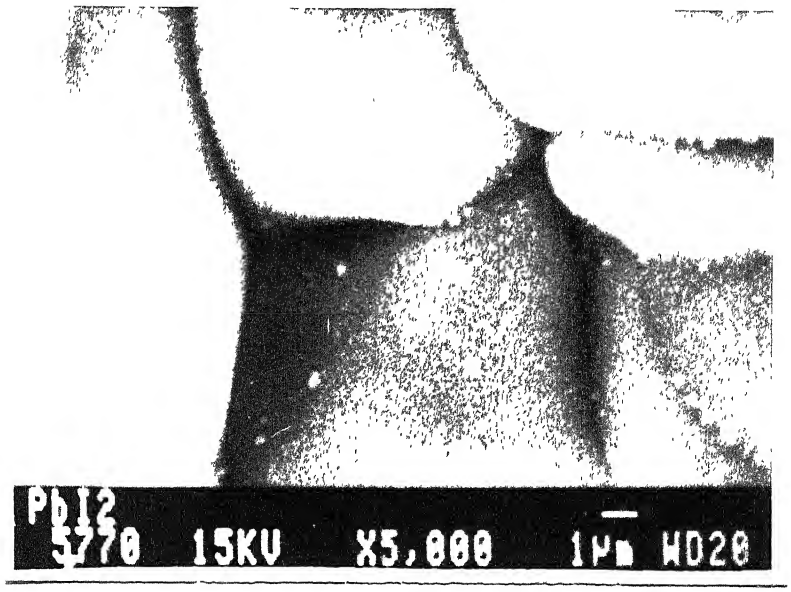

(a)

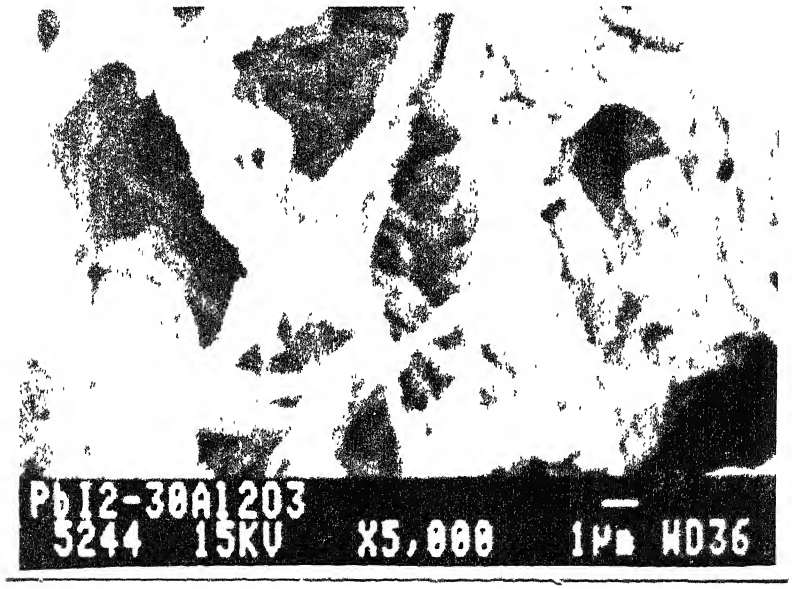

(b)

Fig.4.13 SEM micrographs for (a) PbI_2 and, (b) PbI_2 - 30 m/o Al_2O_3 composite sintered at 320°C.

4.3.4 Conductivity versus Composition :

The dc conductivities of all the samples at various temperatures have been obtained from the complex impedance (z, θ) analysis. Fig.4.14 shows a typical plot of the real part of the impedance (z cosθ) vs imaginary part (z sinθ) of the impedance for pure PbI_2. The near-perfect semicircular impedance spectra clearly suggest that the electrode/solid electrolyte/electrode assembly is equivalent to a parallel combination of a pure resistor and a capacitor. Thus the diameter of the semicircular plot yields the dc resistance which has been used to calculate the conductivity of the samples. The dc conductivity for all the systems investigated in the present work has been calculated in this manner at various different temperatures.

PbI_2-Al_2O_3 composites prepared by the method II show a decrease in the conductivity over that of pure PbI_2. The results are shown in Fig.4.15. The lowering of conductivity may be interpreted in terms of a chemical reaction between the constituents. The XRD, DTA and change of color of the samples suggest that a chemical reaction indeed occurs during the preparation of the samples by the method II. These samples were not studied in further detail. The results and discussion given below pertain to the samples prepared by the method-I only.

The variation of conductivity as a function of concentration (m/o) of Al_2O_3 in PbI_2 at three different temperatures, viz., 100, 150 and 250°C, is shown in Fig. 4.16. It is observed that the conductivity increases only slightly up to about 10 m/o of Al_2O_3

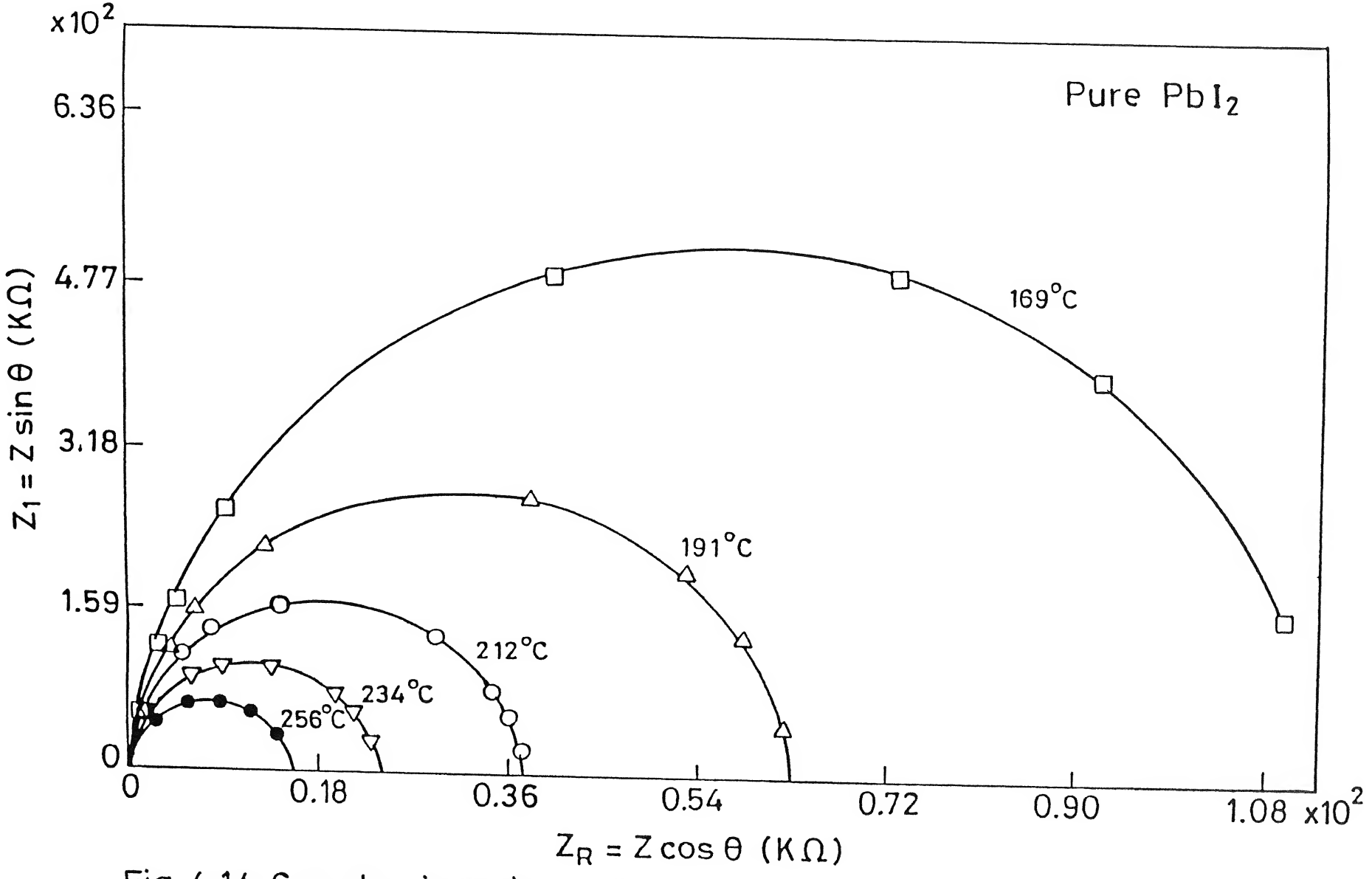

Fig. 4.14 Complex impedance plots for PbI_2 at different temperatures.

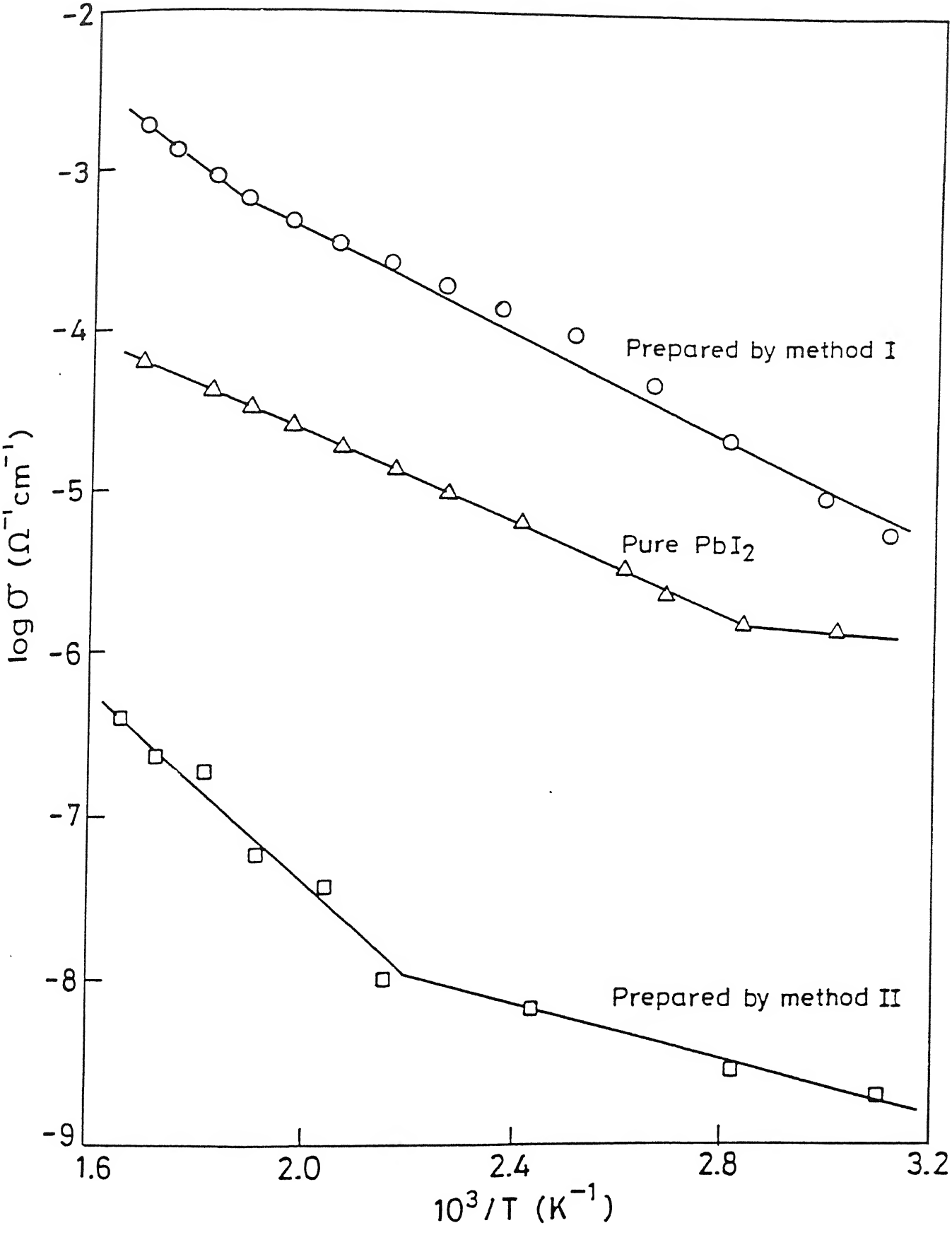

Fig. 4.15 log (σ) vs $10^3/T$ for PbI_2 and PbI_2-30 m/o Al_2O_3 prepared by method-I and method-II.

but rises rapidly subsequently and exhibits a maximum value at ~35 m/o Al_2O_3. As the concentration of Al_2O_3 increases further, the conductivity decreases rather rapidly. Table 4.5 compares the normalized conductivity, the ratio σ(composite)/σ_o(host), for PbI_2-Al_2O_3 composites at 100, 150 and 250°C. The results show that the conductivity of PbI_2 is enhanced by a factor of ~ 25 by the dispersion of Al_2O_3. These results are *distinctly* different from those on $PbCl_2$-Al_2O_3 and $PbBr_2$-Al_2O_3 composites which show a decrease in the conductivity.

Table 4.5

Normalized conductivity (σ/σ_o) for PbI_2-Al_2O_3 composites of various compositions at three different temperatures

composition (Al_2O_3)		σ/σ_o		
(m/o)	(v/o)	(100°C)	(150°C)	(250°C)
0	0	1	1	1
10	4	1.2	1.3	1.4
20	8	2.4	2.2	2.2
25	10	20	17	14
30	13	24	21	19
40	19	25	22	23
43	24	0.17	0.22	0.79
47	27	-	0.06	0.25
50	32	-	0.04	0.14

The fact that PbI_2-Al_2O_3 composites exhibit a maximum conductivity at ~ 35 m/o of Al_2O_3 suggests that some sort of high conducting channels form through the composite material around

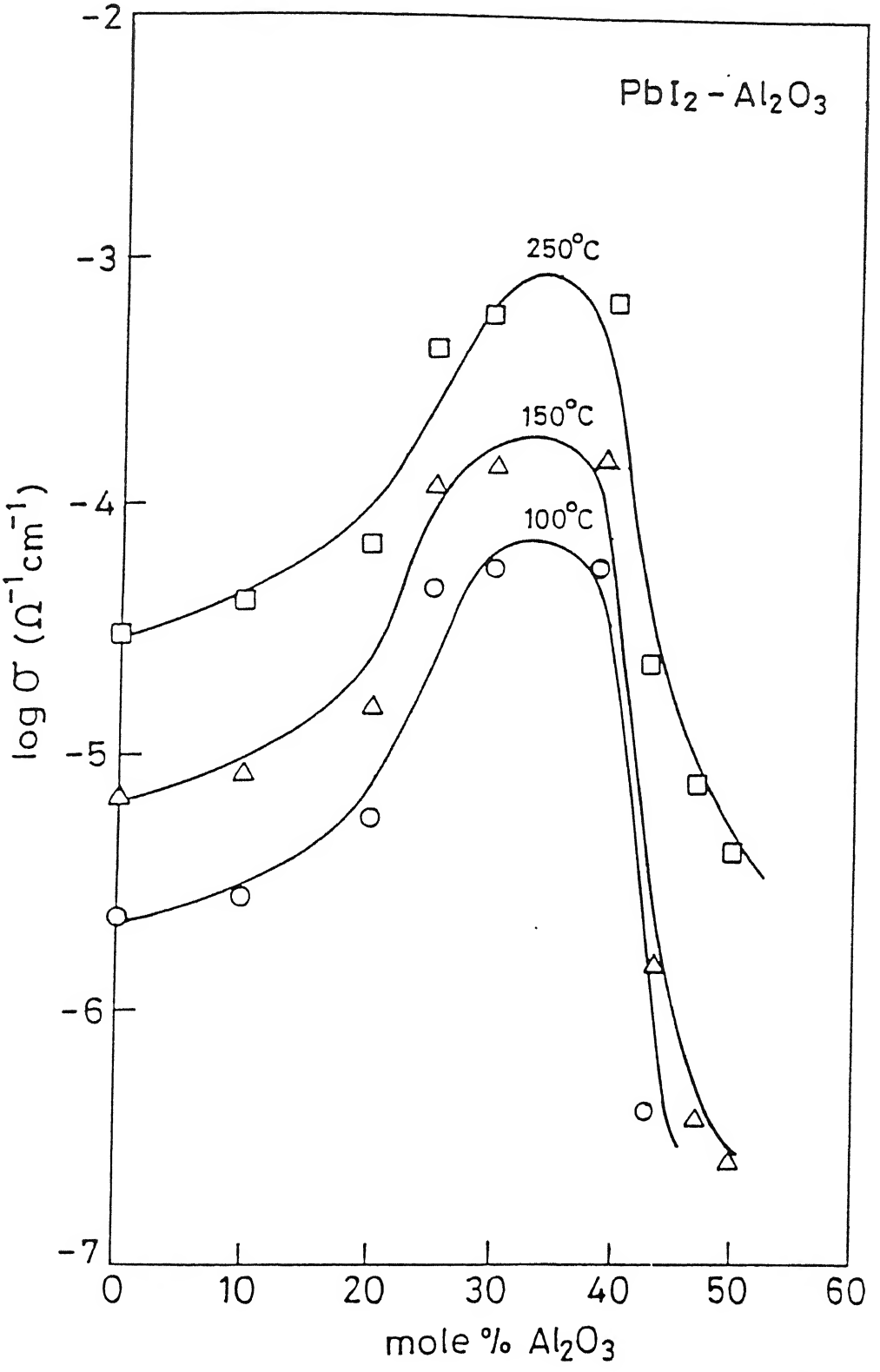

Fig. 4.16 Conductivity vs composition (m/o of Al_2O_3) for PbI_2-Al_2O_3 composites at three different temperatures.

this composition. It could be either due to formation of a high conducting phase or a space charge layer along the interface.

PbI_2 also exhibits Schottky type disorder but, unlike in $PbCl_2$ and $PbBr_2$, both cation and anion vacancies are mobile in PbI_2 (Tubandt,1932; Lingras and Simkovich,1978). A high conducting phase may form as a result of chemical reaction between PbI_2 and Al_2O_3. However, no new phase was detected by XRD at room temperature and DTA below 320°C (samples prepared by the method-I). Alternatively enhanced conductivity phase may result due to the solubility of Al_2O_3 in PbI_2 as follows :

$$Al_2O_3 \Leftrightarrow 2Al^{\cdot}_{Pb} + V^{\cdot}_{I} + 3O'_{I} \qquad (4.4)$$

Thus one molecule of dissolved Al_2O_3 in PbI_2 produces one excess iodide ion vacancy $V^{\cdot}_{I}$. However, if this were the mechanism of conductivity enhancement, only a fraction of a mole percent of the dopant (Al_2O_3) would have been required to achieve the observed enhancement in the conductivity. On the other hand, the experiments show that there is very little enhancement in the conductivity due to the addition of as large as 10 m/o Al_2O_3 and that the maximum enhancement in the conductivity occurs at ~ 35 m/o of Al_2O_3. Therefore the classical doping mechanism does not appear to be operative in these composite solid electrolytes.

The observed enhancement in the conductivity (Fig.4.16) may be explained in terms of a space charge layer that may form at the interface due to interaction between the nucleophilic groups on

the Al_2O_3 surface and the positively charged species. The lead ions may be attracted towards the Al_2O_3 surface causing an increase in the concentration of cation vacancies (V''_{Pb}) in the matrix in the vicinity of the interface and simultaneously *suppressing* the concentration of anion vacancies ($V^{\cdot}_{I}$) as the product of the concentrations of cation and anion vacancies must be constant at a fixed temperature. The lead ion vacancies V''_{Pb} in PbI_2, unlike in $PbCl_2$ and $PbBr_2$, are relatively more mobile probably because of the high polarizability and very large size of the I^- ions (2.16 Å). Under the action of external electric field, the I^- ions are highly polarized, thus reducing the activation barrier for Pb^{2+} ion migration. Therefore, the increased concentration and the relatively large mobility of the lead ion vacancies in the space charge region may result in the enhancement of conductivity in PbI_2-Al_2O_3 composites.

The above results are also consistent with the random resistor network (RRN) model (Bunde et.al.,1985, 1986) which presumes the formation of a high conducting space charge layer along the normal conductor-insulator phase and predicts the existence of two critical concentrations of the dispersoid, viz., p'_c and p''_c. At the lower critical concentration p'_c, the high conducting layers begin to form connected pathways, and at the higher critical concentration p''_c, the connected pathways get disrupted as they begin to from closed loops due to increased concentration of insulating bonds. The results in Fig. 4.16 do show that the conductivity rises rather rapidly initially, passes through a maximum at ~ 35 m/o Al_2O_3 and subsequently drops rather

rapidly. Thus the space charge mechanism appears to control the conductivity in PbI_2-Al_2O_3 composites.

It has been reported previously that the magnitude of enhancement in the conductivity depends upon, among other factors, the morphology or the surface activity (Maier, 1985; Shukla et.al., 1988), the shape (Slade and Thompson,1988) and the size (Nakamura and Goodenough, 1982; Chang et.al, 1984) of the dispersoid. To investigate the effect of surface activity, the Al_2O_3 particles were treated with a basic medium (NaOH; PH=9.6) and it was found that the NaOH-treated particles were almost twice as effective in the conductivity enhancement as the untreated particles (see Section 4.3.6). Table 4.6 summarizes the normalized conductivity of PbI_2-30 m/o Al_2O_3 (as-received) and PbI_2-30 m/o Al_2O_3 (NaOH-treated) at three different temperatures viz.,100,150 and 250°C. The increased effectiveness of NaOH-treated Al_2O_3

Table 4.6

Normalized conductivity (σ/σ_o) for PbI_2-30 m/o Al_2O_3 composites containing dispersion of as-received and NaOH-treated Al_2O_3 at three different temperatures

type of Al_2O_3	σ/σ_o		
	100°C	150°C	250°C
Al_2O_3 (as-received)	24	21	19
Al_2O_3 (NaOH-treated)	49	49	47

particles leads to the conclusion that the surface chemistry and

hence the interface plays a *dominant* role in the conductivity enhancement.

4.3.5 Conductivity Versus Particle Size :

Table 4.7 compares the normalized conductivity of PbI_2-30 m/o Al_2O_3 composites for three different particle sizes at three different temperatures 100, 150 and 250°C. Evidently, the relative enhancement in the conductivity is higher for lower particle sizes of Al_2O_3. These results are comparable to those reported earlier (Jow and Wagner, 1979; Nakamura and Goodenough,1982; Chang et.al., 1984). Various proposed models describe rather empirically, the conductivity enhancement as a function of the inverse of the size of the dispersed particles. Some studies have emphasized the correlation between the enhancement in the conductivity and the effective surface area of the dispersed phase (Slade and Thompson, 1988). However, for a quantitative comparison between the theoretical predictions and the experiment, the electrical conductivity expression given by Maier (1985) (Chapter 2; Section 2.3.2) can be rewritten as :

$$\frac{\sigma}{\sigma_o} = (1-\varphi_A) + \frac{K}{r_A} \qquad (4.5)$$

where, $$K = (3\sqrt{2}/\sigma_o)\ \beta_L\ \varphi_A\ \sqrt{(\varepsilon\varepsilon_o RT/V^m)}\ \mu_v\ \sqrt{N_{vo}} \qquad (4.6)$$

which is a constant at a given temperature (T) and a fixed concentration φ_A of the dispersoid. Other terms have their usual meaning (Section 2.3.2). Thus a plot of the normalized conductivity, σ(composite)/σ_o(host), versus inverse of particle

size ($1/r_A$) should be a straight line whose slope should be equal to the constant K. Thus the constant K can be calculated as well as determined from the experimental data, and hence compared to test the Maier's theory of heterogeneous doping (Eq.4.5).

Table 4.7 lists the particle size (r_A, μm), inverse particle size (r_A^{-1}, cm^{-1}), and the normalized conductivity (σ/σ_o), at 100, 150 and 250°C for PbI_2-30 m/o Al_2O_3 composites. Fig.4.17 shows the plot of normalized conductivity (σ/σ_o) versus inverse particle size ($1/r_A$) at the three temperatures. Even though the graphs are reasonably good straight lines, it need to be stressed that there are, unfortunately, only three data points corresponding to the three different particle sizes of Al_2O_3 that are available. Nevertheless, the conclusions drawn from these results may be fairly reliable especially in view of the fact that the third data corresponding to 0.05 μm ($r_A^{-1}=20\times10^4$ cm^{-1}) size of the Al_2O_3 particle is so *far apart* from the rest and yet falls on the line joining the other two data points (with $r_A^{-1}=3.33\times10^4$ and $1\times10^4 cm^{-1}$). Thus the fact that the plots are linear and their slopes decrease as temperature increases is very much in accordance with the model, which predicts that the slope K should decrease as temperature increases because at a fixed concentration φ_A of the dispersoid,

$$K \propto \frac{\sqrt{T}}{n_v(T)} \qquad (4.7)$$

where $n_v(T)$ is a strong (exponential) function of temperature and thus increases much more rapidly with temperature than $\sqrt{T}$, and

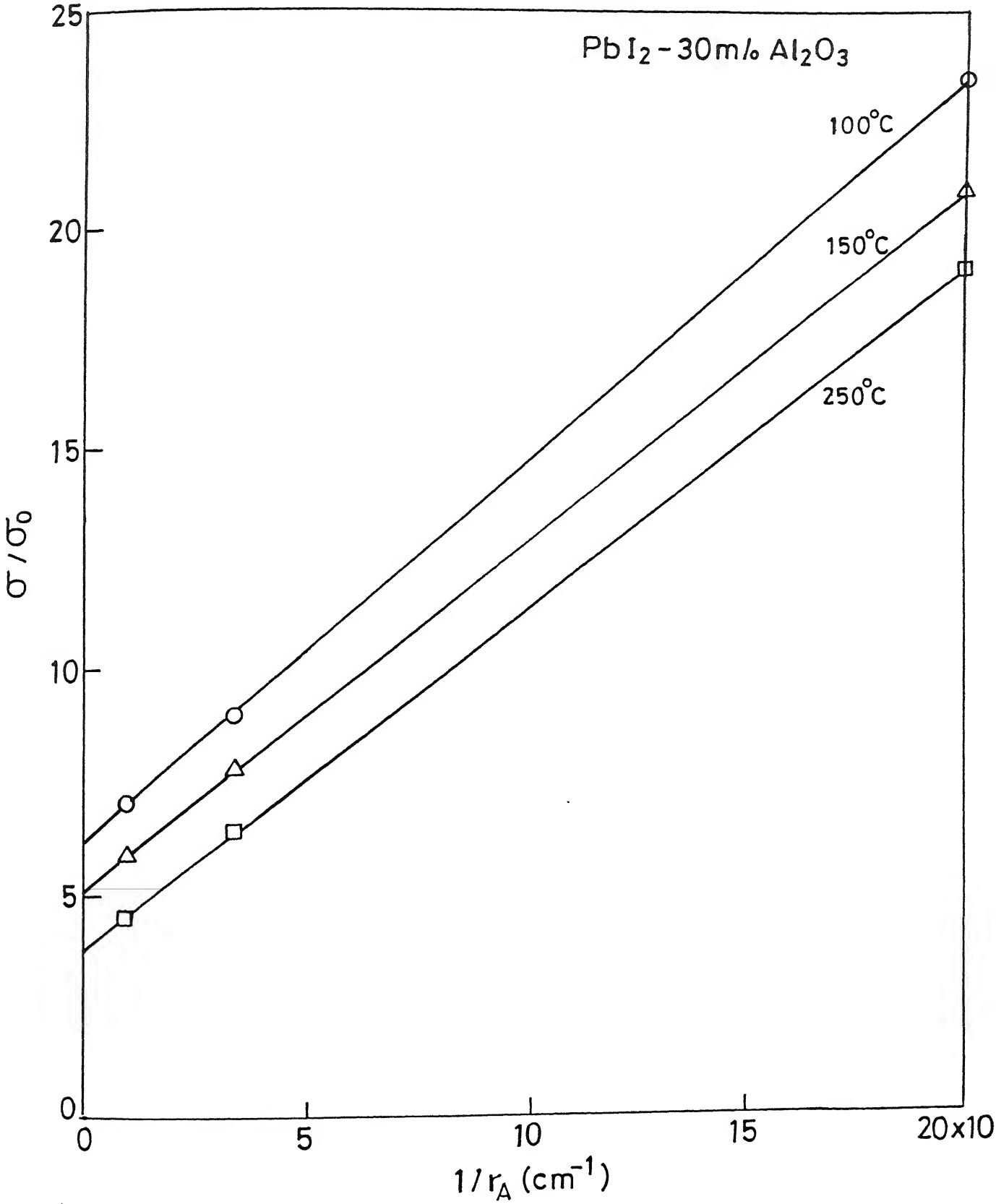

Fig. 4.17 Normalized conductivity (σ/σ_0) vs inverse particle size of Al_2O_3 for PbI_2-30 m/o Al_2O_3 composite at three different temperatures.

hence K should decrease as temperature increases.

The experimental values of the slope (Fig.4.17) are listed in Table 4.8. In the absence of any mobility or diffusion studies on PbI_2, the conductivity of the composites and K values could not be calculated and compared with the observed values. Nevertheless,

Table 4.7

Normalized conductivity (σ/σ_o) for PbI_2-30 m/o Al_2O_3 composite for three different particle sizes of Al_2O_3 at three different temperatures

particle size* of Al_2O_3, r_A (μm)	inverse part.size r_A^{-1} ($10^4 cm^{-1}$)	σ/σ_o (100°C)	(150°C)	(250°C)
0.05	20	24	21	19
0.3	3.3	8.9	7.8	6.5
1.0	1.0	7.1	5.9	4.5

*As quoted by the manufacturers (Buehler Micropolish II, USA).

Table 4.8

Calculated values of the slope of normalized conductivity (σ/σ_o) vs inverse particle size (r_A^{-1}) in PbI_2-30 m/o Al_2O_3 composite

Temperature(°C)	$K_{cal.}$(cm)
300	8.7×10^{-5}
400	7.9×10^{-5}
500	7.7×10^{-5}

the K values obtained from the experimental data (Table 4.8)

appear reasonable as these compare well with those (K values) for $MX-Al_2O_3$ systems for which good agreement is found between the calculated and the observed values (see Chapter 5).

The RRN model (Roman and Yussouff, 1987) is also found to be in qualitative agreement with the observed results. For larger particles, the surface area per unit volume available for forming high conducting bonds is less and hence the enhancement in the conductivity is less than that for smaller particles. The observed dependence of conductivity of $PbI_2-Al_2O_3$ composites on the particle size of Al_2O_3 (Fig.4.17) further supports the view that interface between PbI_2 matrix and dispersoid Al_2O_3 is responsible for the observed conductivity enhancement.

4.3.6 Conductivity vs Temperature :

The logarithm of dc conductivity, $\log(\sigma)$, as a function of inverse temperature for various $PbI_2-Al_2O_3$ composites is shown in Fig.4.18. The preexponential factor (σ_o) and the activation energy (E_a) are given in Table 4.9. Unlike $PbCl_2-Al_2O_3$ and $PbBr_2-Al_2O_3$, the activation energy for conduction remains almost *unchanged* in $PbI_2-Al_2O_3$ composites, at least upto 40 m/o Al_2O_3, which would suggest that the defect and conduction mechanisms in PbI_2 do not change on addition of Al_2O_3. According to the space charge theory discussed earlier, $PbI_2-Al_2O_3$ composites conduct via excess Pb^{2+} ion vacancies. Thus the fact that the migration energies in the composites and pure PbI_2 are nearly equal would suggest that Pb^{2+} ion vacancies also contribute to the conduction process in PbI_2. Unfortunately, the defect and conduction mechanisms in PbI_2

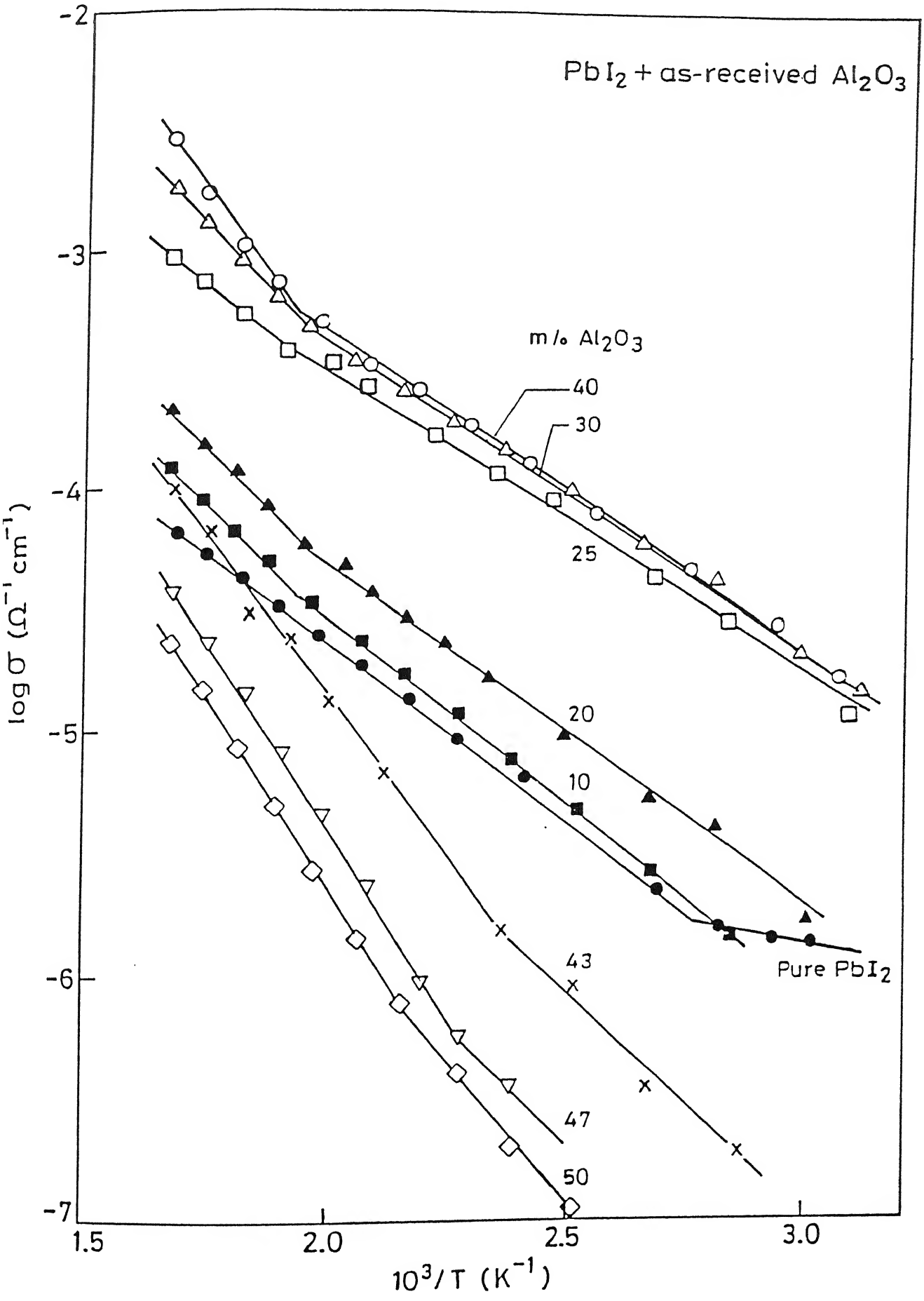

Fig.4.18 log (σ) vs $10^3/T$ for various PbI_2-Al_2O_3 composites

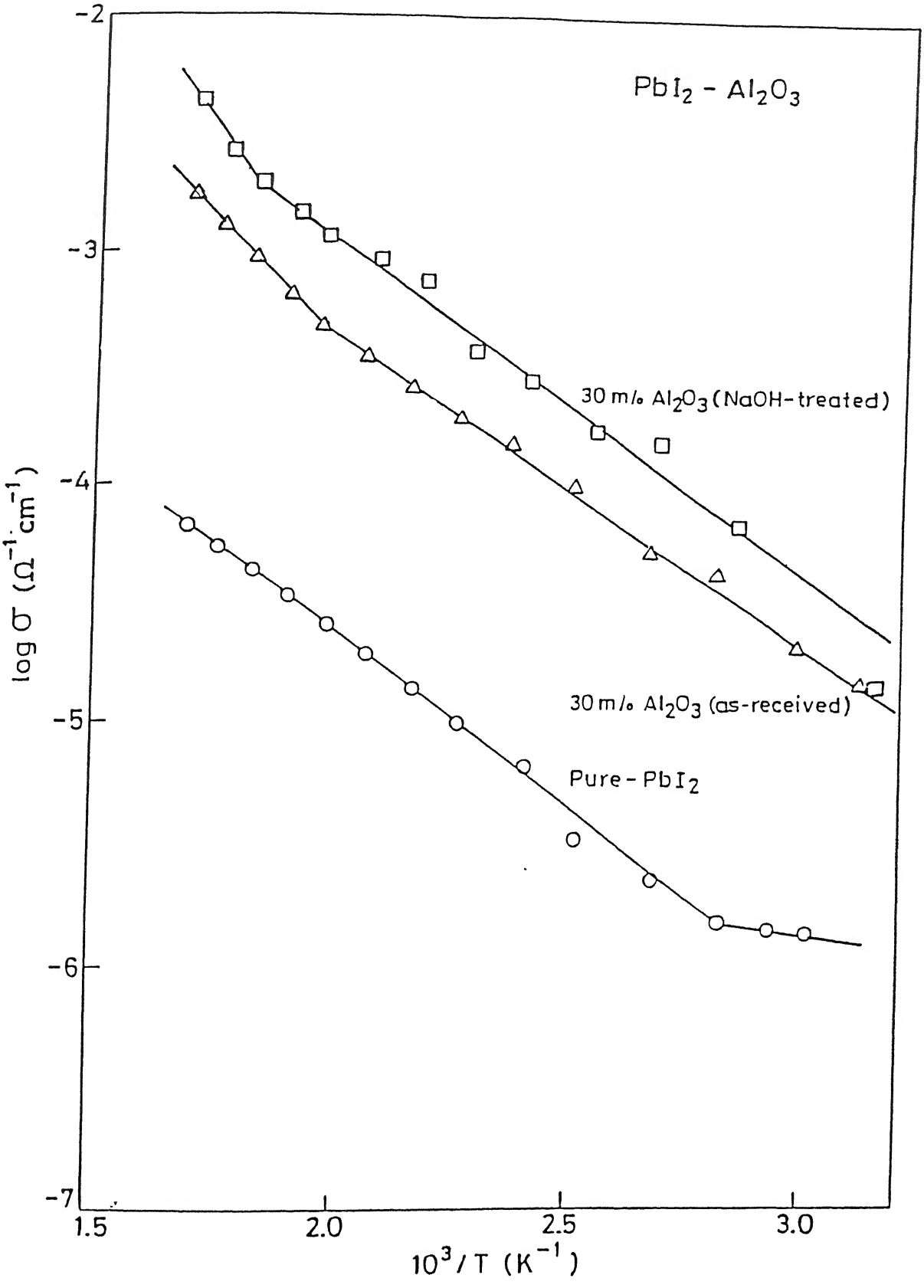

Fig. 4.19 log(σ) vs $10^3/T$ for PbI_2 and PbI_2-30 m/o Al_2O_3 composites with as-received and NaOH-treated Al_2O_3.

is same for the two samples which implies that the basic conduction mechanism remains the same, viz., via Pb^{2+} ion vacancies.

Fig. 4.20 shows the log(σ) vs $10^3/T$ plots for PbI_2-30 m/o Al_2O_3 for three different particle sizes of Al_2O_3, viz., 0.05, 0.3, 1.0 μm. The enhancement in the conductivity is higher for the lower particle size of Al_2O_3. These results have been discussed in Section 4.3.5. The activation energies and the preexponential factors are listed in Table 4.10. It is observed that the activation energy is independent of the particle size which implies that the conduction mechanism remains the same for all the three particle sizes.

Table 4.10

Ionic transport parameters, the activation energy (E_a) and the preexponential factor (σ_o), for PbI_2-30 m/o Al_2O_3 composites for three different particle sizes of Al_2O_3 in the temperature range 100-200°C

Particle size of Al_2O_3 (μm)	E_a (eV)	σ_o $(ohm.cm)^{-1}$
0.05	0.26	1.7×10^{-1}
0.3	0.25	5.0×10^{-2}
1.0	0.24	2.9×10^{-2}

4.4 Summary and Conclusions :

The compositional and particle size dependence of the conductivity of composites suggest that matrix-particle interface plays a *critical* role in the conductivity profiles of the

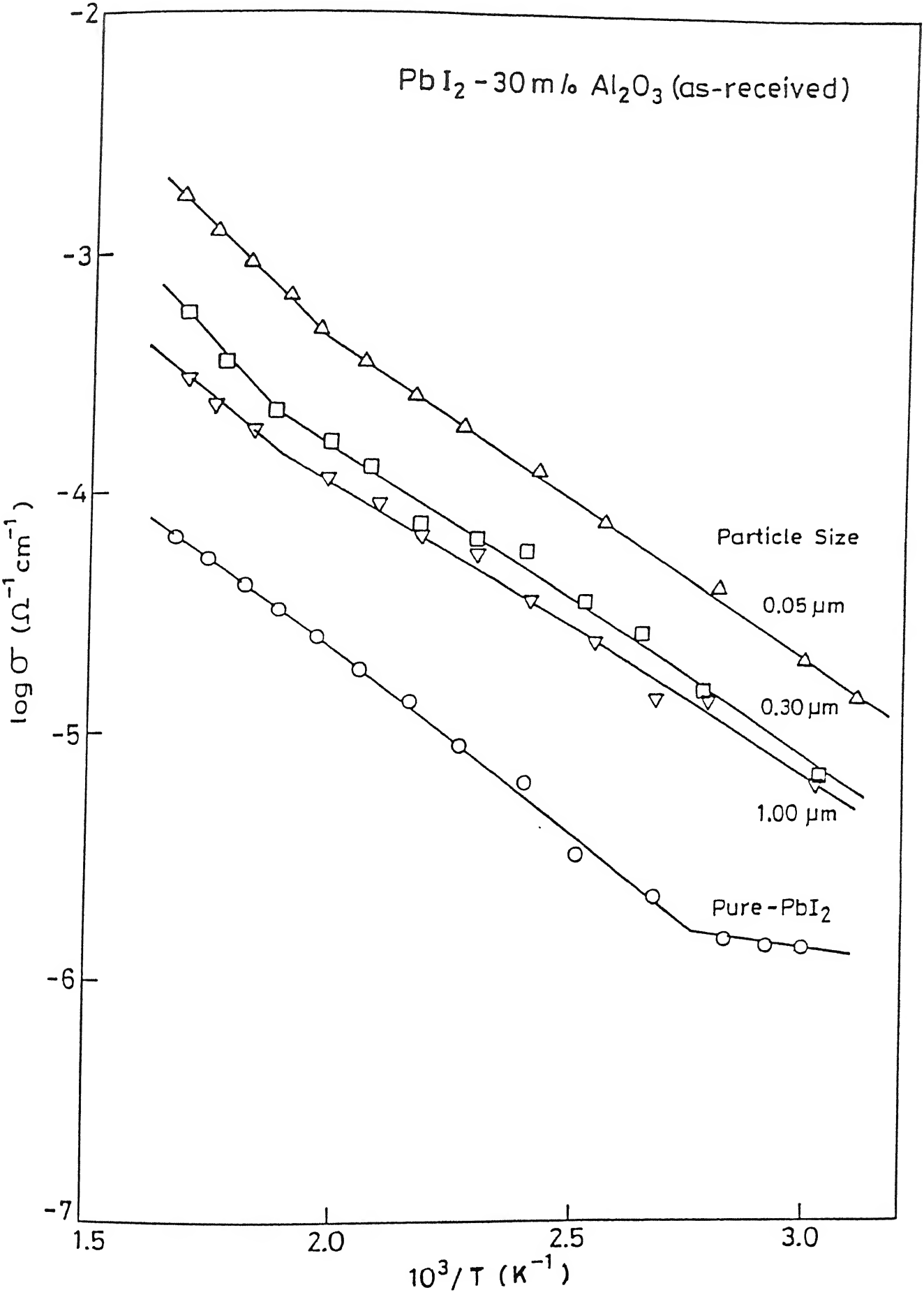

Fig.4.20 log (σ) vs $10^3/T$ for PbI_2 and PbI_2-30 m/o Al_2O_3 comp

composites. The PbI_2-Al_2O_3 composites show enhancement in the conductivity whereas $PbCl_2$-Al_2O_3 and $PbBr_2$-Al_2O_3 composites show a decrease in the conductivity. This behavior has been attributed to the fact that the Pb^{2+} ion vacancies are almost immobile in $PbCl_2$ and $PbBr_2$, but are as mobile as I^- ion vacancies in PbI_2. Due to Al_2O_3 dispersion the positively charged species (Pb^{2+}ions) are attracted towards the Al_2O_3 surface causing an increase in the lead ion vacancies at the interface. As the mobility of Pb^{2+} ion vacancies is comparable to that of anion vacancies $V_I^{\cdot}$ in PbI_2, the space charge regions containing the mobile Pb^{2+}ions around the interface dominate the conduction in PbI_2-Al_2O_3 composites. This behavior is distinctly different from the $PbCl_2$-Al_2O_3 and $PbBr_2$-Al_2O_3 composites wherein the conductivity is depressed due to decreased concentration of dominant charge carriers chloride and bromide ion vacancies respectively. Though the concentration of lead ion vacancies V_{Pb}'' is increased at the interface but their mobility is negligible as compared to that of the anion vacancies. Therefore, the space charge regions at the interface do not control the conduction in $PbCl_2$-Al_2O_3 and $PbBr_2$-Al_2O_3 composite systems. Thus, the results on these systems can be explained satisfactorily on the basis of space charge theory of conduction in composites solid electrolytes.

CHAPTER 5

MCl - Al_2O_3 (M = Na, K, Rb) COMPOSITES

Since the discovery of ionic conductivity enhancement in LiI due to dispersion of Al_2O_3 by Liang (1973), considerable attention has been devoted to the study of composite solid electrolytes to understand the mechanism of conduction in such systems. The conduction in such electrolytes is believed to be different from that in the conventional homogeneously doped ones in that the fulfillment of local electroneutrality condition is decisive in the latter whereas in the case of former, interfaces are utilized to give rise to high ionic conductivity, and the deviations from electroneutrality at the matrix-particle interface are important (Maier, 1985). Superionic conductors such as α-AgI, however, show decrease in ionic conductivity due to dispersion of insulating particles such as Al_2O_3, SiO_2, CeO_2 etc.(Chen Liquan, 1986).

Even though the studies on composite solid electrolytes are numerous and vigorous, the alkali halide based composites, with the exception of lithium salts, have not been investigated. In this work alkali chlorides (MCl; M=Na, K, Rb) have been chosen as host matrix as they (i) do not exhibit any solid-solid transformation,(ii) are well understood with regard to their defect and conduction mechanisms and, (iii) are not very hygroscopic. Thus the effect of Al_2O_3 dispersion can be studied over a wide temperature range which should be helpful in

identifying the mechanism of enhanced conductivity in the composites.

The $MCl-Al_2O_3$ (M = Na, K and Rb) composites of various compositions have been prepared by the conventional method as described in Chapter 3 (Section 3.2.1). The samples of best conducting compositions for all the three systems have also been prepared by the solution casting method as described in the Section 3.2.2. Most of the composite samples have been investigated by SEM for microstructural analysis and by DTA and XRD for phase characterization studies and to examine the solid solubility of Al_2O_3 in the matrix phase. Even though the particle sizes of three different Al_2O_3 samples used in this work are quoted by the manufacturer to be 0.05, 0.3 and 1.0 μm, preliminary investigations using SEM and Coulter counter revealed that the average sizes of the particles were larger than those quoted by the suppliers, which is expected due to the agglomeration before and during processing.

The conductivity for all the samples at each temperature was obtained from the complex impedance analysis. The high frequency semicircular portion of the impedance spectra could be expressed as a constant phase element in parallel with the bulk resistance. The resistance obtained from the high-frequency semicircular portion has been used to calculate the conductivity of various composites.

The detailed results on NaCl-Al_2O_3 system are presented first, followed by those on KCl-Al_2O_3 and RbCl-Al_2O_3 systems.

5.1 NaCl -Al_2O_3 System :

5.1.1 X-ray Diffraction :

Fig.5.1 shows the X-ray diffractograms of NaCl-40 m/o Al_2O_3 composition before (curve a) and after (curve b) heating the mixture at 750°C. The XRD peaks for both the samples are almost identical and could be ascribed either to NaCl or Al_2O_3 phase. These results show no evidence of any chemical reaction or solid solution formation between the constituents. However, since XRD patterns were taken at room temperature and it is possible that a new phase/solid solution may form at higher temperatures, the samples were further examined by differential thermal analysis.

5.1.2 Differential Thermal Analysis :

The DTA traces of NaCl-40 m/o Al_2O_3 samples before and after heating the mixture at 750°C are shown in Fig.5.2 (a and b). The endothermic peaks in both the curves correspond to the melting of NaCl. The absence of any other peak thus rules out the possibility of any chemical reaction or thermal decomposition of any of the constituents. Further, since there is no observable shift in the peak corresponding to the melting of the NaCl in the heat-treated sample (curve b), it is concluded that Al_2O_3 does not dissolve in NaCl either.

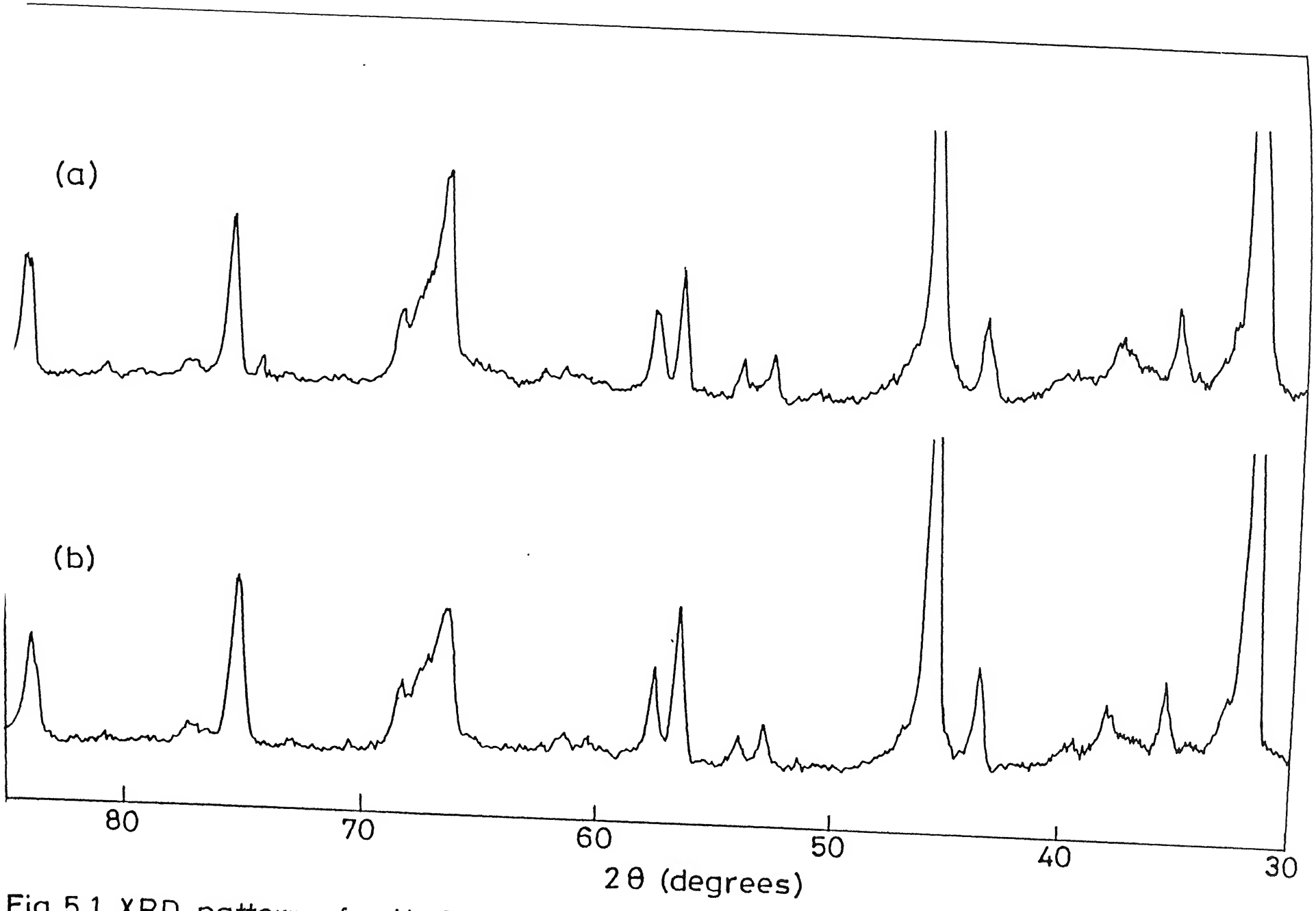

Fig. 5.1 XRD patterns for NaCl-40 m/o Al_2O_3 samples (a) before and, (b) after heat treatment at 750°C

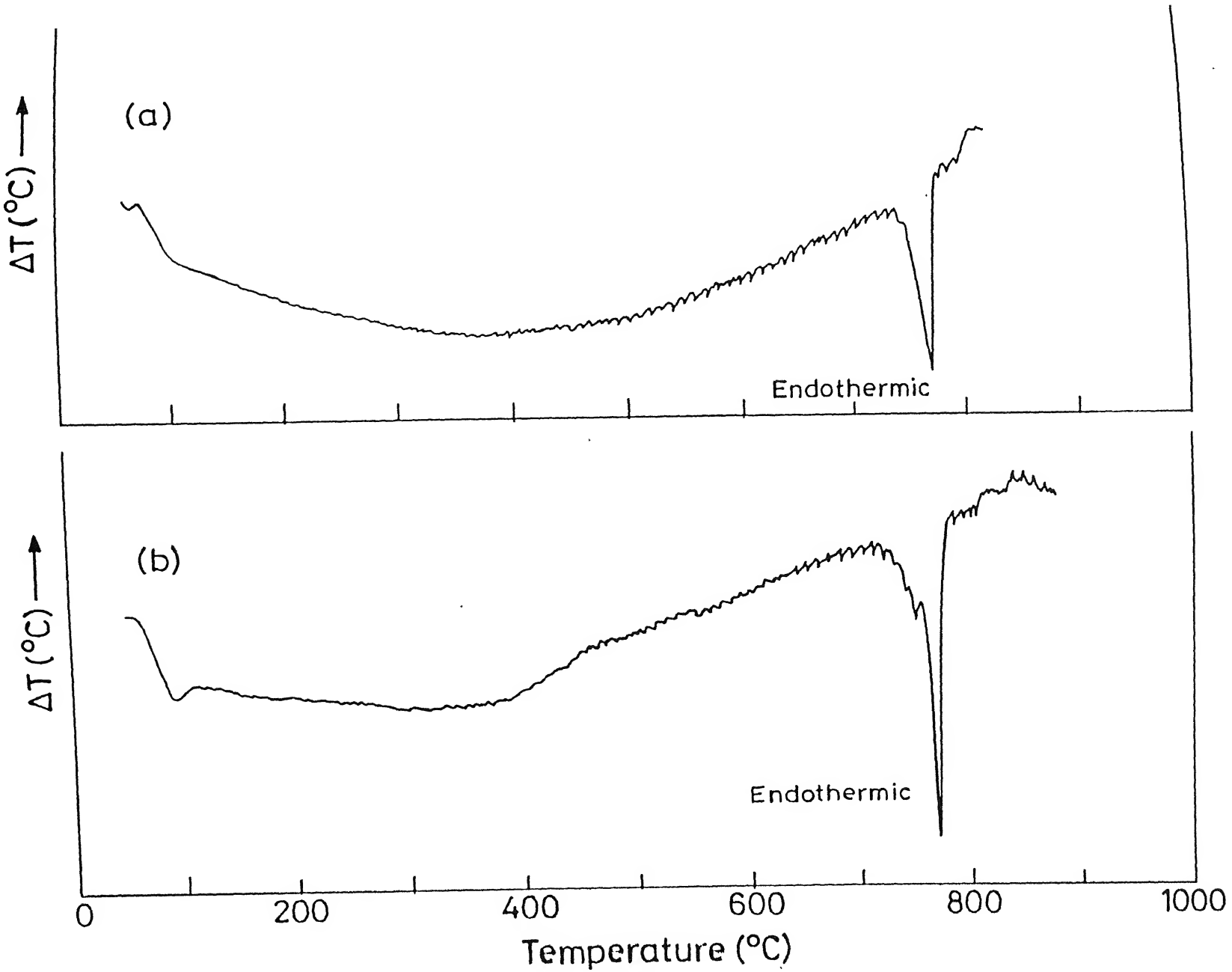

Fig.5.2 DTA curves for NaCl-40 m/o Al_2O_3 composite (a) pre-heated and, (b) after heat treatment at 750°C

5.1.3 Scanning electron microscopy :

The scanning electron micrographs of well polished samples of polycrystalline NaCl and NaCl-30 m/o Al_2O_3 sintered at 750°C are shown in Fig. 5.3. In case of pure NaCl (Fig.5.3a), it is observed that the grains are uniformly distributed whereas in case of NaCl-30 m/o Al_2O_3 (Fig.5.3b) the NaCl and Al_2O_3 grains are uniformly dispersed in the NaCl matrix.

5.1.4 Conductivity Versus Composition:

Fig. 5.4 shows the variation of electrical conductivity as a function of concentration (m/o) of Al_2O_3 in NaCl at three different temperatures, viz., 300, 400 and 500°C. Fig.5.5 shows the conductivity versus composition plots at 500°C for three different particle sizes of Al_2O_3, viz., 0.05, 0.3, 1.0 μm. The conductivity increases sharply as the concentration of Al_2O_3 increases, attains a maximum value at 30-35 m/o Al_2O_3 and starts decreasing subsequently. Table 5.1 compares the normalized conductivity (the ratio of the conductivity of the composite to that of pure salt, σ/σ_o) of various NaCl-Al_2O_3 composites at 300, 400 and 500°C. The data show that a maximum enhancement in conductivity by over two orders of magnitude is obtained for NaCl-30 m/o Al_2O_3 composite system and that the enhancement in conductivity is more pronounced at lower temperatures for a given composite. These features are in general similar to those reported in the literature on other composite systems.

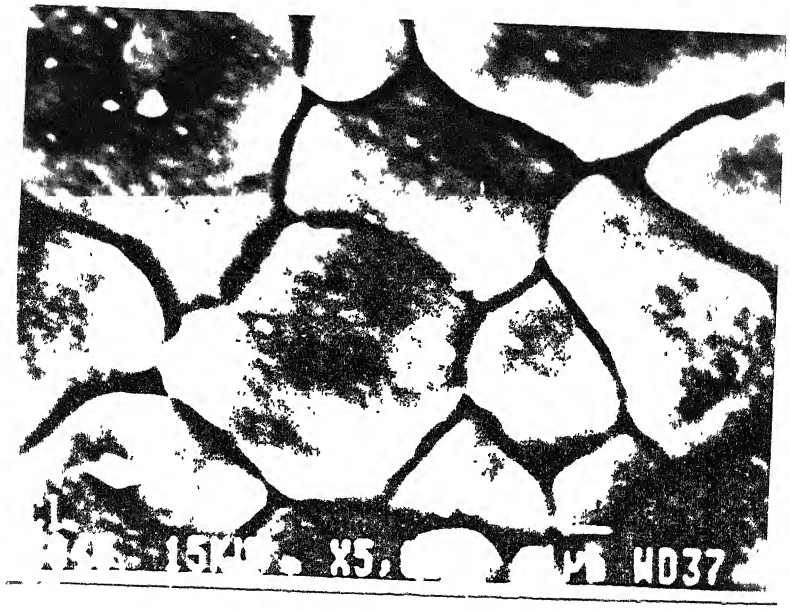

(a)

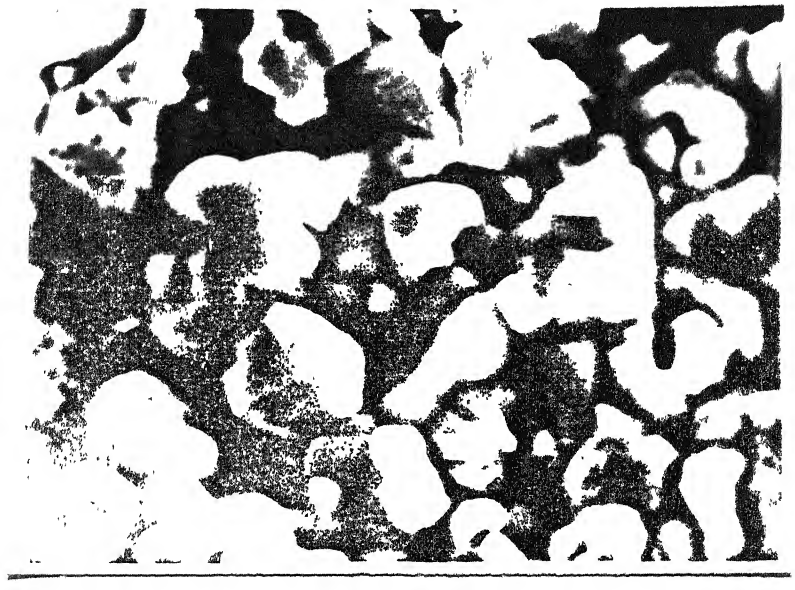

(b)

Fig. 5.3 SEM micrographs for (a) NaCl and, (b) NaCl-30 m/o Al_2O_3 composite sintered at 750°C.

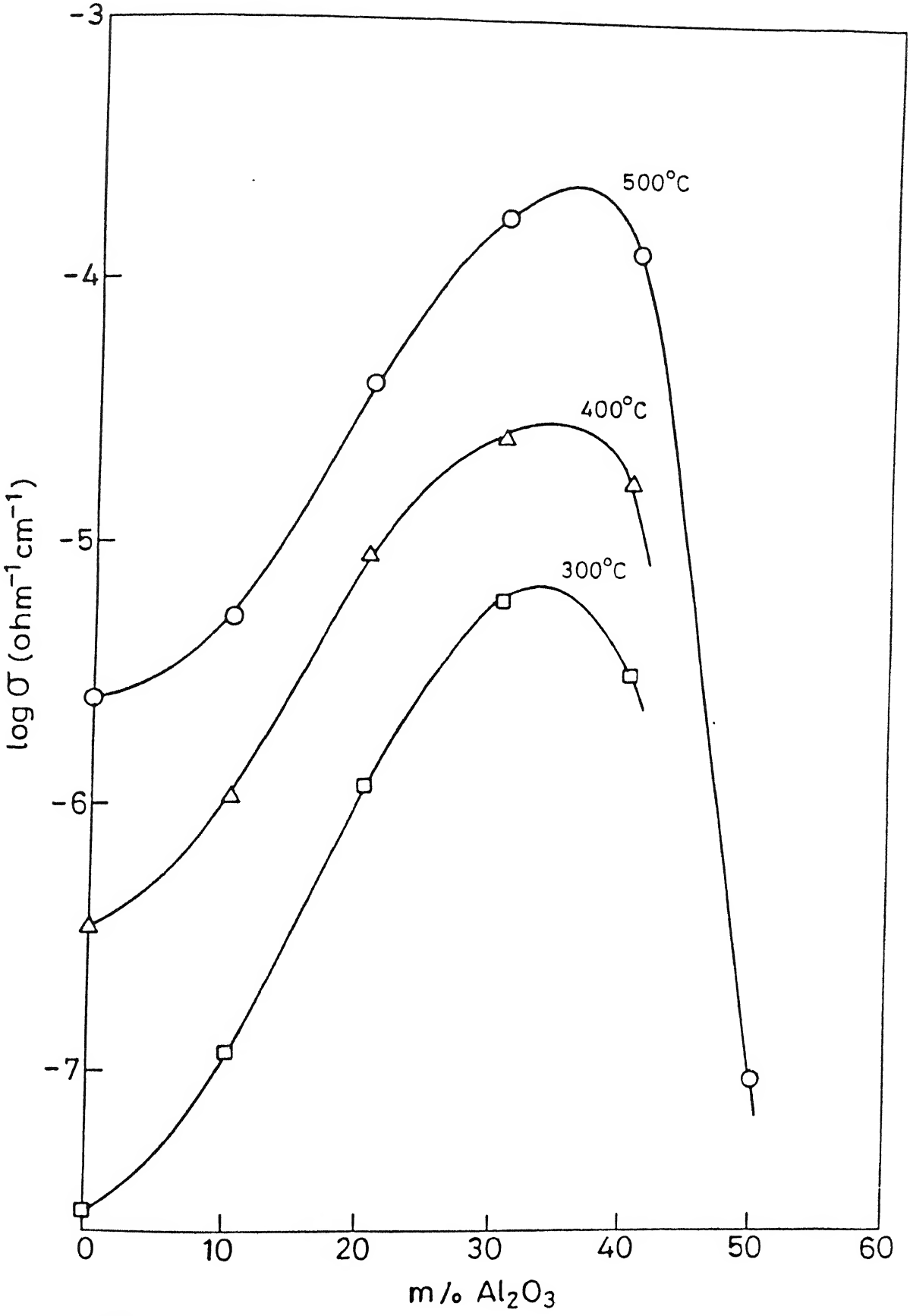

Fig.5.4 log (σ) vs composition (m/o Al_2O_3) for NaCl-Al_2O_3 composites at three different temperatures.

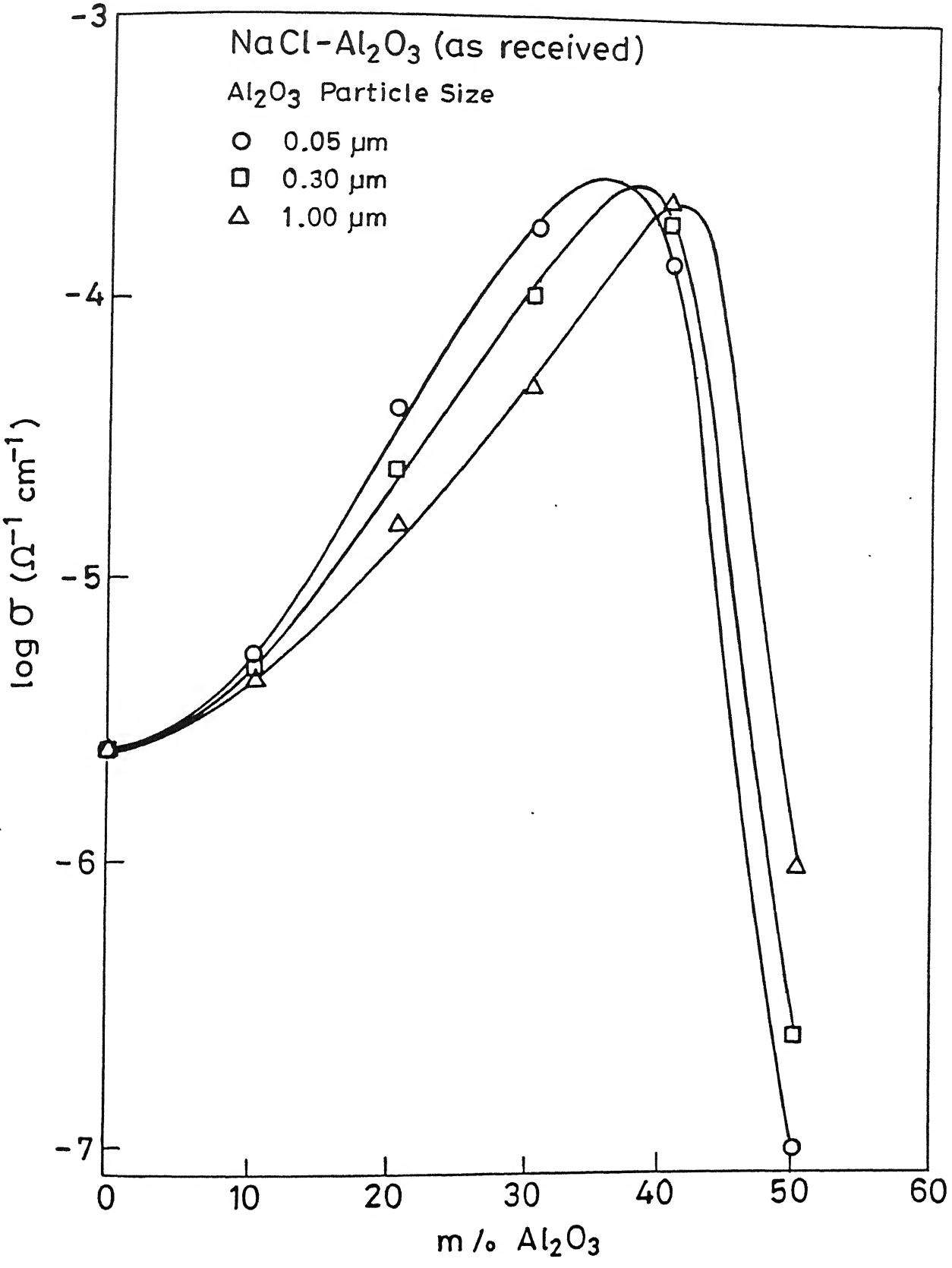

Fig. 5.5 log (σ) vs composition (m/o Al_2O_3) for NaCl - Al_2O_3 composites at 500°C for three different particle size of Al_2O_3.

Table 5.1

Normalized conductivity (σ/σ_o) for NaCl-Al_2O_3 composites of various compositions at three different temperatures

composition (m/o Al_2O_3)	σ/σ_o		
	300°C	400°C	500°C
0	1.0	1	1
10	4.0	3	2
20	40	25	16
30	2.2×10^2	1.2×10^2	72
40	1.2×10^2	77	52
50	-	-	4.0×10^{-2}

Table 5.2 compares the normalized conductivity of NaCl-30 m/o Al_2O_3 samples prepared by (i) conventional and (ii) solution casting methods. It is observed that the enhancement in the conductivity for a given composite is generally more for the sample prepared by the solution casting rather than the conventional method. This may be due to the combined effects of more uniform distribution of Al_2O_3 particles as well as chemisorbed water molecules on their surfaces. Thus these results reinforce the existing view (Pack, 1979; Shahi and Wagner, 1981) that the wet Al_2O_3 is more effective than the dry Al_2O_3 and that the matrix-particle interface plays a dominant role in the conductivity enhancement.

Table 5.2

Normalized conductivity (σ/σ_o) for NaCl-30 m/o Al_2O_3 composites prepared by the conventional and solution casting methods at three different temperatures

composite type	σ/σ_o		
	300°C	400°C	500°C
conventional	2.2×10^2	1.2×10^2	72
solution casting	2.5×10^3	7.0×10^2	3.2×10^2

It is conceivable to attribute the enhanced conductivity to the excess sodium vacancies generated by the dissolution of Al_2O_3 in sodium chloride lattice as follows :

$$Al_2O_3 \Leftrightarrow 2Al^{\cdot\cdot}_{Na} + V'_{Na} + 3O'_{Cl} \qquad (5.1)$$

where the Kröger-Vink notation has been used. Thus one molecule of dissolved Al_2O_3 produces one excess sodium ion vacancy. If this were the mechanism of conductivity enhancement, a simple calculation, using the known mobility value of Na^+ ion vacancy at 300°C (Etzel and Maurer, 1950), would suggest that only a fraction of a mole percent of the dopant (Al_2O_3) would be required to achieve the observed conductivity of ~ 10^{-5} $ohm^{-1}cm^{-1}$ at 300°C. On the other hand, the experiments show that there is very little enhancement in the conductivity due to addition of as large as 10 m/o Al_2O_3 and that the maximum enhancement in conductivity occurs at $\simeq$ 35 m/o Al_2O_3. This clearly suggests that the classical doping mechanism cannot explain the conductivity enhancement in

$NaCl-Al_2O_3$ composite system. It is also conceivable that dispersion of Al_2O_3 increases the dislocation density in the host matrix and the excess space charge at the dislocations may contribute to the excess conductivity. However, the dependence of conductivity on the processing and particle size indicates that the mechanism responsible for conductivity enhancement must involve the matrix-particle interface.

The existence of space charge region near lattice discontinuities (free surface, dislocations and grain boundaries) in an ionic solid was first proposed by Frenkel (1946) and the space charge distribution profiles have been formulated by several researchers (Lehovec, 1953; Kliewer and Koehler, 1965; Eshelby et.al.,1958; Yan et.al.,1977). The origin of space charge is ascribed to the difference in the free energy of formation of the individual vacancies in case of Schottky disorder and of the vacancies and the interstitials in case of Frenkel disorder. If there is a chemically inert second phase instead of vacuum, which means there is no solubility or a global chemical reaction with the crystal, then the space charge profile can be obtained in a similar way as for a crystal in contact with vacuum. Jow and wagner (1979) were the first to use these concepts and proposed that fine dispersoids form well defined space charge regions in contact with the host matrix. The space charge profiles for two phase composites have been formulated by Maier (1985, 1986). According to this author,the dispersoid acts as a nucleophilic surface which attracts positively charged species leaving a space

charge region of cation vacancies in the host crystal at the interface. An increase in the defect concentration in the space charge region gives rise to the excess conductivity in the composite systems.

In pure NaCl crystal at the free surface the formation energy of Na^+ ion vacancy is lower than that of Cl^- ion vacancy (Kliewer and Koehler,1965). As a consequence just beneath the surface there are more cation vacancies than the anion vacancies resulting in a negative space charge region. If there is a second insoluble (Al_2O_3) phase instead of vacuum, one would expect the increased rate of cation disorder reaction. Consequently sodium ions will be enriched at the interface and the concentration of sodium ion vacancies increased in the host crystal which will give rise to the excess conductivity in NaCl-Al_2O_3 composite systems.

Maier's theory has been discussed in Chapter 2 (Section 2.3.2). Accordingly, the total conductivity of a composite, assuming the conductivity of the dispersoid to be neligible, is given by the expression :

$$\sigma = (1-\phi_A)\sigma_o + (3\sqrt{2})\,\beta_L\,(\varphi_A/r_A)\,\sqrt{(\varepsilon\varepsilon_o RT/V^m)}\,\mu_v\,\sqrt{N_{vo}} \qquad (5.2)$$

where the first term corresponds to the conductivity of the matrix phase and the second term corresponds to the space charge layer contribution. φ_A is the volume fraction of the dispersoid, V^m the bulk molar volume of MX, $\varepsilon\varepsilon_o$ the absolute dielectric constant of

the matrix phase, μ_v the mobility of the defect, N_{vo} the mole fraction of defects at the interface and β_L a constant to account for the topology of the dispersoids. Table 5.3 compares the observed conductivity values with those calculated from the above equation for NaCl-Al_2O_3 composites at 300°C. The following values of various parameters have been taken; β_L = 0.5, r_A=0.05 μm, ε(NaCl) ~ 6, $V_m \simeq 27$ cm^3/mole, $N_{vo} \simeq 1$ and the mobility of the sodium ion vacancies μ_{Na^+} (Etzel and Maurer, 1950) :

$$\mu_{Na^+} = \frac{19600}{T} \exp(-9860/T) \quad cm^2\ V^{-1}s^{-1} \tag{5.3}$$

Table 5.3

Observed and calculated conductivities for various NaCl-Al_2O_3 composites at 300°C

composition (Al_2O_3) (m/o)	(v/o)	$\sigma_{obs.}$ (ohm-cm)$^{-1}$	$\sigma_{cal.}$ (ohm-cm)$^{-1}$
0	0	3.1×10^{-8}	3.1×10^{-8}
10	10	1.6×10^{-7}	5.0×10^{-7}
20	19	1.1×10^{-6}	9.3×10^{-7}
30	29	6.3×10^{-6}	1.4×10^{-6}
40	39	3.3×10^{-6}	1.9×10^{-6}

It may be noted from Table 5.3 that the calculated and observed conductivity values agree within a factor of two for all the compositions except for the 30 m/o Al_2O_3 composite which happens to be the composition at which the conductivity is maximum. Despite this minor discrepancy, our results on NaCl-Al_2O_3 composites do provide support to the Maier's microscopic theory of

enhanced conductivity in the composite solid electrolytes.

The conductivity-composition results on $NaCl-Al_2O_3$ system (Figs.5.4 and 5.5) can also be discussed in view of the random resistor network (RRN) model (Bunde et.al.,1985, Roman and Yussouff,1987) which presumes the existence of a highly conducting layer between a normally conducting matrix and a non-conducting dispersoid. This model, in particular, predicts the existence of two critical concentrations, viz., p_c' and p_c'', of the dispersed phase. At the lower critical concentration p_c', the high conducting layers begin to form connected pathways, while at the higher critical concentration p_c'' the connected pathways get disrupted and hence conductivity begins to drop sharply. Even though it is difficult to identify the lower critical concentration p_c', the existence of the higher critical concentration p_c'', where conductivity drops sharply is evident in Figs.5.4 and 5.5, and thus our results appear to be consistent with the macroscopic RRN model.

5.1.5 Conductivity Versus Particle Size :

Almost all the models (Jow and Wagner, 1979; Maier, 1985,1986; Bunde et.al., 1985) discuss the dependence of conductivity enhancement on the particle size of dispersoid and predict an inverse relation, viz., a higher σ enhancement by smaller particles, as observed in most composite solid electrolytes. Nevertheless, for a quantitative comparison of the observed data with the theory, the conductivity expression

(Eq.5.1) given by Maier(1985) can be written as :

$$\frac{\sigma}{\sigma_o} = (1-\varphi_A) + \frac{K}{r_A} \qquad (5.4)$$

where σ_o is the bulk conductivity of the matrix phase, and at a fixed temperature T and concentration φ_A of the dispersoid, K is a constant which from Eqs.(5.1) and (5.3) is given by :

$$K = (3\sqrt{2}/\sigma_o)\ \beta_L\ \varphi_A\ \sqrt{(\varepsilon\varepsilon_o RT/V^m)}\ \mu_v\ \sqrt{N_{vo}} \qquad (5.5)$$

Thus a plot of normalized conductivity, σ(composite)/σ_o(host), versus inverse particle size (r_A^{-1}) should be a straight line whose slope equals the constant K (Eq.5.5).

Table 5.4 lists the normalized conductivity (σ/σ_o) for NaCl-30 m/o Al_2O_3 composites for three different particle sizes of Al_2O_3 at 300, 400 and 500°C. Fig.5.6 shows the plot of normalized conductivity versus inverse particle size at the three temperatures. Even though the graphs are reasonably good straight lines, it need to be stressed that there are, unfortunately, only three data points corresponding to the three different particle sizes of Al_2O_3 which are available. Nevertheless, the conclusions drawn from these results may be fairly reliable, especially in view of the fact that the third data corresponding to 0.05 μm (r_A^{-1}=20x10^4 cm^{-1}) size of the Al_2O_3 particle is so *far apart* from the rest and yet falls on the line joining the other two data points (with r_A^{-1}= 3.33x10^4 and 1x10^4 cm^{-1}). Moreover, the fact

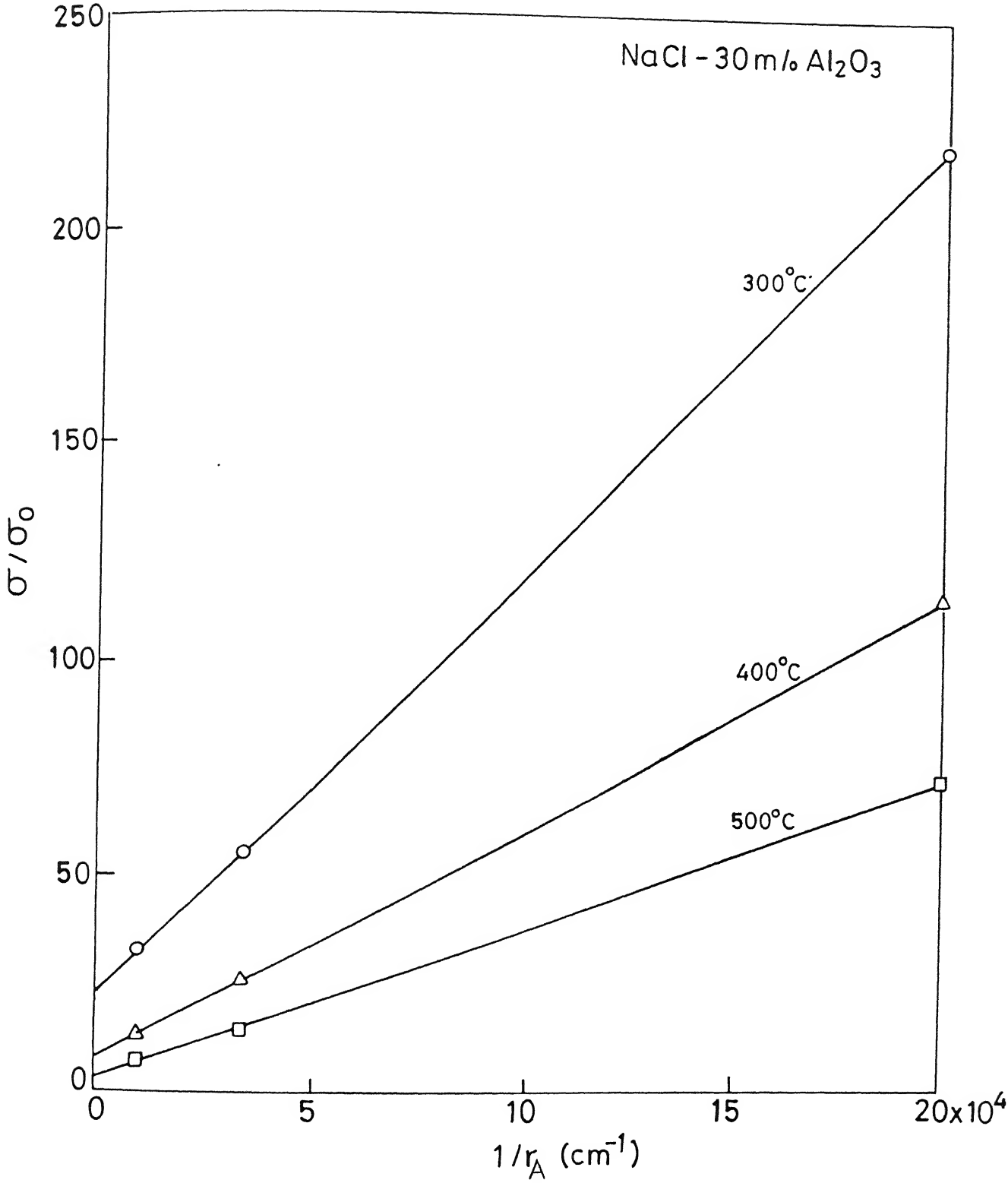

Fig.5.6 Normalized conductivity (σ/σ_0) vs inverse of particle size of Al_2O_3 for NaCl - 30 m/o Al_2O_3 at three different temperatures.

that the slope of the linear plot decreases as temperature increases is very much in accordance with the model, which predicts that the slope K should decrease as temperature increases because, according to Eq.5.5, at a fixed concentration φ_A of the dispersoid,

$$K \alpha \frac{\sqrt{T}}{n_v(T)} \tag{5.6}$$

where $n_v(T)$ is a strong (exponential) function of temperature and increases rapidly with temperature resulting in the decrease of K.

Table 5.4

Normalized conductivity (σ/σ_o) for NaCl-30 m/o Al_2O_3 composites for three different particle sizes of Al_2O_3 at three different temperatures

particle size* of Al_2O_3 (r_A, μm)	inverse part.size r_A^{-1} ($10^4 cm^{-1}$)	σ/σ_o (300°C)	(400°C)	(500°C)
0.05	20	220	114	72
0.3	3.3	55	25	14
1.0	1.0	32	13	7

*As quoted by the manufacturers (Buehler Micropolish II, USA).

The observed and calculated values of the slope (Fig.5.6 and Eq.5.5 respectively) are compared in Table 5.5. It should be pointed out that there is a reasonable agreement between the calculated and the observed values, which once again lends a

strong support to the Maier's theory of heterogeneous doping. It may, however, be noted that the agreement between the calculated and observed values of K is better at higher temperatures.

Table 5.5

Comparison of observed and calculated values of the slope of normalized conductivity (σ/σ_o) vs inverse particle size (r_A^{-1}) in NaCl-30 m/o Al_2O_3 composites

Temperature(^oC)	$K_{obs.}$(cm)	$K_{cal.}$(cm)
300	$9.9x10^{-4}$	$2.2x10^{-4}$
400	$5.4x10^{-4}$	$2.3x10^{-4}$
500	$3.5x10^{-4}$	$2.3x10^{-4}$

The RRN model also qualitatively explains the dependence of conductivity on the particle size of Al_2O_3. Fig. 5.5 shows the variation of conductivity as a function of composition (m/o Al_2O_3) at 500^oC for three different particle sizes of Al_2O_3, viz., 0.05, 0.3 and 1.0 μm). The finer particles have higher specific surface area for a given concentration (m/o) of Al_2O_3, and thus the optimum interface required for maximum conductivity is attained at a lower concentration of the dispersoid. The results of Fig. 5.5 show that the conductivity peak shifts to the right (i.e. towards higher concentration of Al_2O_3) as particle size increases (i.e. specific surface area decreases) and are thus consistent with the RRN model.

5.1.6 Conductivity Vs Temperature :

The log(σ) versus $10^3/T$ behavior for various NaCl-Al_2O_3 composites is shown in Fig. 5.7. The transport parameters, viz., the preexponential factor (σ_o) and the activation energy (E_a), are given in Table 5.6. It is evident from these results that the effect of dispersion is to enhance the conductivity. These results are consistent with those reported earlier for various composite systems.

Table 5.6

Ionic transport parameters, the activation energy (E_a) and the preexponential factor (σ_o), for various NaCl-Al_2O_3 composites

composition (Al_2O_3) (m/o)	(v/o)	temperature range (^oC)	E_a (eV)	σ_o (ohm-cm)$^{-1}$
0	0	300-600	0.82	4.8×10^{-1}
10	10	300-600	0.72	2.6×10^{-1}
20	19	300-600	0.68	1.1
30	29	300-600	0.62	1.7
40	39	300-600	0.69	3.9
50	49	450-600	1.53	9.3×10^{2}

The activation energy obtained for various NaCl-Al_2O_3 composites ($\simeq$ 0.71±0.04 ev) is comparable to the enthalpy of migration for Na^+ ion vacancies reported for pure NaCl (0.8 eV; Dreyfus and Nowick, 1962). This is in accordance with the space charge theory that the excess sodium ion vacancies are induced in the matrix at the interface.

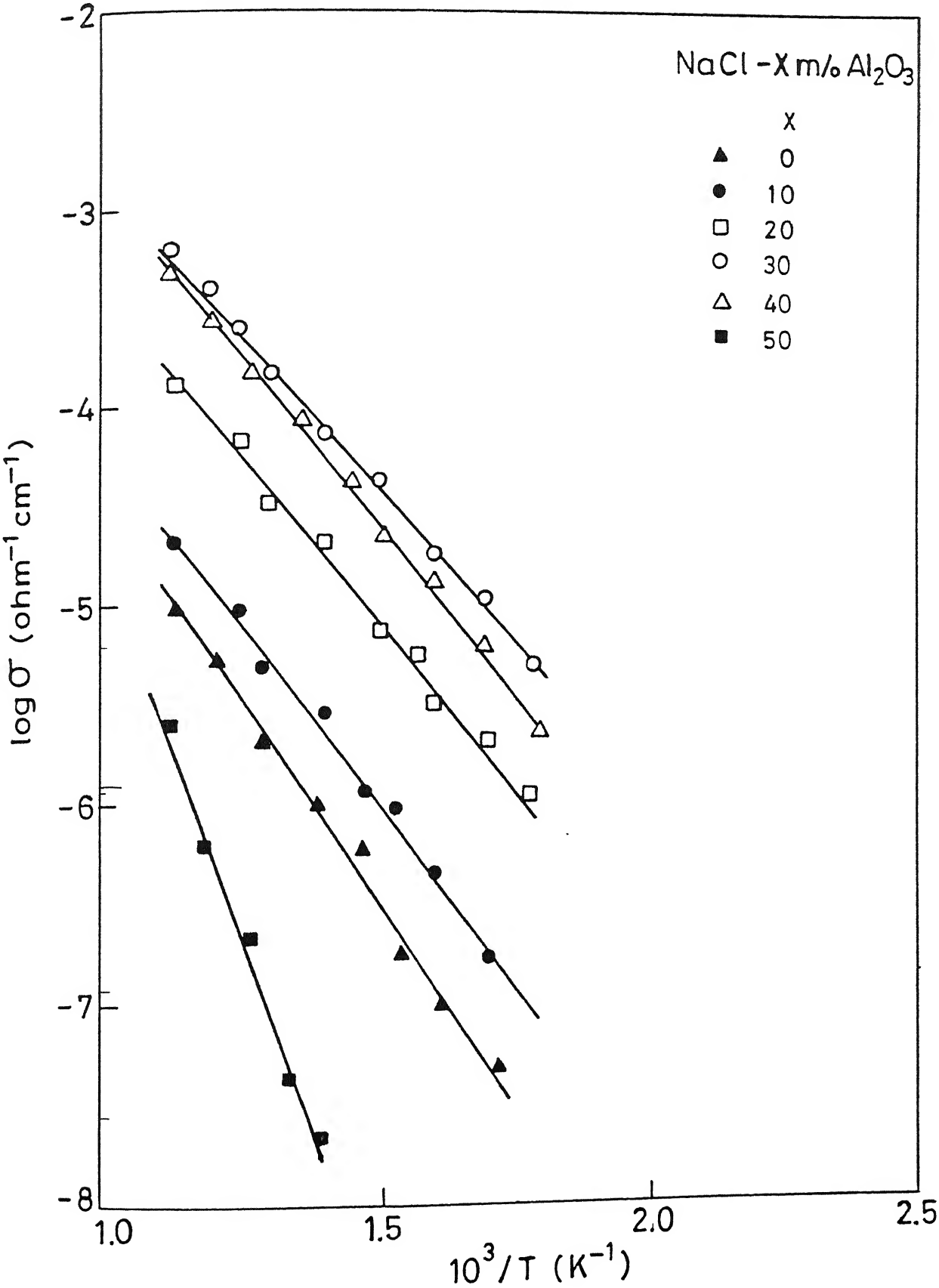

Fig. 5.7 Conductivity as a function of temperature inverse for various NaCl - Al_2O_3 composites.

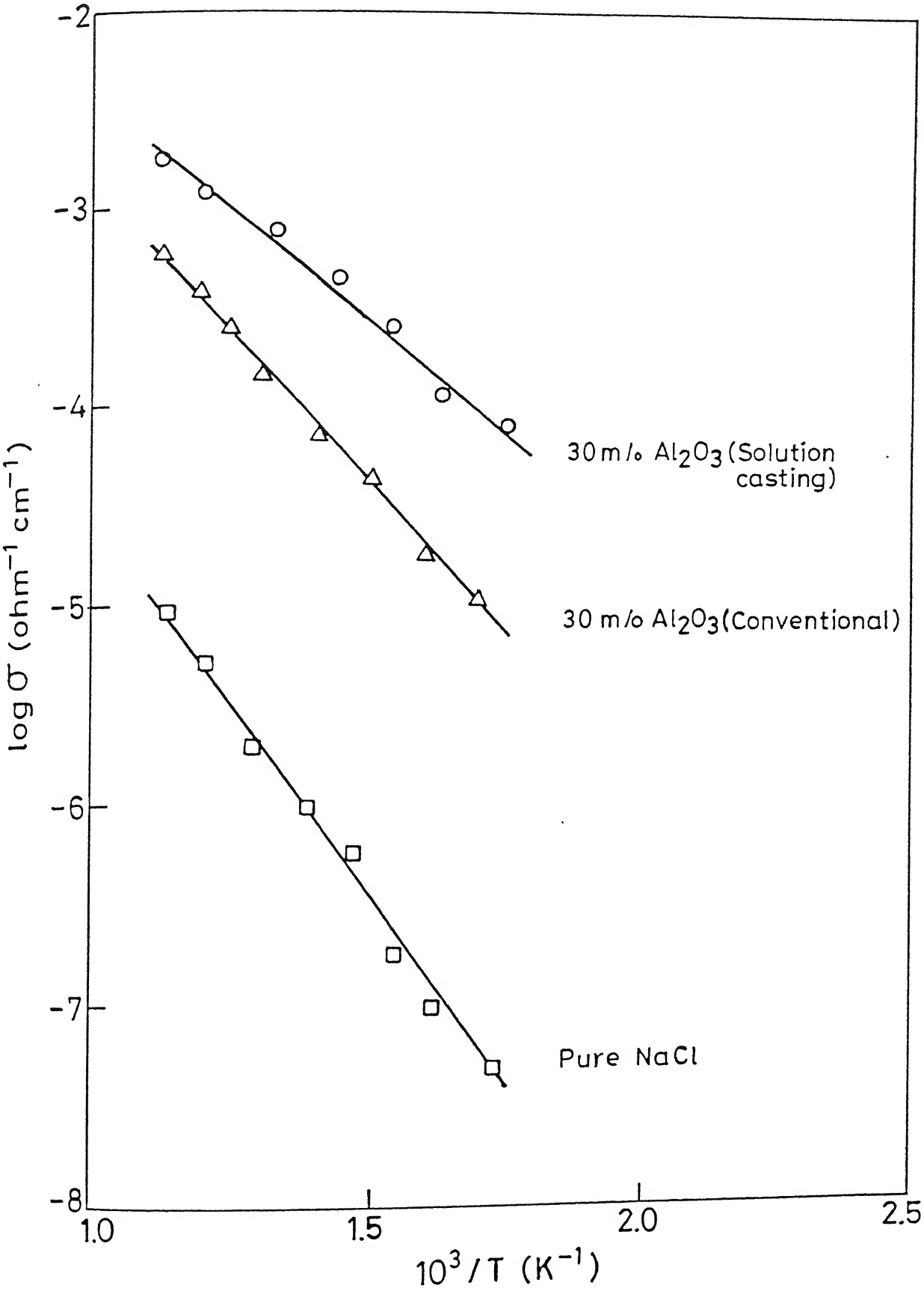

Fig. 5.8 log(σ) vs $10^3/T$ for NaCl-30 m/o Al_2O_3 samples prepared by conventional and solution casting methods.

Fig. 5.8 compares the log(σ) versus $10^3/T$ plots for NaCl-30 m/o Al_2O_3 prepared by the (i) conventional and (ii) solution casting methods. The samples prepared by the latter method show about an order of magnitude higher enhancement in the conductivity as compared to those prepared by conventional method. This result further indicates that the enhancement in conductivity could be due to chemisorbed water molecules on the Al_2O_3 surface. This result is consistent with the space charge theory. The presence of chemical species such as water at the interface may increase the cation disorder reaction giving rise to higher concentration of sodium ion vacancies than in case of dry Al_2O_3 particles.

5.2 KCl-Al_2O_3 System

5.2.1 X-ray Diffraction :

XRD patterns of KCl-40 m/o Al_2O_3 samples before and after heat treatment at 650^{o}C revealed that the samples were biphasic and no additional peak was observed which could be attributed to a new phase. As shown in Fig. 5.9 no difference is discernible between the XRD patterns of the pre-heated (Fig.5.9a) and the post-heated (Fig.5.9b) mixtures of KCl-40 m/o Al_2O_3 samples indicating that the heat treatment merely affected the densification of the mixtures.

5.2.2 Differential Thermal Analysis :

DTA curves (Fig.5.10) for the same samples also show no evidence of any chemical reaction between KCl and Al_2O_3. There is

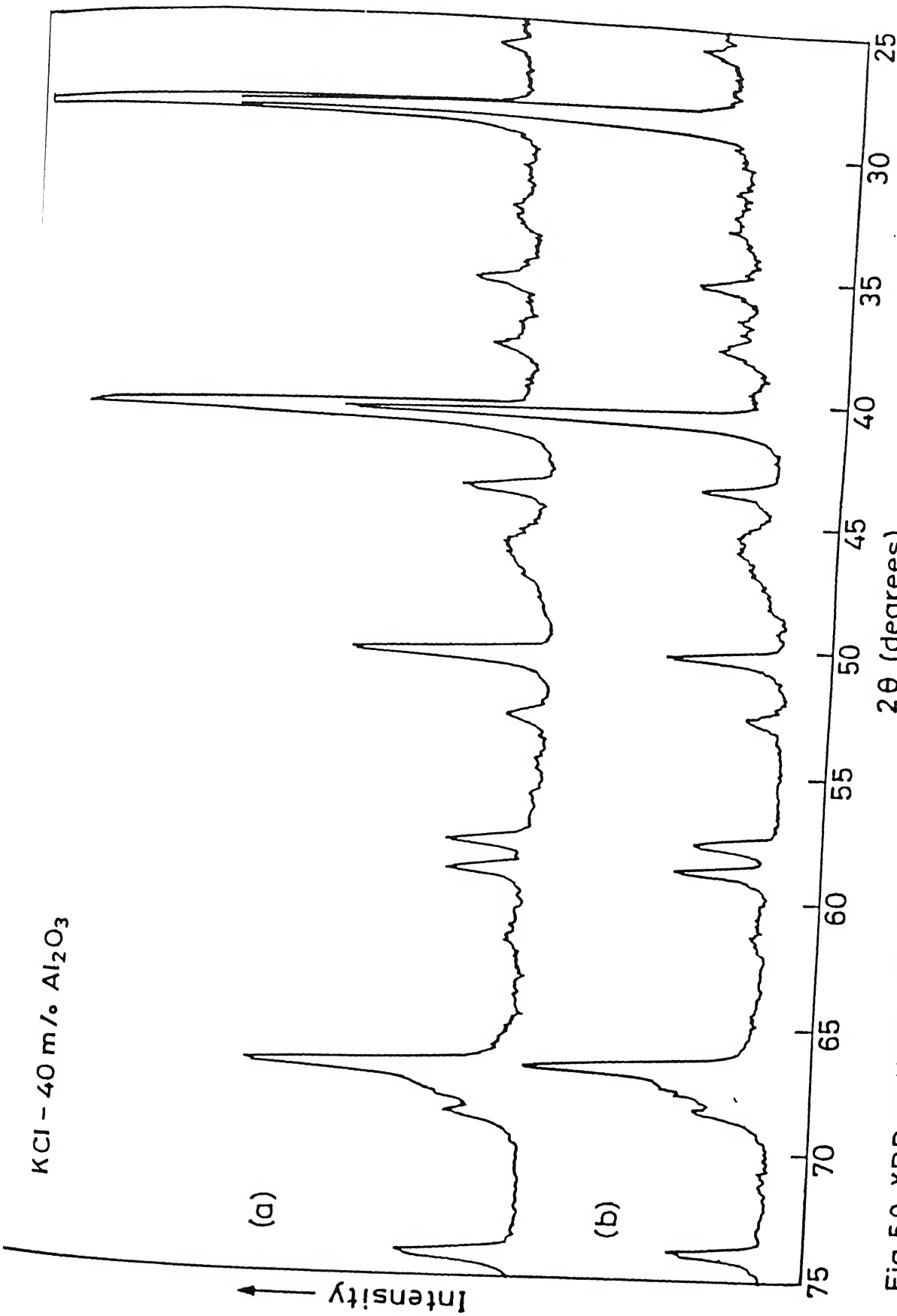

Fig.5.9 XRD patterns for KCl-40 m/o Al_2O_3 samples (a) pre-heated, (b) post-heated at 650°C.

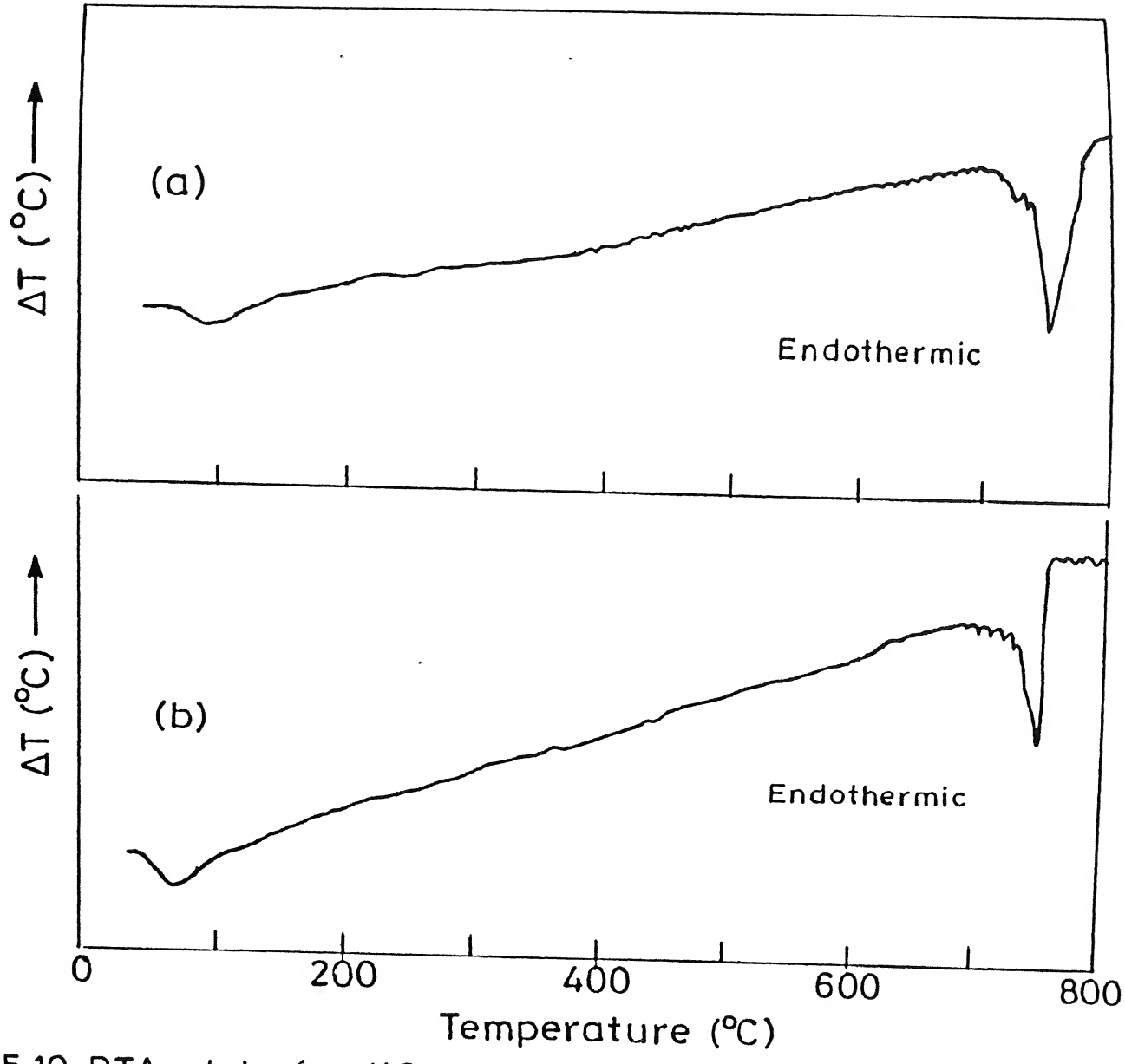

Fig.5.10 DTA plots for KCl -40 m/o Al_2O_3 samples (a) pre-heated (b) post-heated at 650°C.

no apparent shift in the endothermic peak position (curve b) due to the heat treatment, which suggests that there is no solubility of Al_2O_3 in KCl and thus KCl-Al_2O_3 system forms a two-phase composite.

5.2.3 Scanning Electron Microscopy :

SEM micrographs of polished samples of polycrystalline KCl and KCl-30 m/o Al_2O_3 composite sintered at 650°C are shown in Fig.5.11. Fig.5.11a shows that the grains of pure KCl are uniformly distributed. In case of KCl-30 m/o Al_2O_3 sample, the grains are interspersed with the Al_2O_3 particles as shown in Fig. 5.11b. The micrographs suggest that KCl-Al_2O_3 system is a two-phase mixture.

5.2.4 Conductivity vs Composition :

Fig. 5.12 shows the variation of the conductivity as a function of concentration (m/o) of Al_2O_3 in KCl at 500°C for three different sizes of Al_2O_3 particles (0.05, 0.3,and 1.0 μm). Table 5.7 compares the normalized conductivity of various KCl-Al_2O_3 composites at three different temperatures, viz., 300, 400 and 500°C. It is observed that as the concentration of Al_2O_3 increases, the conductivity initially increases slowly, then rather rapidly before it peaks at ~ 45 m/o Al_2O_3. Moreover, as the particle size increases, the enhancement in the conductivity decreases and the maximum in the conductivity occurs at a slightly higher concentration of Al_2O_3. A maximum enhancement in the conductivity by over an order of magnitude occurs for KCl-45 m/o

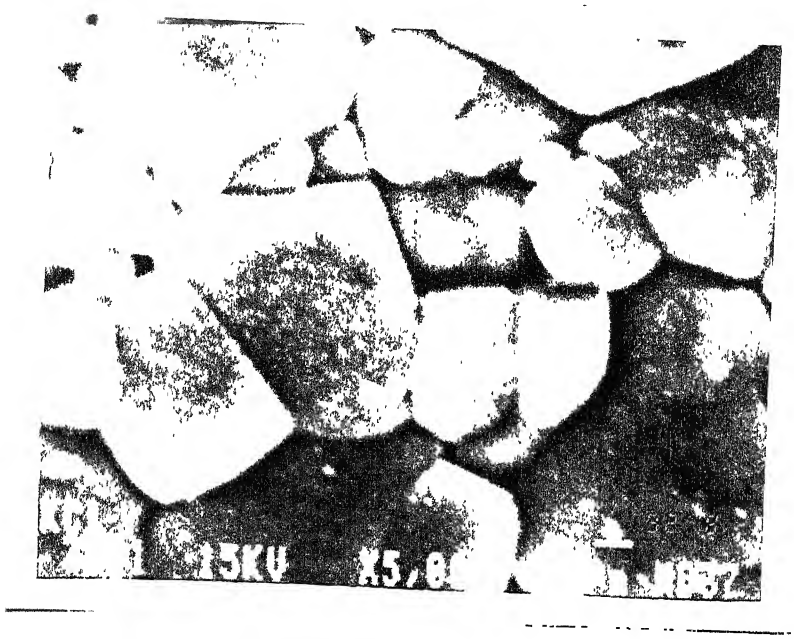

(a)

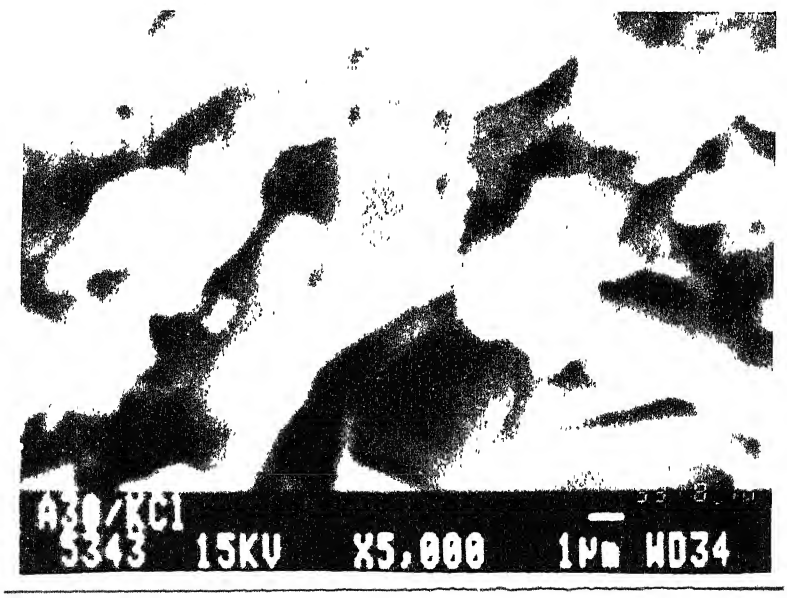

(b)

Fig.5.11 SEM micrographs (a) KCl and, (b) KCl-30 m/o Al_2O_3 composite sintered at 650°C.

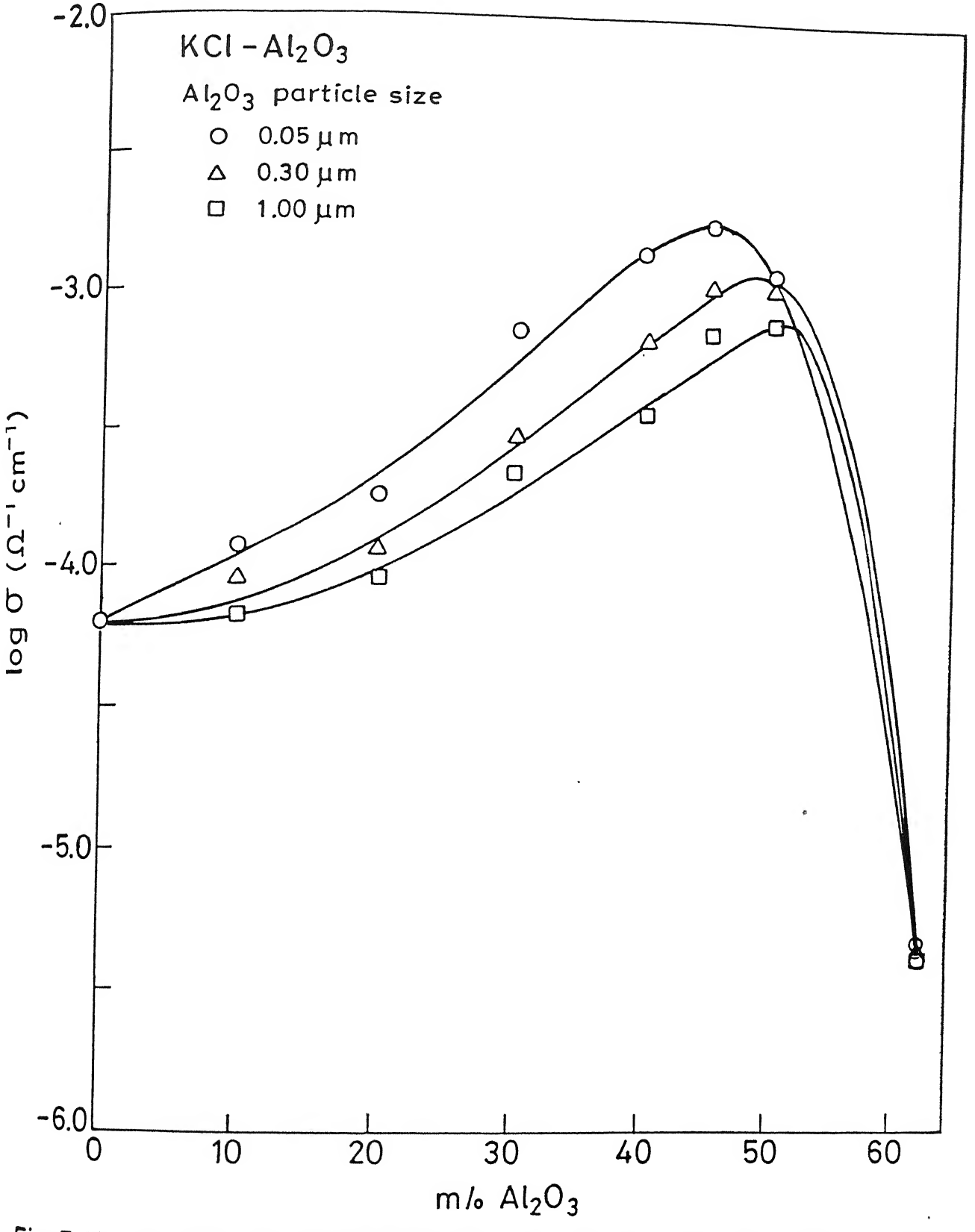

Fig. 5.12 log (σ) vs composition (m/o Al_2O_3) for KCl-Al_2O_3 composites at 500°C for three different particle size of Al_2O_3.

Al_2O_3 composite.

As in case of NaCl-Al_2O_3 and, indeed, other composite systems, one may be inclined to ascribe the conductivity enhancement in KCl-Al_2O_3 composites also to the excess defects (K^+ ion vacancies) generated by the dissolution of Al_2O_3 (in KCl) according to the following equation :

$$Al_2O_3 \Leftrightarrow 2Al_K^{\cdot\cdot} + V_K' + 3O_{Cl}' \qquad (5.7)$$

Thus one molecule of dissolved Al_2O_3 produces one excess cation vacancy. If this were the mechanism of conductivity enhancement in KCl-Al_2O_3 composite systems, a simple calculation using the known mobility values of K^+ ion vacancies (Beaumont and Jacobs, 1966)

Table 5.7

Normalized conductivity (σ/σ_o) for KCl-Al_2O_3 composites of different compositions at three different temperatures

composition (Al_2O_3)		σ/σ_o		
(m/o	(v/o)	(300°C)	(400°C)	(500°C)
0	0	1	1	1
10	7	2.3	2.1	1.8
20	15	4.7	3.5	2.9
30	23	15	12	12
40	31	35	26	22
45	36	80	42	28
50	41	11	15	19

would suggest that only a fraction of a mole percent of Al_2O_3 is required to achieve the observed conductivity enhancement. On the other hand, the experiments show that there is very little enhancement in the conductivity of KCl even by the addition of as large as 10 m/o Al_2O_3 and the maximum enhancement in the conductivity occurs at $\simeq$ 45 m/o Al_2O_3. This clearly suggests that the classical doping mechanism cannot be used to explain the conductivity enhancement in KCl-Al_2O_3 composites. The dispersion of Al_2O_3 may also increase the dislocation density in the host matrix and the excess space charge at the dislocation may contribute to the excess conductivity. However, the dependence of conductivity on the processing parameters and the particle size indicates that the mechanism responsible for conductivity enhancement must involve the matrix-particle interface. The fact that KCl-Al_2O_3 composites exhibit a maximum conductivity at ~45 m/o Al_2O_3 suggests that some sort of high conducting channel forms through the conductor around this composition. It could be either due to formation of a high conducting phase or a space charge layer along the interface.

As brought out in Section 5.1 on NaCl-Al_2O_3 system, Maier's semiquantitative theory appears quite relevant to the composite solid electrolytes, and hence it would be reasonable to discuss the results on KCl-Al_2O_3 system also in view of the above model. Pure KCl, like NaCl, also exhibits Schottky disorder and conducts primarily via cation vacancies below 600^{o}C (Dreyfus and Nowick, 1962; Fuller and Reilly, 1967). The cation and anion vacancies are

formed according to the reaction :

$$O \Leftrightarrow V'_K + V^{\cdot}_{Cl} \qquad (5.8)$$

Due to the condition of local electroneutrality, the concentration of defects (cation and anion vacancies) in the bulk is fixed by the Schottky constant. However, as in case of NaCl crystal, in KCl also near any inhomogeneity, there are more cation vacancies than anion vacancies as the free energy of formation of a cation vacancy $V^{\cdot}_K$ is lower than that of an anion vacancy $V^{\cdot}_{Cl}$ (Dreyfus and Nowick, 1962; Yan et.al., 1977). The introduction of dispersoid causes the cations to be attracted towards the surface of the dispersoid, leaving a depletion zone with a greater concentration of cation vacancies. This depletion zone is the high conducting space charge layer along the matrix-particle interface. The activation energies observed for conduction in various $KCl-Al_2O_3$ composites are comparable to the migration enthalpies of K^+ ion vacancies in pure KCl (Dreyfus and Nowick, 1962). This is consistent with the theory that the excess cation vacancies are induced in the matrix at the interface.

Table 5.8 lists the calculated and observed conductivities for $KCl-Al_2O_3$ composites at 300^oC. The values have been calculated from Eq.(5.2) by taking β_L = 0.5, r_A=0.05 μm, ε(KCl) ≃ 6, V^m=37.6 cm^3/mol, $N_{vo} \simeq 1$ and the following expression for mobility of K^+ ion vacancies μ_{K^+} (Beaumont and Jacobs, 1966) :

$$\mu_{K^+} = \frac{1275}{T} \exp(-8232/T) \qquad cm^2\ V^{-1}s^{-1} \qquad (5.9)$$

Table 5.8

Observed and calculated conductivities for various $KCl-Al_2O_3$ composites at 300°C

composition (Al_2O_3) (m/o)	(v/o)	$\sigma_{obs.}$ (ohm-cm)$^{-1}$	$\sigma_{cal.}$ (ohm-cm)$^{-1}$
0	0	2.6×10^{-7}	2.6×10^{-7}
10	7	6.3×10^{-7}	5.8×10^{-7}
20	15	1.2×10^{-6}	9.3×10^{-7}
30	23	4.0×10^{-6}	1.3×10^{-6}
40	31	9.1×10^{-6}	1.7×10^{-6}
45	36	2.1×10^{-5}	1.8×10^{-6}

The calculated and the observed values of conductivities are in reasonably good agreement especially at lower concentrations of Al_2O_3 which implies that the space charge layer mechanism of conduction is appropriate for the composites. However, it may be pointed out that the theoretical Eq.5.2 consistently underestimates the calculated values of conductivity at higher concentrations of the dispersoid. Similar discrepancy was also observed in case of $NaCl-Al_2O_3$ system (Table 5.3).

The electrical conductivity data on $KCl-Al_2O_3$ composite system also appear to be consistent with the random resistor network model (Roman et.al., 1986) which predicts, as pointed out earlier, two critical concentrations, p_c' and p_c'' of the

dispersoid. Below p_c' the conductivity of the composite does not change much and beyond p_c'' it drops rapidly because the connected pathways get disrupted as they begin to form closed loops at higher concentrations of Al_2O_3. An inspection of Fig.5.12 indeed reveals that the conductivity (σ) of KCl containing Al_2O_3 particles, especially of 1 μm size, remains almost unaffected upto a concentration of (p_c'=) 10 m/o and drops rapidly beyond (p_c''=) 50 m/o Al_2O_3. This latter value of 50 m/o for p_c'' is larger than that (~35 m/o) observed in case of NaCl-Al_2O_3 system (Fig.5.4).

5.2.5 Conductivity Versus Particle Size :

As discussed in Section 5.1.5, almost all the models presume formation of space charge layer and predict faster ion transport due to finer particles of dispersed phase. Equally true is the fact that almost all investigations on composite solid electrolytes are *qualitatively* in conformity with the above prediction. However, for a direct, quantitative comparison of the theory (Eq.5.4), with the experiment, the conductivity data on KCl-Al_2O_3 system may be plotted in the form of (σ/σ_o) vs inverse particle size ($1/r_A$) of Al_2O_3.

Table 5.9 lists the normalized conductivity, σ(composite)/σ_o (salt), for KCl containing 45 m/o Al_2O_3 of three different particle sizes, viz., 0.05, 0.3, 1.0 μm, at three different temperatures. Inverse particle size ($1/r_A$) of Al_2O_3 is also listed in Table 5.9. Even a crude inspection of this data immediately discloses the inverse relation between the conductivity and the

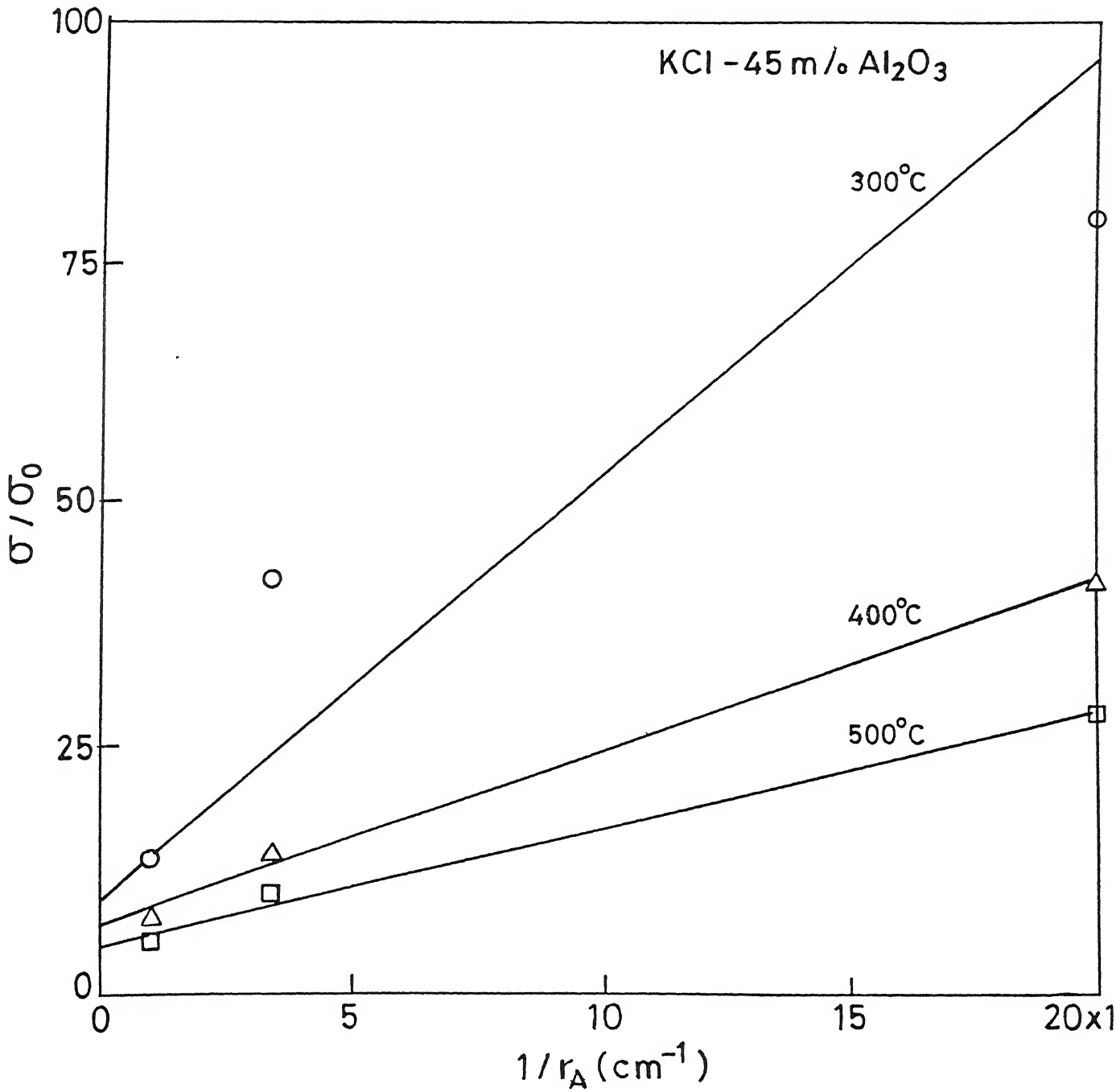

Fig. 5.13 Normalized conductivity (σ/σ_0) vs inverse particle size of Al_2O_3 for KCl - 45 m/o Al_2O_3 composite at three different temperatures.

noticed, however, that there is a serious discrepancy between the observed and calculated values. The reasons are not immediately clear. It may be mentioned that a reasonably good agreement was found in case of $NaCl-Al_2O_3$ (Section 5.1.1) and $RbCl-Al_2O_3$ systems (to be discussed in Section 5.3.5). The above discrepancy may perhaps arise due to inaccurate values of mobility of K^+ ion vacancies (Eq.5.9) used in the calculation.

The RRN model also qualitatively explains the dependence of conductivity on the particle size of Al_2O_3. The finer particles have higher surface area for a given concentration (m/o) of Al_2O_3, and thus the optimum interface required for maximum conductivity is attained at a lower concentration for finer Al_2O_3 particles. The results in Fig. 5.12 show that the conductivity peak shifts towards the higher concentration of Al_2O_3 as particle size increases (i.e. surface area decreases). Thus the results are consistent with the random resistor network model which assumes the formation of a high-conducting layer at the matrix/particle interface and therefore provide support to the Maier's space charge theory. Fig.5.12 also shows that at a given temperature and composition, the conductivity is lower for a higher particle size of Al_2O_3. The results in Table 5.9 also show that as the particle size increases the conductivity decreases and the enhancement in conductivity is higher at lower temperatures. These observations are in conformity with the results reported earlier for a variety of systems and are consistent with the space charge theory

5.2.5 Conductivity vs Temperature :

The log(σ) vs 10^3/T plots for various KCl-Al_2O_3 composites are shown in Fig.5.14. It is evident that the effect of dispersion of Al_2O_3 is to increase the conductivity appreciably. The logσ vs 1/T plots for all the composites are linear as expected. The transport parameters, viz., the preexponential factor (σ_o) and the activation energy (E_a), are given in Table 5.11 for all the KCl-Al_2O_3 composites studied in this work.

Table 5.11

Ionic transport parameters, the activation energy (E_a) and the preexponential factor (σ_o), for various KCl-Al_2O_3 composites

composition (Al_2O_3) (m/o)	(v/o)	temperature range (^oC)	E_a (eV)	σ_o $(ohm\text{-}cm)^{-1}$
0	0	300-600	1.03	3.2×10^2
10	7	300-600	0.99	3.4×10^2
20	15	300-600	0.93	2.0×10^2
30	23	300-600	1.09	2.0×10^3
40	31	300-600	0.94	1.8×10^3
45	36	300-600	0.89	1.2×10^3
50	41	300-600	0.99	2.0×10^3
60	51	450-600	1.83	3.1×10^6

The ionic conductivity values and the transport parameters for pure KCl are in agreement with the literature values (Beaumont and Jacobs, 1966). While the KCl-Al_2O_3 composites exhibit

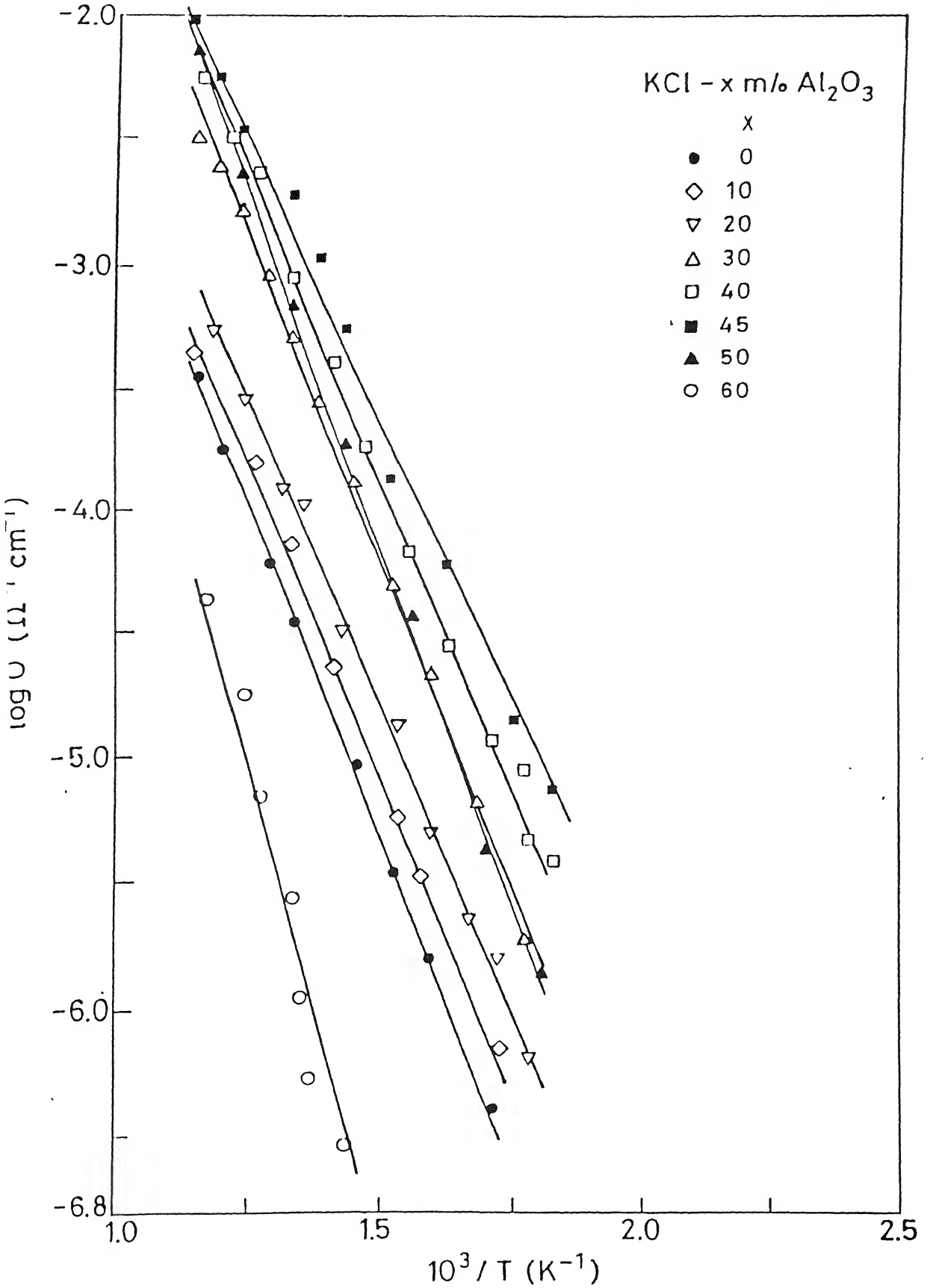

ig.5.14 log (σ) vs 10^3/T for various KCl - Al_2O_3 composites.

appreciably higher conductivity, their activation energies remain almost nearly constant within ±10 %; the average activation energy being ~0.97 eV which is very close to that of pure KCl, which implies that the dominant conduction mechanism in the composites is same as that in pure KCl, viz., via K^+ ion vacancies. This reaffirms the earlier assertion that the positively charged species (K^+ ions) are attracted towards the surface of the dispersoids (Al_2O_3) particles and thereby excess K^+ ion vacancies are created in the interface region leading to the enhanced conductivity.

Fig.5.15 compares the logσ versus $10^3/T$ behavior for KCl-45 m/o Al_2O_3 samples prepared by the (i) conventional and (ii) solution casting methods. It is evident that the samples prepared by the solution casting method show about an order of magnitude higher conductivity than those prepared by conventional method. As pointed out earlier, in the solution casting method, Al_2O_3 is added in the solution containing ionized alkali salts. This may lead to better stabilization of cations at the interface resulting in higher concentrations of cation vacancies in the space charge layer in the vicinity of Al_2O_3 particles. Thus these results suggest that the matrix-particle interface plays a dominant role in the conductivity enhancement. Larger concentration of defects is introduced in the space charge region in the samples prepared by the solution casting method resulting in higher enhancement in conductivity.

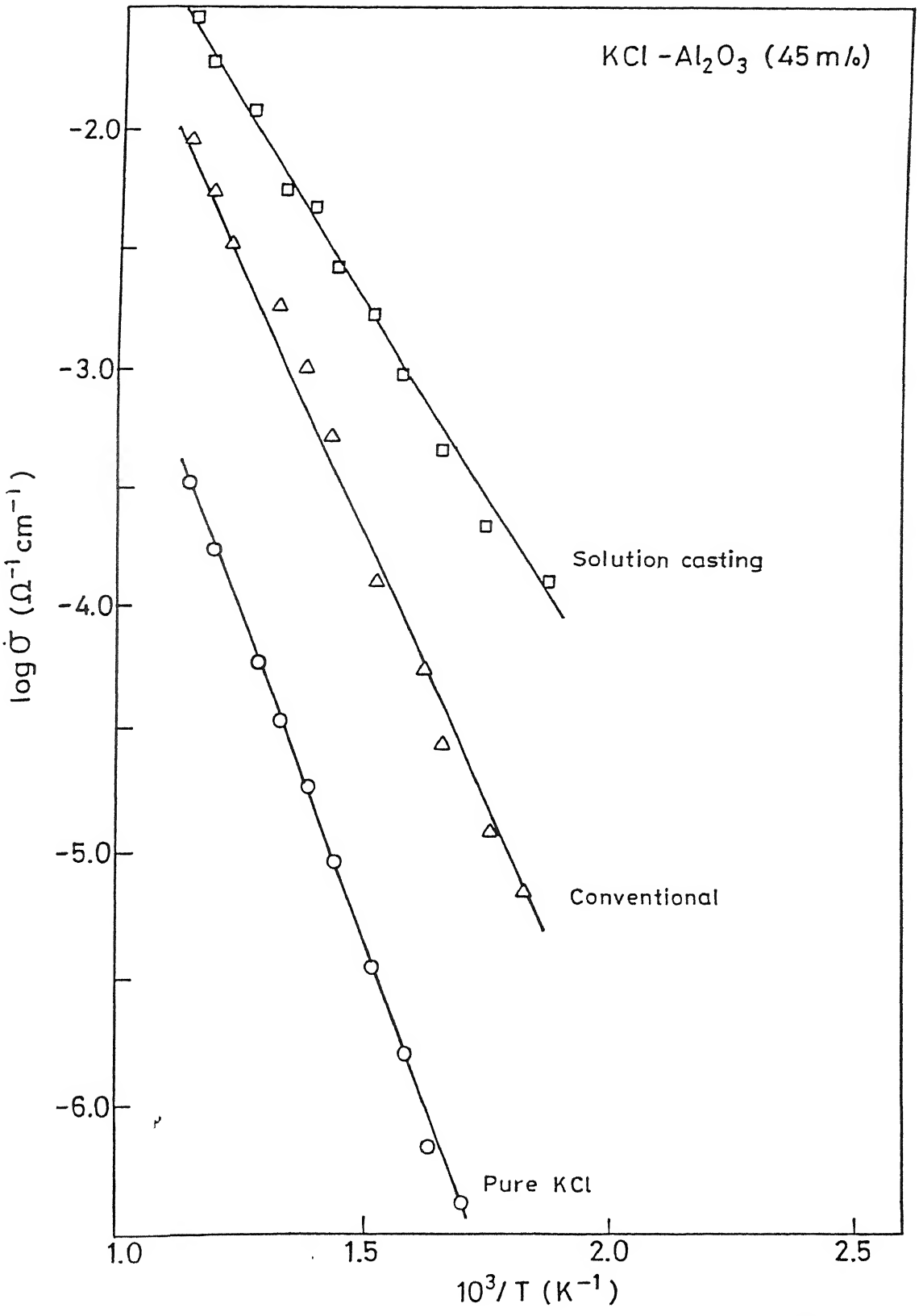

Fig.5.15 Conductivity vs temperature inverse for KCl - 45 m/o Al_2O_3 samples prepared by conventional and solution casting methods

5.3 RbCl - Al_2O_3 Systems :

5.3.1 X-ray Diffraction :

Fig.5.16 shows the room temperature XRD patterns of RbCl-40 m/o Al_2O_3 samples before (curve a) and after (curve b) heat treatment at 600°C. No additional peak was observed after the heat treatment which could be attributed to a new phase. This indicates that the heat treatment merely affected the densification of the mixture and samples remain biphasic mixture of RbCl and Al_2O_3.

5.3.2 Differential Thermal Analysis :

The DTA curves (Fig.5.17) for pure RbCl and RbCl-40 m/o Al_2O_3 also show no evidence of any chemical reaction between RbCl and Al_2O_3. The endothermic peak corresponding to the melting point of RbCl (curve a) remains unaffected due to the dispersion of Al_2O_3 which suggests that there is no solubility of Al_2O_3 in RbCl (curve b) even at the elevated temperatures near the melting point.

5.3.3 Scanning Electron Microscopy :

SEM micrographs of well polished samples of polycrystalline RbCl and RbCl-30 m/o Al_2O_3 sintered at 600°C are shown in Fig.5.18. It is observed that the RbCl grains are uniformly distributed (Fig.5.18a) whereas in case of RbCl-30 m/o Al_2O_3 the grains are interspersed with the Al_2O_3 particles as shown in Fig.5.18b which signifies that RbCl-Al_2O_3 system is a two-phase composite.

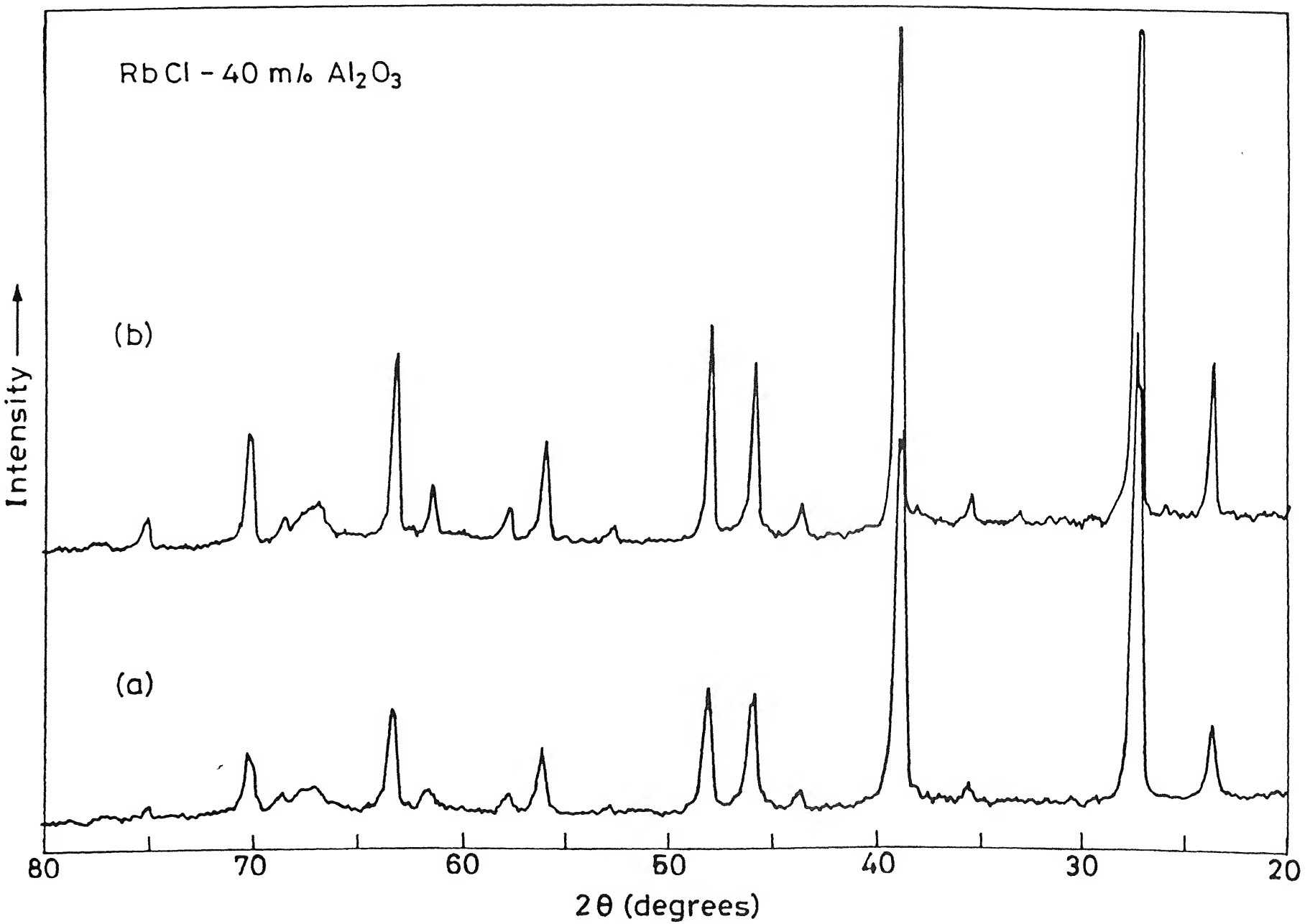

Fig. 5.16 XRD patters for RbCl-40 m/o Al_2O_3 (a) pre-heated, (b) post-heated at 600°C

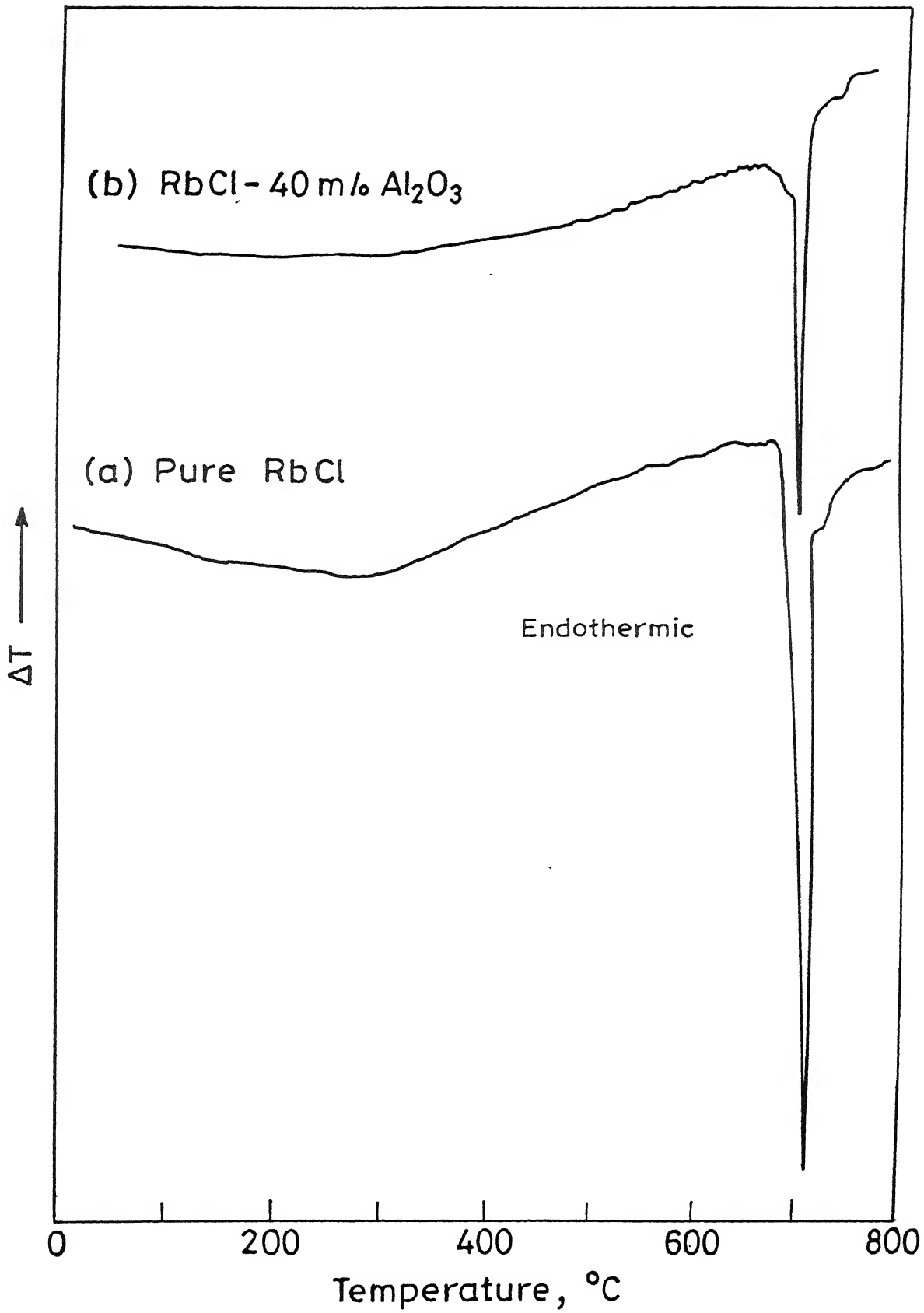

Fig. 5.17 DTA curves for (a) pure RbCl, (b) RbCl-40 m/o Al_2O_3 samples.

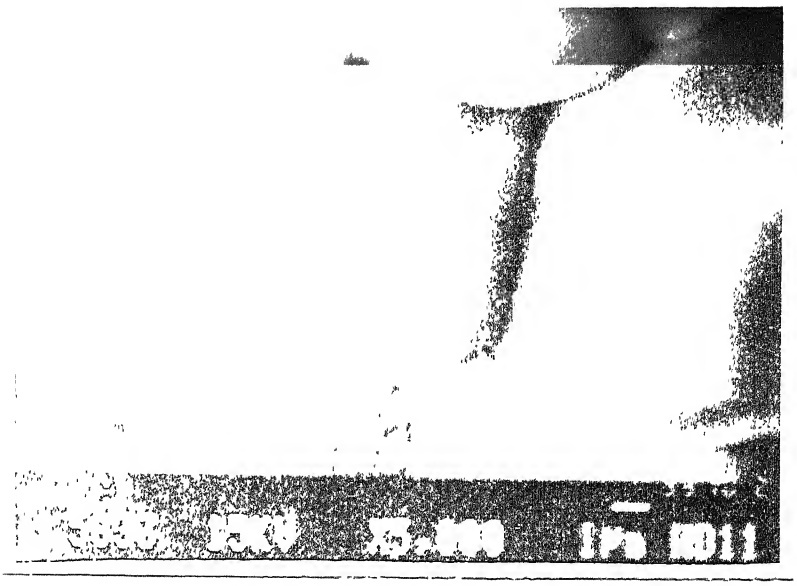

(a)

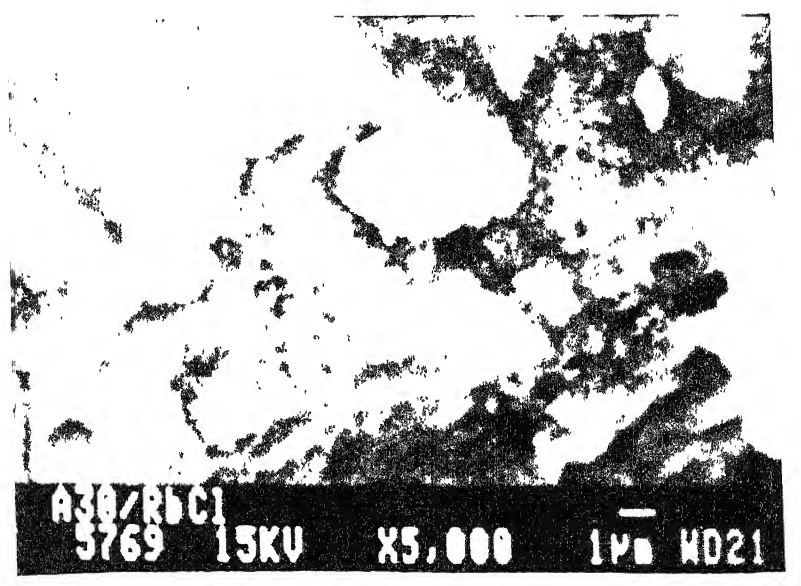

(b)

Fig. 5.18 SEM micrographs for (a) RbCl and, (b) RbCl-30 m/o Al_2O_3 composite sintered at 600°C.

5.3.4 Conductivity vs Composition :

Fig.5.19 shows the conductivity versus composition behavior for RbCl-Al_2O_3 composite system at 500°C for three different particle sizes of Al_2O_3, viz., 0.05, 0.3 and 1.0 μm. Table 5.12 compares the normalized conductivity, σ(composite)/σ_o(host), for various RbCl-Al_2O_3 composites at 300, 400 and 500°C. These results show that as the concentration of Al_2O_3 increases, the conductivity increases before it peaks at ~ 40 m/o Al_2O_3. As the particle size increases the enhancement in conductivity decreases and also the maximum in the conductivity is obtained at lower concentrations of Al_2O_3. Table 5.12 shows that the enhancement in conductivity is by over two orders of magnitude for RbCl-40 m/o Al_2O_3 system, and the enhancement in σ is more pronounced at lower temperatures for a given composite.

Table 5.12

Normalized conductivity (σ/σ_o) for RbCl-Al_2O_3 composites of various compositions at three different temperatures

composition (Al_2O_3)		σ/σ_o		
(m/o)	(v/o)	(300°C)	(400°C)	(500°C)
0	0	1	1	1
10	6	75	71	36
20	13	3.8×10^2	3.3×10^2	1.2×10^2
30	20	5.0×10^2	4.5×10^2	2.8×10^2
40	28	7.9×10^2	5.0×10^2	4.2×10^2
50	37	1.3×10^2	2.5×10^2	1.8×10^2
55	42	-	6.5	10

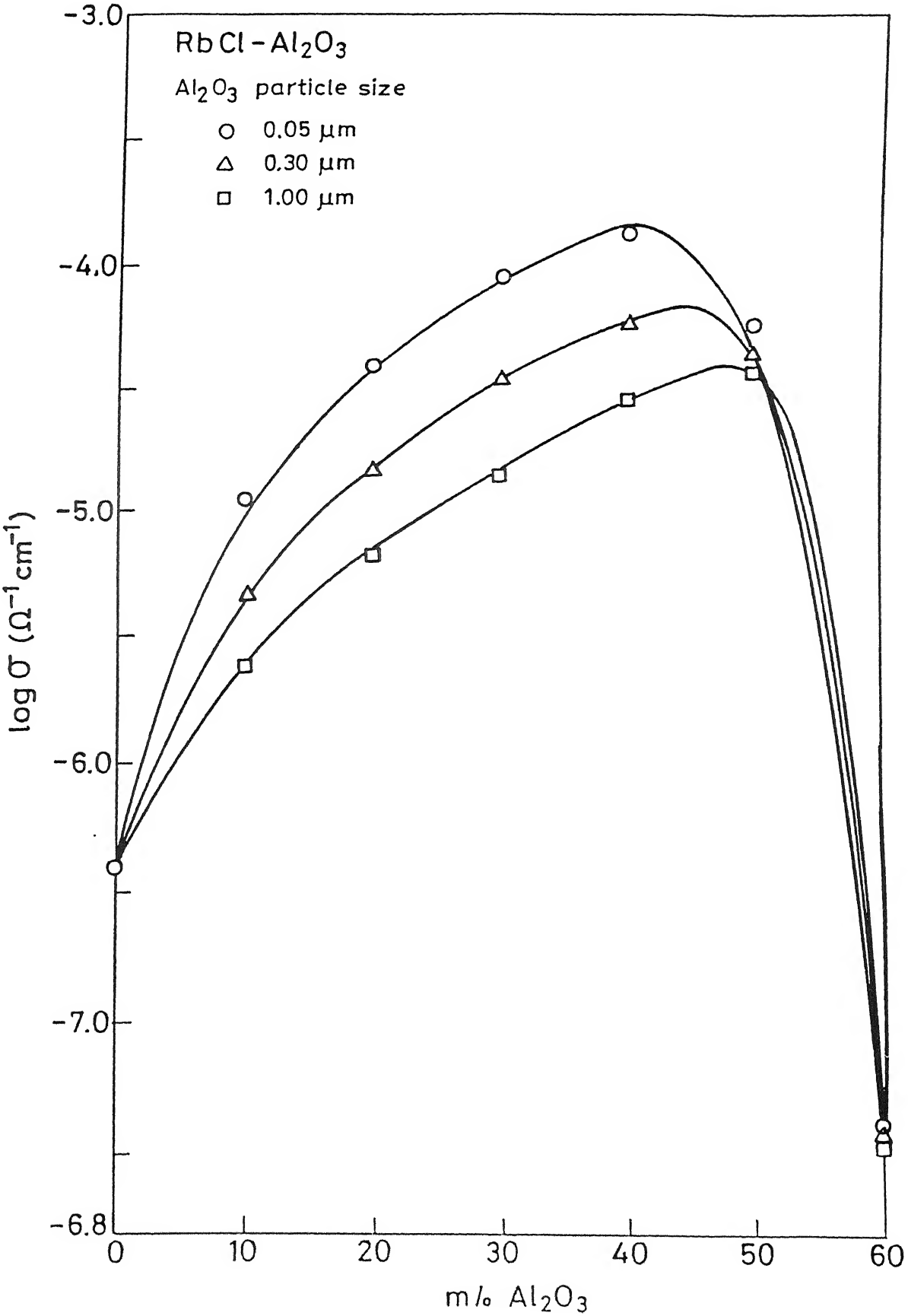

Fig.5.19 log (σ) vs composition (m/o Al_2O_3) for RbCl-Al_2O_3 composites at 500°C for three different particle sizes of Al_2O_3.

As discussed previously, the classical doping mechanism cannot be used to explain the enhancement in the conductivity of $RbCl-Al_2O_3$ system also, because the dissolution of Al_2O_3 in RbCl will produce excess of Rb^+ ion vacancies according to the following relation :

$$Al_2O_3 \Leftrightarrow 2Al^{\cdot\cdot}_{Rb} + V'_{Rb} + 3O'_{Cl} \qquad (5.10)$$

Thus, as a simple calculation using known mobility values of Rb^+ ion vacancy in RbCl (Laurent and Benard, 1957) would demonstrate, only a fraction of a mole percent of Al_2O_3 is required to achieve the observed conductivity enhancement at 300^oC. On the other hand the experiments show that there is only a nominal enhancement in the conductivity of RbCl even with the addition of as large as 10 m/o of Al_2O_3, and that the maximum enhancement in conductivity occurs at ~40 m/o Al_2O_3 for $RbCl-Al_2O_3$. This clearly suggests that the classical doping mechanism cannot explain the conductivity enhancement in $RbCl-Al_2O_3$ composites. The dispersion of Al_2O_3 may also increase the dislocation density in the host matrices and the excess space charge at the dislocation may contribute to the excess conductivity. However, the dependence of conductivity on the processing and particle size indicates that the mechanism responsible for conductivity enhancement must involve the matrix-particle interface. The activation energies for various $RbCl-Al_2O_3$ composites are comparable to the Rb^+ vacancy migration enthalpies reported for pure RbCl (Fuller et.al.1968). This is in

accordance with the space charge theory that the excess cation vacancies are induced in the matrix at the interface. It would therefore be only appropriate to discuss the conductivity versus composition results on $RbCl-Al_2O_3$ also in view of space charge theory advanced by Jow and Wagner (1982) and developed by Maier (1984,1985,1986,1987).

The enhanced conductivity of a composite solid electrolyte, according to space charge theory (Maier, 1985) is given by Eq.(5.2). The σ values for $RbCl-Al_2O_3$ have been calculated from this equation using, β_L = 0.5, r_A=0.05 μm, $\varepsilon \simeq 6$, V^m=43.2 cm^3/mol and $N_{vo} \simeq 1$. In the absence of any report on the mobility of charge carriers in RbCl at lower temperatures, we have relied on the extrapolated values of mobility of Rb^+ ion vacancies in RbCl. A value of $D_o \simeq 1x10^{-3}$ cm^2/s (Arai and Mullen, 1966) and $E_a \simeq 0.33$ eV in the extrinsic region obtained in this work (see Section 5.3.6) have been used to calculate the diffusion coefficient D_{Rb^+} and hence mobility, (μ_{Rb^+}), from the Nernst-Einstein relation μ=eD/kT, of the Rb^+ ion vacancies in RbCl at different temperatures. The mobility of Rb^+ ion vacancies so obtained is given below :

$$\mu_{Rb^+} = \frac{12}{T}\exp(-3826/T) \qquad cm^2\ V^{-1}s^{-1} \qquad (5.11)$$

The calculated values of conductivity are compared with the observed values in Table 5.13. There is a fair agreement between the two values except for the 10 m/o Al_2O_3 sample for which the calculated value is nearly four times higher than the observed

one. Nevertheless, the overall agreement between the calculated and observed values suggests that the space charge theory of electrical conductivity is appropriate for the composites.

Table 5.13

Observed and calculated values of conductivity for various $RbCl-Al_2O_3$ composites at 300^oC

composition (Al_2O_3) (m/o)	(v/o)	$\sigma_{obs.}$ $(ohm-cm)^{-1}$	$\sigma_{cal.}$ $(ohm-cm)^{-1}$
0	0	$1.6x10^{-8}$	$1.6x10^{-8}$
10	6	$1.2x10^{-6}$	$5.2x10^{-6}$
20	13	$5.3x10^{-6}$	$1.1x10^{-5}$
30	20	$8.0x10^{-6}$	$1.7x10^{-5}$
40	28	$1.3x10^{-5}$	$2.4x10^{-5}$

The macroscopic random resistor network (RRN) model (Roman et.al.,1986) also appears reasonable in view of the data on $RBCl-Al_2O_3$ system. That the conductivity versus composition behavior (Fig.5.19) exhibits a sharp maximum at ~ 40 m/o Al_2O_3, and the σ drops rapidly beyond ~ 45 m/o Al_2O_3 and the maximum in the conductivity curve shifts to higher concentration of Al_2O_3 for larger particle size of Al_2O_3, are all consistent with the RRN model. The only discrepancy that may be noted is the lack of evidence for a lower critical concentration (p_c') of Al_2O_3 because there is substantial enhancement in the conductivity of RbCl containing just 10 m/o Al_2O_3.

5.1.5 Conductivity Versus Particle Size :

Space charge theory (Jow and Wagner, 1979; Maier, 1985,1986; Bunde et.al., 1985) can be further tested in view of the conductivity (σ) versus particle size (r_A) of the dispersoid (Al_2O_3) data on RbCl-Al_2O_3 system. The above theory predicts an inverse relation between the normalized conductivity, σ(composite)/σ_o(host), and the particle size (r_A) of the dispersoid as given by Eq.(5.4), rewritten below for ready reference :

$$\frac{\sigma}{\sigma_o} = (1-\varphi_A) + \frac{K}{r_A} \qquad (5.4)$$

where the symbols have their usual meaning (Section 5.1.5). Table 5.14 lists the particle size, inverse particle size and the experimental values of (σ/σ_o) for RbCl-40 m/o Al_2O_3 at three different temperatures, viz., 300, 400, 500^oC. Even a glance of the data shown in Table 5.14 reveals the inverse relationship between the conductivity and the the particle size, as predicted by the theory (Eq.5.2). However, for a closer comparison, (σ/σ_o) is plotted against $1/r_A$ in Fig.5.20. It is observed that all the three graphs are fairly good straight lines, and their slope decreases as the temperature increases which is consistent with the prediction of the model (Eq.5.5).

Lastly, the observed and the calculated values of the slope (Fig.5.20 and Eq.5.4 respectively) are compared in Table 5.15. It should be pointed out that the agreement between the calculated and the observed values is surprisingly good, which once again

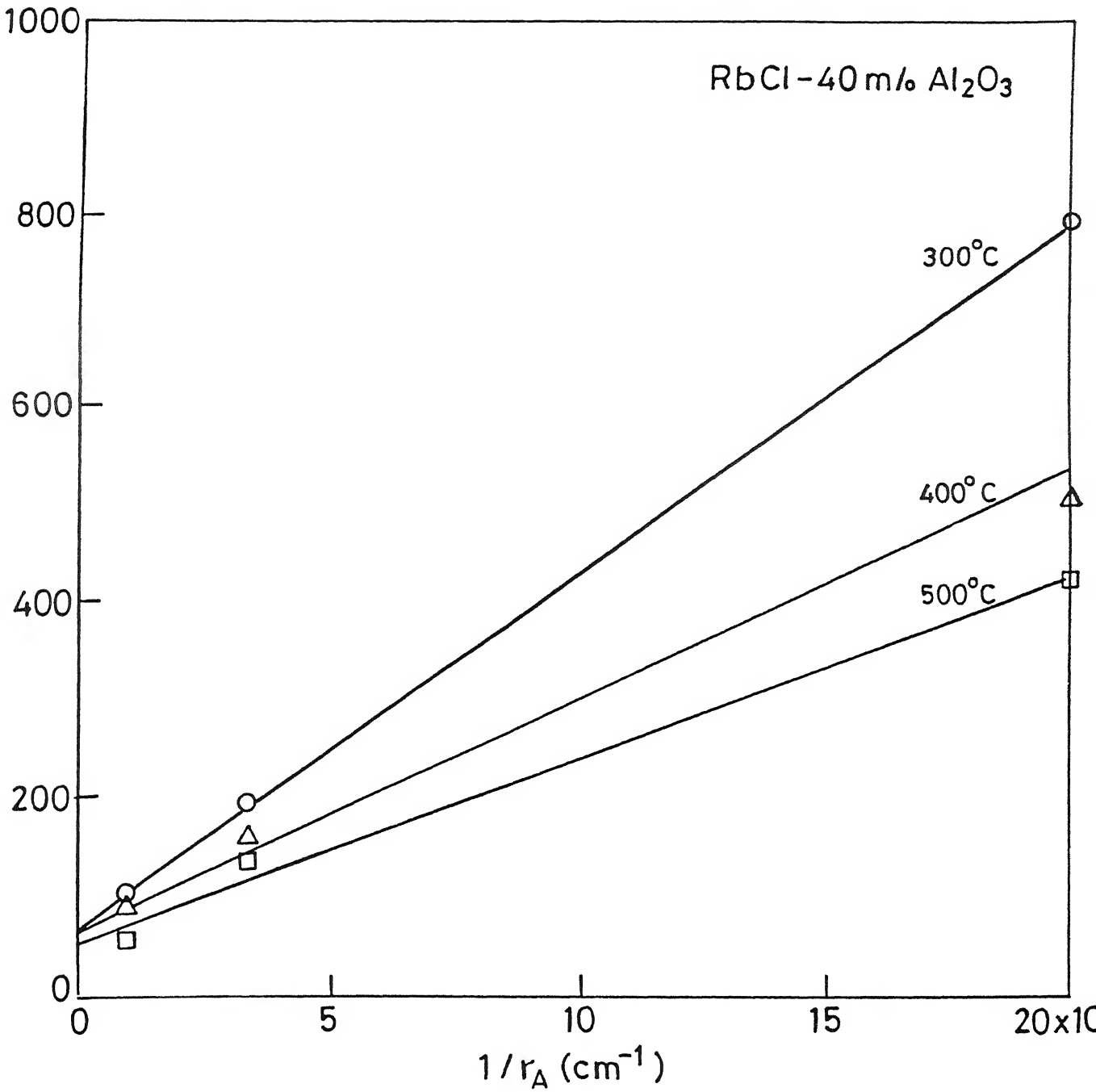

Fig. 5.20 Normalized conductivity (σ/σ_0) vs inverse particle size of Al_2O_3 for RbCl-40 m/o Al_2O_3 composite at three different temperatures.

lends a strong support to the Maier's theory of heterogeneous doping.

Table 5.14

Normalized conductivity (σ/σ_o) for RbCl-40 m/o Al_2O_3 composites for three different particle sizes of Al_2O_3 at three different temperatures

particle size* of Al_2O_3, r_A (r_A, μm)	inverse part.size r_A^{-1} ($10^4 cm^{-1}$)	σ/σ_o (300°C)	σ/σ_o (400°C)	σ/σ_o (500°C)
0.05	20	7.9×10^2	5.0×10^2	4.2×10^2
0.3	3.3	1.9×10^2	1.6×10^2	1.3×10^2
1.0	1.0	1.0×10^2	84	53

*As quoted by the manufacturers (Buehler Micropolish II, USA).

Table 5.15

Comparison of observed and calculated values of the slope of the normalized conductivity (σ/σ_o) vs inverse particle size (r_A^{-1}) in RbCl-40 m/o Al_2O_3

Temperature(°C)	$K_{obs.}$(cm)	$K_{cal.}$(cm)
300	3.7×10^{-3}	7.4×10^{-3}
400	2.4×10^{-3}	6.3×10^{-3}
500	1.9×10^{-3}	1.6×10^{-3}

The RRN model is also consistent with the results on RbCl-Al_2O_3 (Fig.5.19) which show that the conductivity peak shifts to the right (i.e. towards higher concentration of Al_2O_3) as particle size increases (i.e. specific surface area decreases).

The finer particles have higher specific surface area for a given concentration (m/o) of Al_2O_3, and thus the optimum interface required for maximum conductivity is attained at a lower concentration of the dispersoid.

5.3.6 Conductivity versus Temperature :

The log σ vs $10^3/T$ plots for various RbCl-Al_2O_3 composite systems are shown in Fig.5.21. The plots in general consist of two linear segments; a low temperature segment called extrinsic region and a high temperature segment known as intrinsic region. The latter is associated with a higher activation energy. As the concentration of Al_2O_3 in RbCl increases, the conductivity increases as expected. Moreover, the extrinsic-intrinsic transition (or knee) temperature also increases. The transport parameters, the preexponential factor (σ_o) and the activation energy (E_a) for all the composites are listed in Table 5.16. The σ_o and E_a values for pure RbCl found in this work are comparable to those reported in the literature (Pierce, 1961; Arai and Mullen, 1966; Fuller and Reilly, 1967). As the concentration of Al_2O_3 in the RbCl-Al_2O_3 composite increases, the activation energy in the low temperature (extrinsic) region is not seriously affected; $E_a \simeq 0.35$ eV in the composites is comparable to that in the pure RbCl ($\simeq 0.33$ eV; Pierce, 1961), which suggests that the dominant conduction mechanism in RbCl and RbCl-Al_2O_3 composites is same, viz., via Rb^+ ion vacancies. Thus the results reinforce the space charge mechanism which postulates that the positively charged species (Rb^+ion) are attracted towards the Al_2O_3 surface

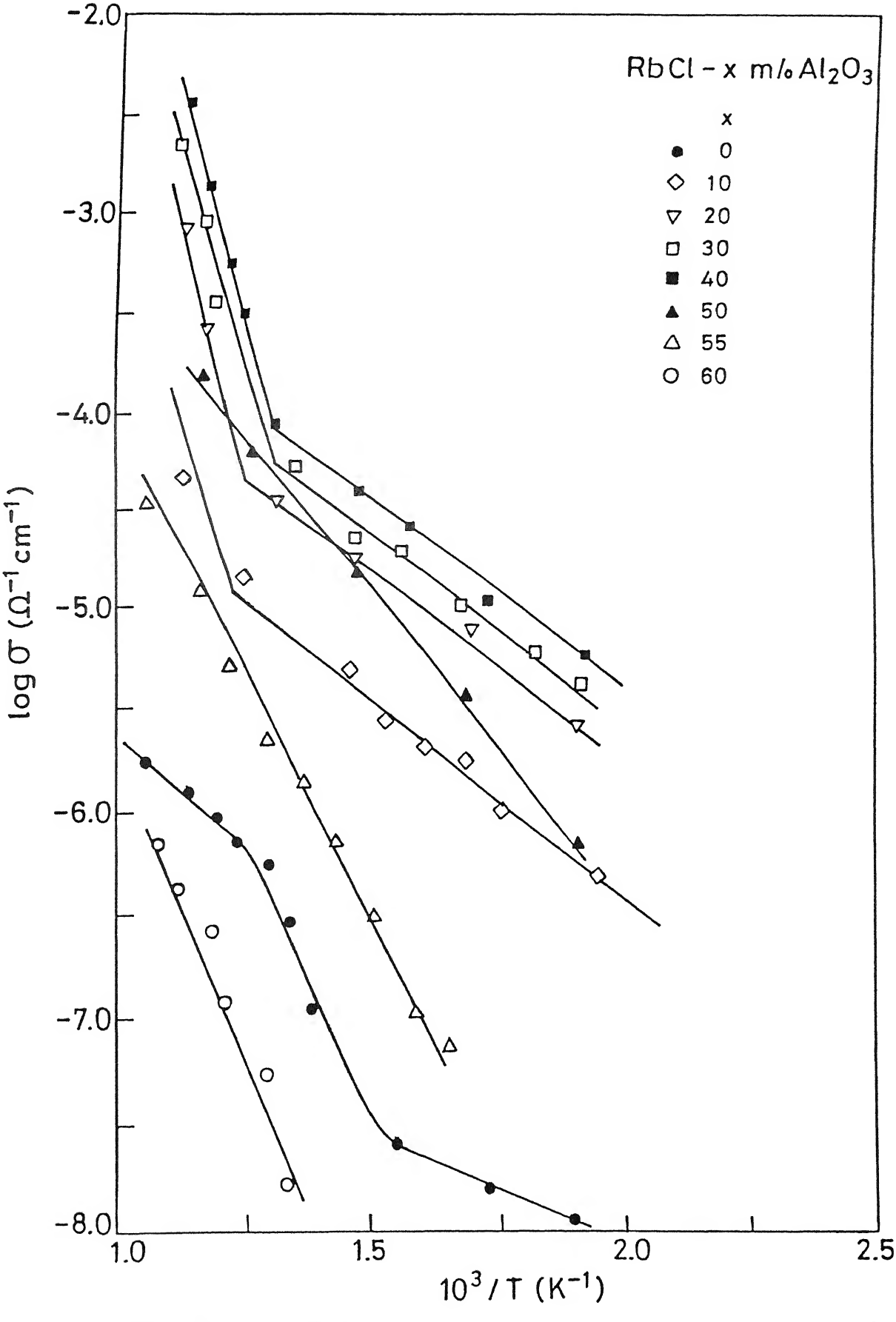

Fig.5.21 Conductivity vs temperature inverse for variou
RbCl-Al_2O_3 composites.

and thereby create excess of Rb^+ ion vacancies in the intefacial region leading to higher conductivity.

Fig.5.22 compares the log σ versus $10^3/T$ plots for RbCl-40 m/o Al_2O_3 samples prepared by the (i) conventional and (ii)

Table 5.16

Ionic transport parameters, the activation energy (E_a) and the preexponential factor (σ_o), for various RbCl-Al_2O_3 composites

composition (Al_2O_3) (m/o)	(v/o)	temperature range (°C)	E_a (eV)	σ_o (ohm cm)$^{-1}$
0	0	500-600	0.39	2.1×10^{-4}
		600- -	-	-
10	6	200-550	0.40	4.1×10^{-3}
		550-600	1.87	4.0×10^{6}
20	13	200-500	0.38	1.4×10^{-2}
		550-600	1.90	8.2×10^{7}
30	20	200-450	0.33	1.3×10^{-2}
		500-600	1.69	9.2×10^{6}
40	28	200-450	0.31	3.3×10^{-2}
		500-600	1.80	7.1×10^{7}
50	37	250-600	0.62	6.1×10^{-1}
55	42	400-600	0.98	7.2
60	47	500-600	1.20	2.2

solution casting methods. The samples prepared by the latter technique show about an order of magnitude higher conductivity than those prepared by the former method. These results which are similar to those observed in MX-Al_2O_3 (M=Na, K), underline once

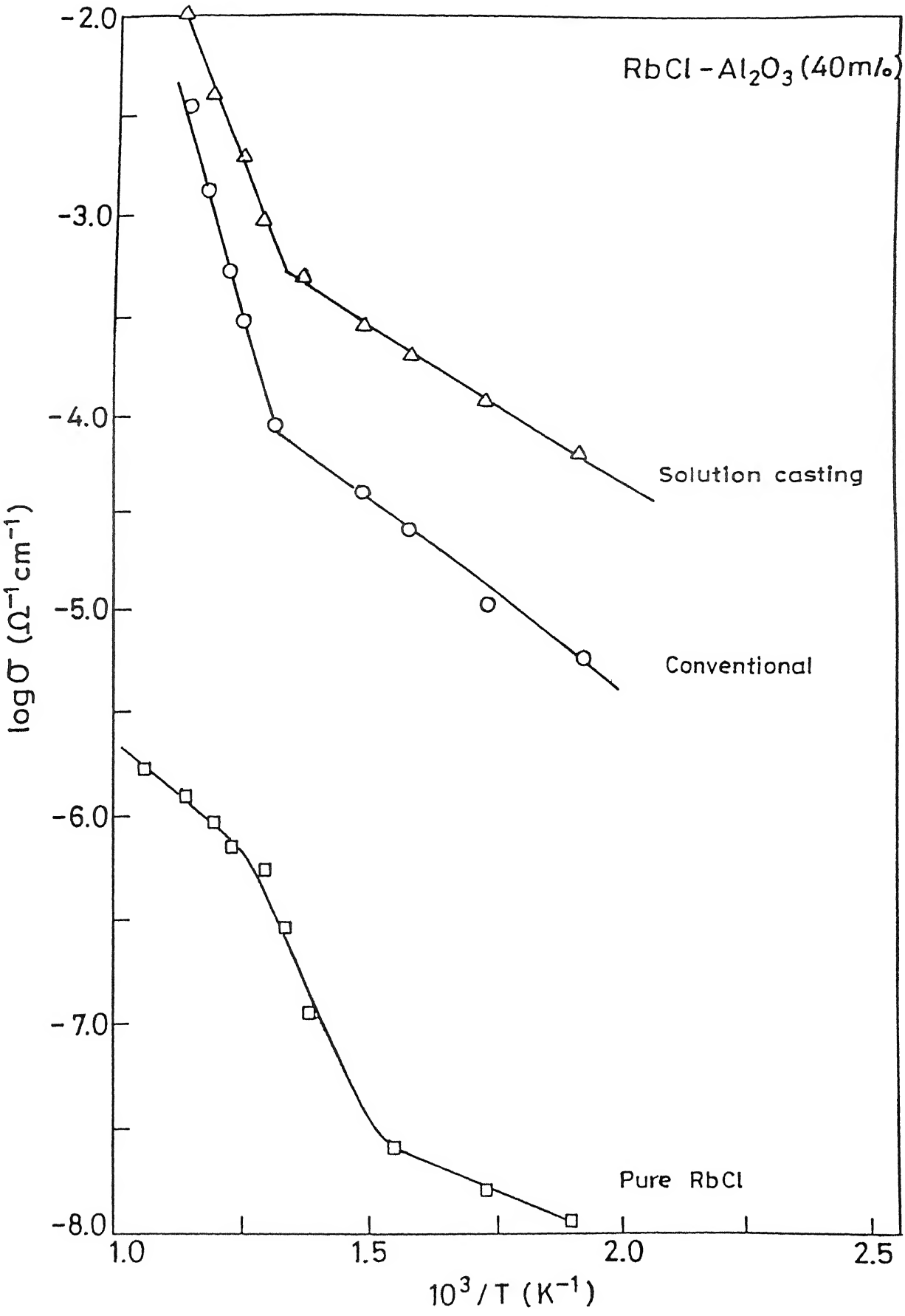

Fig. 5.22 log(σ) vs $10^3/T$ for RbCl-40 m/o Al_2O_3 composites

again the critical role played by the interfaces. The preparation of samples by the solution casting method results into a better dispersion of particles and perhaps, more importantly, more efficient stabilization of cations at the interface resulting in higher concentrations of cation vacancies in the space charge layer, and hence a higher conductivity.

5.4 Summary and Conclusions :

1. The XRD, DTA and SEM studies confirm that the MCl-Al_2O_3 (M=Na, K, Rb) form two-phase composite solid electrolyte systems.

2. The following observed facts that :

(i) The dispersion of as-received Al_2O_3 in the salts MCl (M=Na, K and Rb) leads to 2 to 3 orders of magnitude enhancement in the conductivity.

(ii) The samples prepared by the solution casting method exhibit higher conductivity values than those prepared by the conventional method, and

(iii) The enhancement in σ is larger due to finer Al_2O_3 particles, and that the conductivity maximum shifts to higher concentrations of Al_2O_3 as the particle size decreases.

All underline the critical role played by the interfaces.

3. The good agreement between the observed and the calculated values of conductivity, and the observed linear dependence of the normalized conductivity (σ/σ_o) versus inverse particle size ($1/r_A$) plots and a fair agreement between the experimental and calculated values of their slope (K), strongly support the Maier's space charge theory of conduction in the composite solid electrolytes.

4. The results on all the three systems are, by and large, consistent with the random resistor network (RRN) model.

5. Lastly, the NaCl-30 m/o Al_2O_3 composite prepared by solution casting method which exhibits a $\sigma \sim 10^{-4}$ $(ohm\text{-}cm)^{-1}$ (at 300^oC) that is comparable to to that of Na-β-Al_2O_3, may be further developed and considered for Na/S battery.

CHAPTER 6

CsCl - Al_2O_3 SYSTEM

It is widely accepted that in heterogeneously doped two phase mixtures, the increase in the conductivity occurs due to increased concentration of defects in the matrix-phase adjoining the dispersoid (space charge layer) due to internal adsorption (Jow and Wagner, 1979; Wagner, 1980; Bunde et.al.,1985; Wang and Dudney, 1986; Maier, 1984,1985,1986). However, the direct evidence of the existence of the space charge layer is still a subject of intensive investigation.

This chapter reports the conduction characteristics of CsCl-Al_2O_3 composites. CsCl has been chosen not only because it is a member of the alkali metal chloride family which has been investigated in this work but also it is the only member which undergoes a structural phase transformation and its both B1 (NaCl structure) and B2 (CsCl structure) phases are normal ionic conductors (Wood et.al., 1958). Thus the effect of Al_2O_3 dispersion on the B1$\longleftrightarrow$B2 structural phase transition can also be studied besides the composite solid electrolyte effect.

CsCl-Al_2O_3 composites of various compositions have been prepared by conventional as well as solution casting methods as described in section 3.2. The samples are sintered at 450^{o}C for ~ 24 h. Most of the samples are investigated by DTA, XRD and SEM

techniques for phase analysis and microstructural characterization.

The dc electrical conductivity of the samples at different temperatures is obtained from the complex impedance analysis. The complex impedance spectra for various samples were consistent with that of a constant phase element in parallel with a resistance. The diameter of the high frequency semicircular plot yields the dc resistance of the samples which is used to calculate the conductivity of the samples.

6.1 X - ray Diffraction :

Fig. 6.1 shows the XRD patterns at room temperature of CsCl-40 m/o Al_2O_3 samples without heat treatment (curve a), after sintering at 400°C (curve b) and at 600°C (curve c). That there are no new peaks and no shift in the XRD peaks due to the heat treatment, leads to the conclusion that no new phase is formed as a result of chemical reaction or solid solution formation between Al_2O_3 and CsCl.

6.2 Differential Thermal Analysis :

Fig.6.2 shows the DTA curves for pure CsCl and CsCl-Al_2O_3 composites of three different compositions, viz., 5, 30 and 50 m/o Al_2O_3. There are two thermal events in each case corresponding to the B1$\longleftrightarrow$B2 phase transition and the melting transition of CsCl. The absence of any new peak, and the fact that there is no shift in the positions of the two peaks suggest that neither there is a

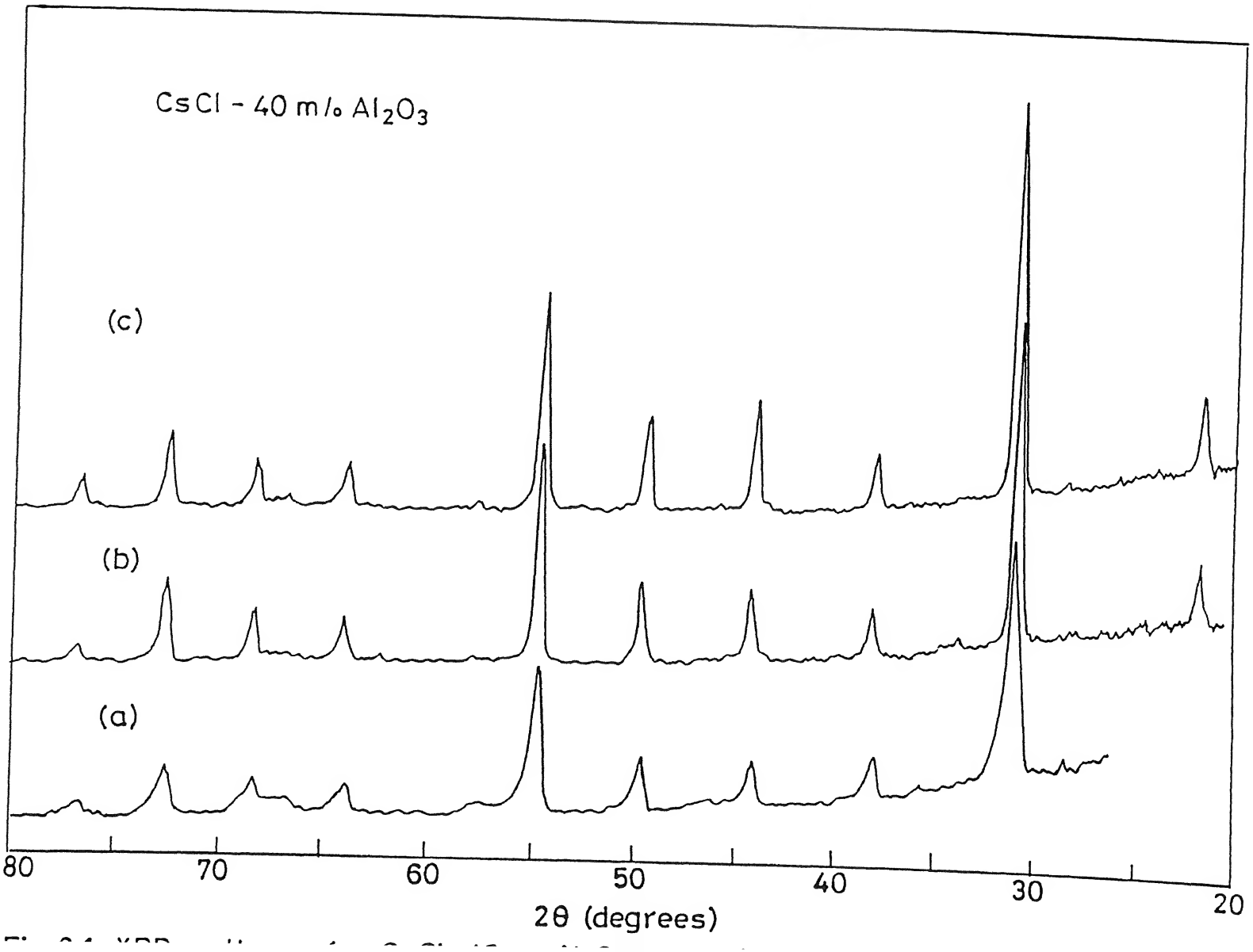
CsCl - 40 m/o Al_2O_3
(c)
(b)
(a)
80
70
60
50
40
30
20
2θ (degrees)

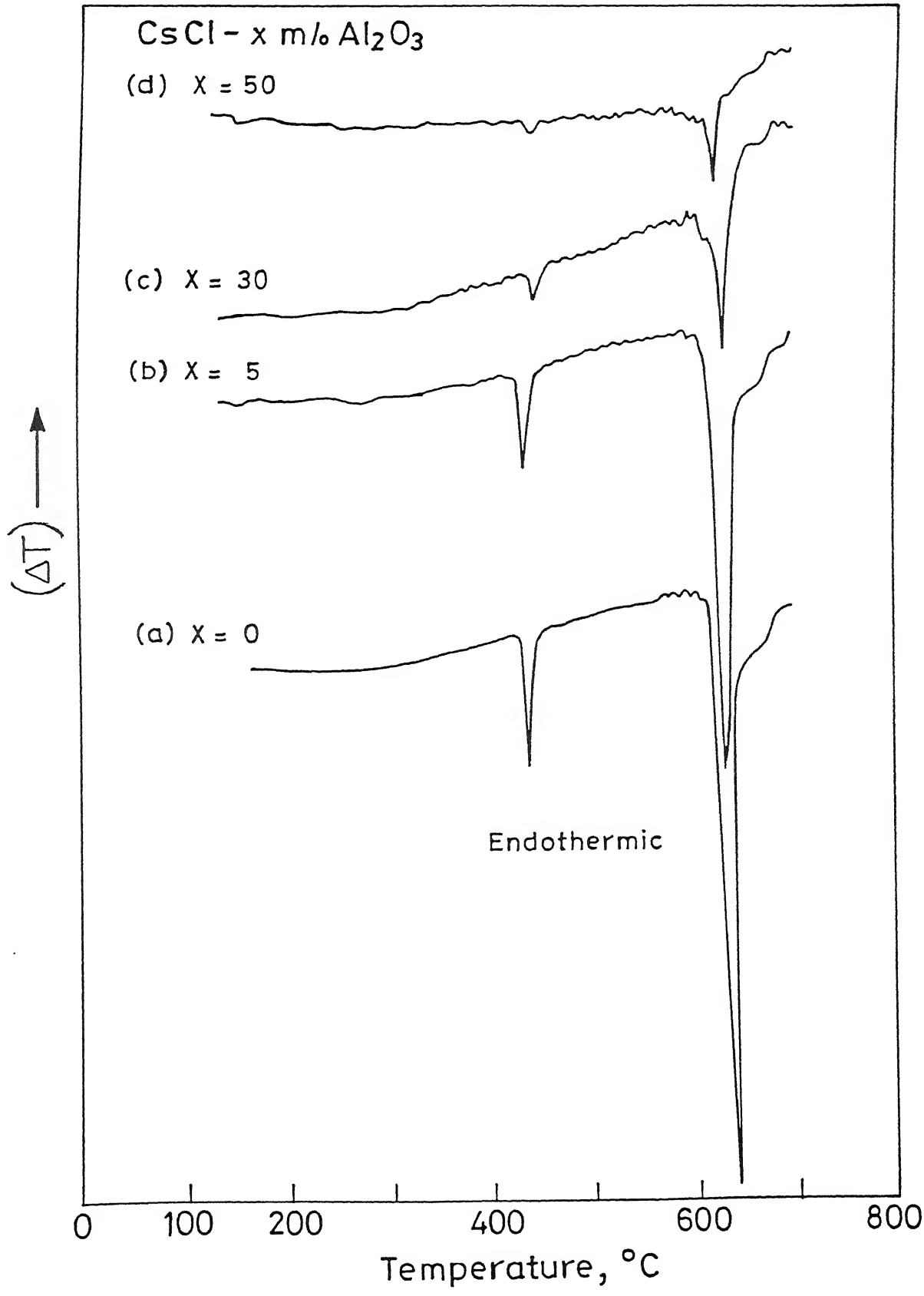

Fig. 6.2 DTA curves for various CsCl-Al_2O_3 composites.

chemical reaction nor solid solution formation between CsCl and Al_2O_3. Thus Al_2O_3 exists as a separate phase in CsCl, and does not affect the structural (B1$\longleftrightarrow$B2) and the melting transition temperatures of CsCl.

6.3 Scanning Electron Microscopy :

The scanning electron micrographs for pure CsCl and CsCl - 40 m/o Al_2O_3 composite sintered at 450°C are shown in Fig.6.3. In case of pure CsCl (Fig.6.3a) the grains are uniformly distributed, whereas in case of CsCl-40 m/o Al_2O_3 the two phase microstructure of CsCl grains interspersed with Al_2O_3 particles is observed (Fig.6.3b).

6.4 Conductivity vs Composition :

Fig. 6.4 shows the variation of conductivity as a function of concentration (m/o) of Al_2O_3 at three different temperatures, viz., 300, 400 and 500°C. Table 6.1 lists the normalized conductivity (σ/σ_o) of various CsCl-Al_2O_3 composites at 300, 400 and 500°C. The results show that the maximum enhancement in the conductivity occurs around 40 m/o Al_2O_3. These results are in general similar to those reported earlier in this work and indeed for a variety of systems elsewhere. However, unlike the general trend, a higher enhancement in the conductivity is observed at higher temperatures (Table 6.1) in this system. This is due to the fact that the high temperature B1 phase (stable above ~470°C) is a normally conducting phase with a lower conductivity and a higher activation energy. Thus the relative enhancement in the

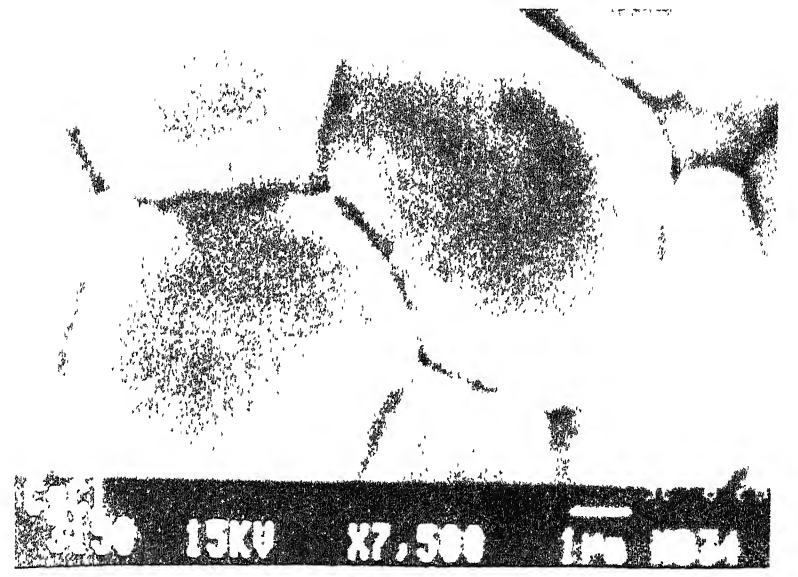

(a)

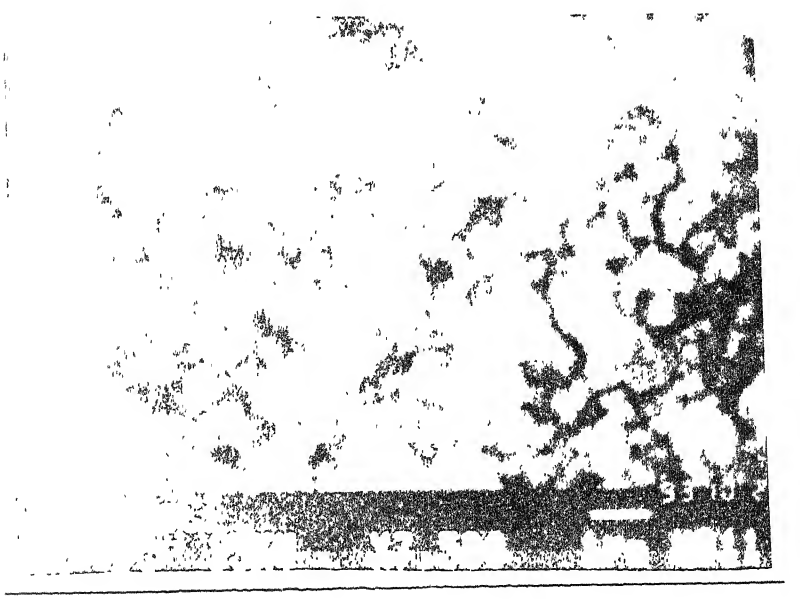

(b)

Fig. 6.3 SEM micrographs for (a) CsCl and, (b) CsCl - 40 m/o Al_2O_3 composite sintered at 500°C.

conductivity is higher at higher temperatures.

Table 6.1

Normalized conductivity (σ/σ_o) for CsCl-Al_2O_3 composites of various compositions at three different temperatures

composition (Al_2O_3)		σ/σ_o		
m/o	v/o	300°C	400°C	500°C
0	0	1	1	1
5	3	1.3	1.5	9.5
10	6	2.4	3.0	18
20	13	3.4	4.5	36
30	21	5.0	6.0	40
40	29	9.0	17	2.0×10^2
50	38	2.0	3.0	24

CsCl is also a Schottky disordered material but, unlike in NaCl, KCl and RbCl, in CsCl the anion vacancies are more mobile than the cation vacancies and a structural phase transition occurs around ~470°C (Wood et.al.,1958; Hoodless and Morrison, 1962; Arends and Nijboer, 1967). However, the mobilities of Cs^+ and Cl^- ion vacancies are comparable (Laurent and Benard, 1957; Harvey and Hoodless, 1967). As in case of other systems (Chapter 5) here also the classical doping mechanism cannot explain the observed enhancement in the conductivity because one molecule of dissolved Al_2O_3 in CsCl will provide one cesium ion vacancy (V_{Cs}^+) as per the following reaction,

$$Al_2O_3 \Leftrightarrow 2Al_{Cs}^{\cdot\cdot} + V_{Cs}^{\prime} + 3O_{Cl}^{\prime} \qquad (6.1)$$

and thus, as a simple calculation using known mobility values of Cs^+ ion vacancies at 300°C would suggest, only a fraction of a mole percent of Al_2O_3 would suffice to obtain the observed enhancement in the conductivity. However, very little enhancement in the conductivity is observed due to addition of as high as 5 m/o Al_2O_3 and the maximum enhancement in any case is less than an order of magnitude at '40 m/o Al_2O_3. This clearly suggests that the classical doping mechanism cannot explain the conductivity enhancement in $CsCl-Al_2O_3$ composites.

As in case of $PbI_2-Al_2O_3$ and $MCl-Al_2O_3$ (M = Na, K, Rb) (Chapters 4 and 5, the observed enhancement in the conductivity of $CsCl-Al_2O_3$ system may also be discussed in terms of space charge layer formation at the interface due to stabilization of positively charged species Cs^+ ions at the Al_2O_3 surface, thereby creating excess Cs^+ ion vacancies at the interface. Thus as the concentration of cation vacancies ($V_{Cs}+$) increases, that of anion vacancies ($V_{Cl}-$) must simultaneously decrease in order to keep the product of two concentrations ($V'_{Cs}.V^{\cdot}_{Cl}$) constant at a given temperature. Though the mobility of Cs^+ ion vacancies is less than that of Cl^- ion vacancies, the increased concentration of Cs^+ ion vacancies in the space charge region results in a net enhancement in the conductivity of $CsCl-Al_2O_3$ composites.

The calculated value of conductivity on the basis of the space charge theory (Eq.2.45) is quite sensitive to the value of mobility data. For instance, if we use the mobility values of

Cs^+ ion vacancies obtained from the tracer diffusion data of Laurent and Benard (1957), viz., $D=10^{-5}\exp(-0.7/kT)$, one obtains a conductivity of ~ 10^{-9} to 10^{-10} $ohm^{-1}cm^{-1}$ at 400°C for the space charge region, which is 3 to 4 orders of magnitude smaller than the conductivity of bulk (CsCl) phase at the same temperature. Thus, if this is the case than there should be no enhancement in the conductivity of CsCl-Al_2O_3 composites, which contradicts the observation (Fig.6.5). This implies that either the above diffusion data are unreliable or the space charge theory is inadequate for this system.

6.5 Conductivity vs Temperature :

The conductivity versus inverse temperature behavior for various CsCl-Al_2O_3 composites is shown in Fig.6.5. The transport parameters, viz.,the preexponential factor (σ_o) and the activation energy (E_a) for pure CsCl are compared with the literature values in Table 6.2. Our values of σ_o and E_a are in reasonable agreement with those on polycrystalline CsCl samples (Harpur et.al.,1955; Morlin, 1966), but somewhat lower than those on single crystalline CsCl samples (Hoodless and Morrison, 1962; Harvey and Hoodless, 1967).

It is observed that the dispersion of Al_2O_3 in CsCl, like in other alkali chlorides, enhances the conductivity (Fig.6.5). However, it is noteworthy that the dispersion of even ~5m/o Al_2O_3 in CsCl is not only sufficient to *suppress* the abrupt (discontinuous) change in the conductivity at the B1⟷B2 phase

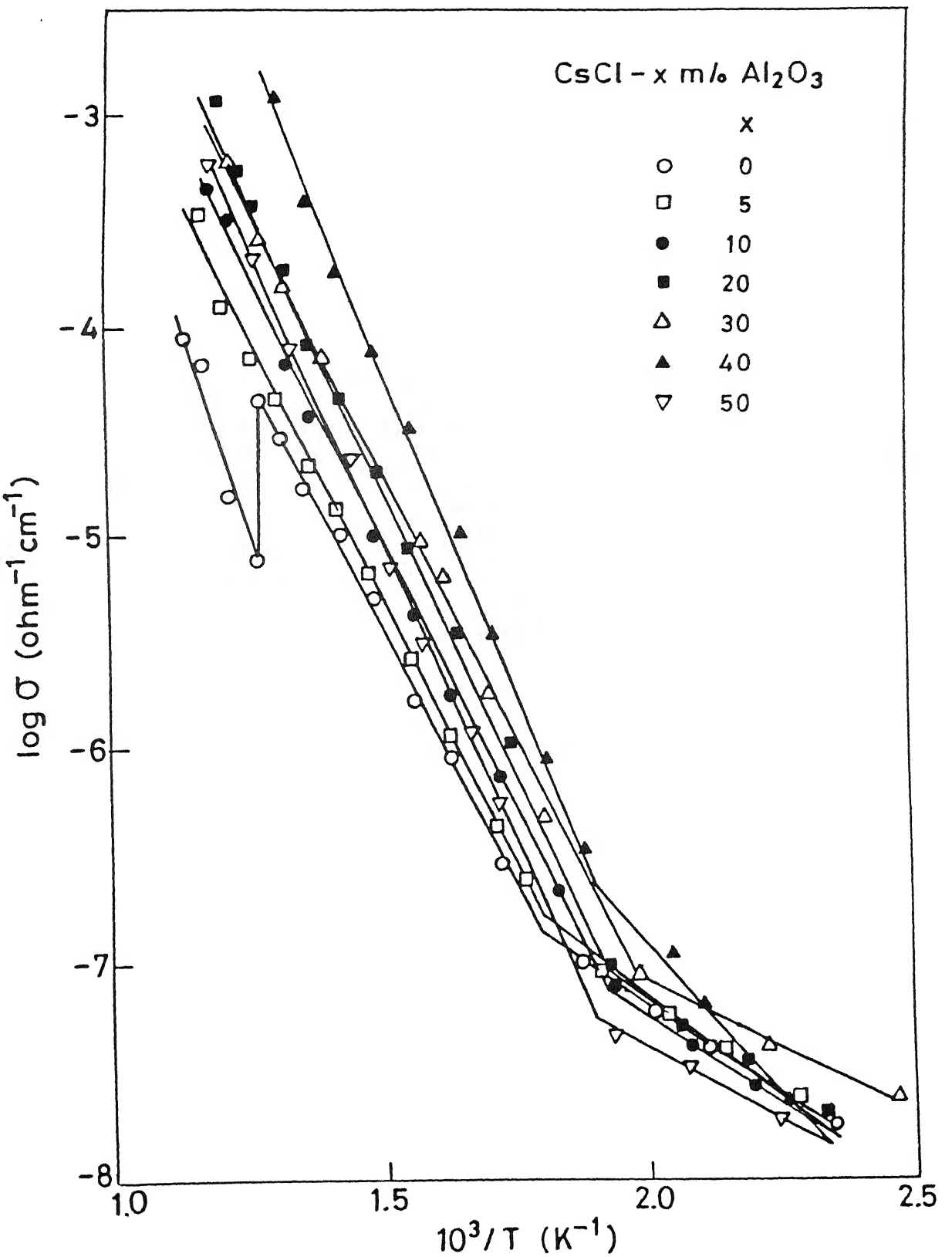

Fig.6.5 log σ vs $10^3/T$ for various CsCl-Al_2O_3 composites.

Table 6.2

Ionic transport parameters, the activation energy (E_a) and the preexponential factor (σ_o), for CsCl

form*	temperature range	E_a (eV)	σ_o $(ohm.cm)^{-1}$	reference
pc	290-450	0.97	85	This work
pc	300-470	1.04	50	Harpur et.al.(1955)
pc	150-460	1.05	100	Morlin (1966)
sc	280-470	1.22	2.3×10^4	Hoodless and Morrison (1962)
sc	290-460	1.26	4.1×10^4	Harvey and Hoodless (1967)

* pc refers to polycrystalline and sc to single crystalline form.

transition temperature (~470°C) but also, and more importantly, any change in the slope of $\ln\sigma$ vs T^{-1} linear plots. As pointed out earlier, (Section 6.2), the differential thermal analyses detect the B1⟷B2 transition in both CsCl and CsCl-Al_2O_3 composites (Fig.6.2). This means that the B1⟷B2 transition indeed occurs in the composite samples as well, but their both $\ln\sigma$ as well as its derivative $d(\ln\sigma)/d(10^3/T)$ versus 1/T curves are continuous at the B1⟷B2 transition temperature (Fig.6.6). The conclusion is therefore inescapable, viz., the conduction in the composites is *independent* of and hence *unaffected* by the events in the bulk CsCl matrix phase. These results therefore provide perhaps the most unambiguous evidence of the direct role of the interfaces in the conduction in the composite electrolytes.

The preexponential factor (σ_o) and the activation energy (E_a)

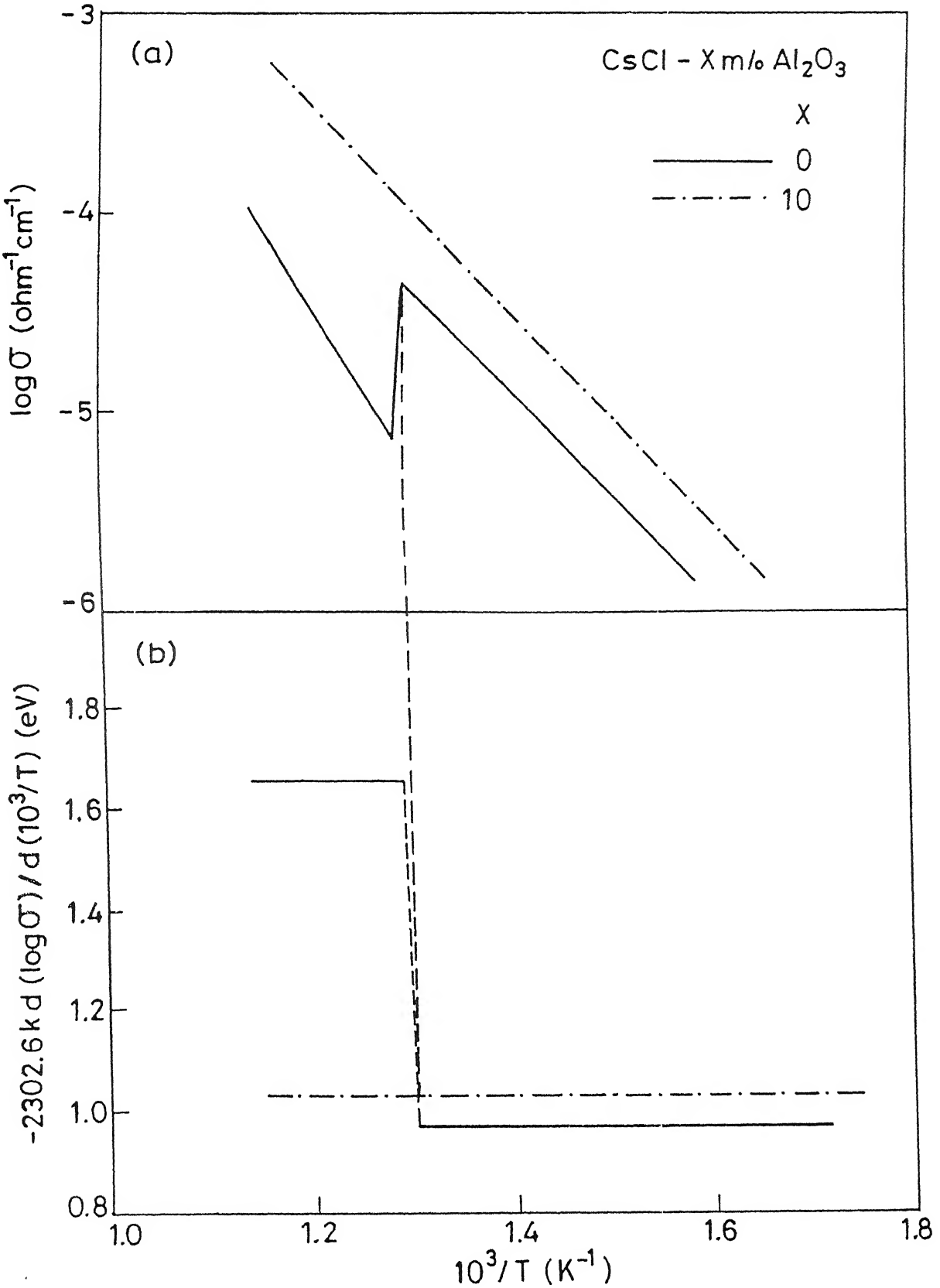

Fig. 6.6 (a) $\log\sigma$ vs $10^3/T$, (b) derivative of $\log\sigma$ w.r.t. $10^3/T$, viz., $[-2302.6\,k\cdot d(\log\sigma)/d(10^3/T)]$ vs $10^3/T$ for CsCl and CsCl-10 m/o Al_2O_3 composite.

of various CsCl-Al_2O_3 composites are listed in Table 6.3. It is observed that there is a slight increase in the activation energy as the concentration of Al_2O_3 increases in the composites. It would appear that as the concentration of Al_2O_3 increases, the conduction is increasingly dominated by the Cs^+ ion vacancies, which have a higher activation energy (Harvey and Hoodless, 1967) and hence the overall activation energy increases. The data of Table 6.3 show once again that the activation energy is continuous across the B1$\longleftrightarrow$B2 phase transition temperature, and hence a single mechanism operates in both the phases.

Fig.6.7 compares the conductivity-temperature behavior for CsCl-40 m/o Al_2O_3 composites prepared by the (i) conventional and (ii) solution casting methods. Also shown in this figure are the

Table 6.3

The ionic transport parameters, the activation energy (E_a) and the preexponential factor (σ_o) for various CsCl-Al_2O_3 composites

composition(Al_2O_3) (m/o)	(v/o)	temperature range (°C)	E_a (eV)	σ_o $(ohm\text{-}cm)^{-1}$
0	0	250-450	0.97	85
		500-600	1.66	3.1×10^5
5	3	250-600	1.01	2.2×10^2
10	6	250-600	1.03	5.6×10^2
20	13	250-600	1.06	1.8×10^3
30	21	250-600	1.00	7.5×10^2
40	29	250-600	1.22	1.1×10^5
50	38	250-600	1.14	3.9×10^5

results of pure CsCl. Table 6.4 compares the normalized conductivity of CsCl-40 m/o Al_2O_3 composites prepared by the conventional and solution casting methods at 300, 400, 500°C. It

Table 6.4

Normalized conductivity (σ/σ_o) for CsCl-40 m/o Al_2O_3 composites prepared by the conventional and solution casting methods

composite type	σ/σ_o		
	(300°C)	(400°C)	(500°C)
conventional	9	17	199
solution casting	158	126	708

is observed that the solution casting method show higher σ than those prepared by the conventional method. These results further indicate that the enhancement in σ is due to the surface induced defects. The higher enhancement in the conductivity could be due to the presence of chemical species such as water molecules which increases the rate of cation disorder reaction and hence the concentration of cation vacancies in the space charge layer at the matrix-particle interface.

6.6 Summary and Conclusions:

The CsCl-Al_2O_3 composites exhibit enhanced conductivity over pure CsCl. The combined results of the electrical conductivity and the DTA directly show the evidence of the existence of the space charge layer in the composite systems. The results are consistent with the Maier's space charge theory of electrical transport in CSEs. The composites prepared by the solution casting method show

conductivity values higher than those prepared by the conventional method which once again underlines the importance of interfacial mechanism of conduction in composites solid electrolytes.

SUMMARY AND CONCLUSIONS

1. The DTA, XRD and SEM studies confirm that Al_2O_3 is not soluble in any of the seven host materials, viz., PbX_2 (X = Cl, Br, I) and MCl (M = Na, K, Rb, Cs), and that the PbX_2-Al_2O_3 and MCl-Al_2O_3 systems are two-phase composites.

2. The following results suggest that the interface plays a critical role in the conduction in the composite solid electrolytes :

(i) The dispersion of as-received Al_2O_3 in PbI_2 and MCl (M = Na, K, Rb, Cs) enhances the conductivity by one to three orders of magnitude.

(ii) The composites prepared by the solution casting method exhibit higher conductivity values than those prepared by the conventional method.

(iii) The base-treated Al_2O_3 is more effective in the conductivity enhancement than the untreated one.

(iv) The enhancement in the conductivity is larger due to dispersion of finer Al_2O_3 particles and the conductivity maximum shifts to higher concentrations of Al_2O_3 as the particle size increases, and *more importantly*,

(v) The conductivity versus temperature studies on $CsCl-Al_2O_3$ composites do not show any evidence of the B1 (NaCl) $\longleftrightarrow$ B2 (CsCl) structural phase transformation which actually occurs and is detected by DTA at ~ $470^{o}C$, implying that the conductivity in the composites is *independent of*, and hence *unaffected by* the events in the bulk matrix phase.

3. The following results support the Maier's space charge theory of transport in composite solid electrolytes :

(i) While the conductivity in $PbCl_2$ and $PbBr_2$ decreases, that in PbI_2 increases due to dispersion of Al_2O_3. This is attributed to the fact that the Pb^{2+} ion vacancies are almost immobile in the former two salts while they are as mobile as Cl^{-} ion vacancies in PbI_2. Thus though their mobility is lower, the increased concentration of Pb^{+} ion vacancies at the $PbI_2-Al_2O_3$ interface gives rise to a net enhancement in the conductivity.

(ii) All the three composites, viz., $MCl-Al_2O_3$ (M = Na, K, Rb) exhibit enhanced conductivity which is attributable to the generation of *excess* as well as *more mobile* cation vacancies in the space charge region at the $MCl-Al_2O_3$ interface.

(iii) The calculated values of the conductivity on the basis of space charge theory are found to be comparable with the observed values in the $MCl-Al_2O_3$ (M = Na, K, Rb) composite systems.

(iv) The conductivity versus inverse particle size (r_A^{-1}) plots are found to be linear within the experimental error. Moreover, the observed slopes agree well with the calculated ones in case of $MCl\text{-}Al_2O_3$ (M = Na, K, Rb) systems.

(v) Though the mobility of Cs^+ ion vacancies is lower, though comparable to that of the Cl^- ion vacancies in CsCl, the increased concentration of Cs^+ion vacancies at the $CsCl\text{-}Al_2O_3$ interface leads to the enhancement in the conductivity.

4. NaCl-(30-40) m/o Al_2O_3 composite prepared by the solution casting method show a conductivity ~ 10^{-4} $ohm^{-1}cm^{-1}$ at 300^oC which is comparable to the conductivity of Na-β-Al_2O_3 at that temperature, and hence is worth considering for further development and application in Na/S batteries.

REFERENCES

Akila R and Jacob K T (1987) Solid State Ionics 25, 217.

Almond D P and West A R (1983) Solid State Ionics **11**, 57.

Arai G and Mullen J G (1966) Phys. Rev. **143**, 663.

Archer W I and Armstrong R D (1980) in : *Electrochemistry* **vol.7**, ed. Thirsk H R, (The Chemical Society, London), p.157.

Arends J and Nijboer H (1967) Solid State Commun. **5**, 163.

Armand M B, Chabagno J M and Duclot M J (1979) in :*Fast Ion Transport in Solids*, eds. Vashishta P, Mundy J N and Shenoy G K, (Elsevier, North Holland, Amsterdam), p.131.

Armand M B (1986) Ann. Rev. Mater. Sci. **16**, 245.

Bauerle J E (1969) J Phys. Chem. Solids **30**, 2657.

Beaumont J H and Jacobs P W M (1966) J. Chem.Phys. **45**, 1496.

Beevers C A and Ross M A S (1937) Z. Krist **97**, 59.

Bollmann W and Henniger H (1972) Phys. Stat Sol. (a) **11**, 367.

Bollmann W and Reimann R (1973) Phys. Stat. Sol. (a) **16**, 187.

Bradley J N and Greene P D (1966) Trans Faraday Soc. **62**, 2069.

Bradley J N and Greene P D (1967) Trans Faraday Soc. **63**, 424.

Braekken H (1932) Z. Krist **83**, 222.

Brune A and Wagner J B Jr. (1987) Solid State Ionics **25**, 165.

Bunde A, Dieterich W and Roman H E (1985) Phys. Rev. Lett.**55**, 5.

Bunde A, Dieterich W and Roman H E (1986) Solid State Ionics **18/19**, 147.

Burley G (1963) Am. Miner **48**, 1266.

Burley G (1967) Acta Cryst. **23**, 1.

Carrillo-Cabrera W, Thomas J O and Farrington G C (1988) Solid State Ionics 28-30, 317.

Chang M R-W, Shahi K and Wagner J B Jr. (1984) J. Electrochem. Soc. **131**, 1213.

Chen Liquan, Zhao Zongyuan, Wang Chaoying and Li Zirong (1985) Acta Physica Sinica, **34**, 1027.

Chen Liquan (1986) in : *Materials for Solid State Batteries*, eds. Chowdhary B V R and Radhakrishna S, (World Scientific Publ. Co., Singapore), pp 69-82.

Chowdhary P, Tare V B and Wagner J B Jr. (1985) J. Electrochem. Soc. **132**, 123.

Cotterill P and Mould P R (1976) in : *Recrystallization and Grain Growth in Metals*,(Newyork, Wiley), pp. 5-29, 180-249.

Crosbie G M (1978) J Solid State Chem. 25, 367.

Derrington C E, Lindner A and O'Keeffe M (1975), J. Solid State Chem. **15**, 171.

De Vries K J and Van Santen J H (1963) Physica **29**, 482.

Dreyfus R W and Nowick A S (1962) Phys. Rev. **126**, 1367.

Dudney N J (1985) J.Am. Ceram. Soc. **68**, 538.

Dudney N J (1988) Solid State Ionics **28-30**, 1065.

Ebert I and Tetlow J (1955) Ann. Physik (Leipzig) **15**, 268.

Eshelby J D, Newey C W A, Pratt P L and Lidiard A B (1958) Phil. Mag.**8**, 75.

Etsell T H and Flengas S N (1970) Chem. Rev. **70**, 339.

Etzel H W and Maurer R J (1950) J. Chem. Phys. **18**, 1003.

Faraday M (1839) in : *Experimental investigations in electricity*, (Quaritch, London), No.1340.

Farrington G C and Briant J L (1978) Mat. Res. Bull. **13**, 763.

Farrington G C and Dunn B (1982) Solid State Ionics **7**, 267.

Farrington G C, Dunn B and Thomas J O (1983) Appl. Phys.A **32**, 159.

Fenton D E, Parker J M and Wright P V (1973) Polymer **14**, 589.

Fijitsu S, Miyayama M, Koumoto K, Yanagida H and Kanazawa T (1985) J. Mat. Sci. **20**, 2103.

Fijitsu S, Koumoto K and Yanagida H (1986) Solid State Ionics **18/19**, 1146.

Frenkel J (1926) Z.Physik 35, 652.

Frenkel J (1946) in : *Kinetic theory of liquids*, (Oxford University Press, New York), p.36.

Friauf R J (1972) in : *Physics of Electrolytes* **Vol.1**, ed. Hladik J, (Academic Press, London, New York), p.153.

Fuller R G and Reilly M H (1967) Phys. Rev.**19**, 113.

Geller G (1976) Phys. Rev. B **14**, 4345.

Goodenough J B, Hong H Y-P and Kafalas J A (1976) Mat. Res. Bull. **11**, 203.

Gyulai Z (1931) Z. Phys. 67, 812.

Harvey P J and Hoodless I M (1967) Phil. Mag.**16**, 543.

Harpur W W, Moss R L and Ubbelohde A R (1955) Proc. Roy. Soc. A **232**, 196.

Hartwig P and Weppner W (1981) Solid State Ionics **3/4**, 249.

Haven Y (1950) Rec. Trav. Chim. pays-Bas 69, 1471.

Haven Y and Verkerk B (1965) Phys. Chem. Glasses **6**, 38.

Hodge I M, Ingram M D and West A R (1976) J. Electroanal. Chem. **74**, 125.

Hoodless I M and Morrison J A (1962) J. Phys. Chem., **66**, 557.

Hooper A (1977) J. Phys. D: **10**, 1487.

Hoshino H, Yamazaki M, Nakamura Y and Shimoji M (1969) J. Phys. Soc. Japan **26**, 1422.

Hoshino H, Yokose S and Shimoji M (1973) J.Solid State Chem. **7**, 1.

Huggins R A (1977) Electrochim Acta 22, 773.

Hughes K and Isard J O (1972) in : *Physics of electrolytes* vol.1, ed. Hladik J (Academic Press, London, Newyork) p 351.

Ingram M D (1980) J Am. Ceram. Soc. 63, 248.

Jacobs P W M and Tompkins F C (1952) Q. Rev. Chem. Soc. 6, 238.

Jander W (1929) Angew. Chem. 42, 462.

Johannesen O and Mckelvy M (1985) Solid State Ionics 17, 251.

Johannesen O and Mckelvy M (1986) J. Phys. Chem. Solids 47, 265.

Joshi A V and Wagner J B Jr. (1975) J.Electrochem.Soc. 122, 1071.

Jow T and Wagner J B Jr. (1979) J. Electrochem. Soc. 126, 1963.

Kelting H and Witt H (1949) Z. Physik 126, 697.

Kennedy J H (1977) J. Electrochem.Soc. 124, 865.

Ketelaar J A A (1938) Trans Faraday Soc. 34, 874.

Khandkar A C and Wagner J B Jr. (1986) Solid State Ionics 20, 267.

Khandkar A C, Tare V B and Wagner J B Jr. (1986) Rev. Chim. Miner. 23, 274.

Kingrey W D, Bowen H K and Uhlmann D R (1976) in :*Introduction to Ceramics*, (Newyork, Wiley), p.250.

Kiukkola K and Wagner C (1957) J. Electrochem. Soc. 104, 308, 379.

Kliewer K L and Koehler J (1965) Phys. Rev. 140, A1126.

Kliewer K L (1966) J. Phys. Chem. Solids 27, 705.

Koch E and Wagner C (1937) Z. Phys. Chem. B 38, 295.

Koularausch W (1882) Ann. Phys. 17, 642.

Kvist A and Lunden A (1965) Z. Naturf. 20a, 235.

Landauer R (1952) J. Appl. Phys. 23, 779.

Lange F F and Hirlinger M M (1987) J. Am. Ceram. Soc. 70, 827.

Laurent J F and Benard J (1957) J. Phys. Chem. Solids 3, 7.

Lehfeldt W (1933) Z. Physik 85, 717.

Lehovec K (1953) J. Chem. Phys. 21, 1123.

Liang C C (1973) J. Electrochem. Soc. 120, 1289.

Liang C C, Joshi A V and Hamilton N E (1978) J. Appl. Electrochem. 8, 445.

Lidiard A B (1957) in : *Handbuch der physik*, ed. Flugge S vol.20, (Springer-verlag, Berlin), p.246.

Lieser K H (1954) Z. Phys. Chem. (N.F.) 2, 238.

Lingras A P and Simkovich G (1978) J. Phys. Chem. Solids 39, 1225.

Liu S H, Kaplan T and Gray L J (1986) Solid State Ionics 18/19, 65.

Lumsden J (1966) in : *Thermodynamics of molten salt mixtures*, (Academic Press, London).

Maier J (1984) Ber. Bunsenges. Phys. Chem. 88,1057; Phys. Stat. Sol.(b) 123, K89.

Maier J (1985) Mat. Res. Bull. 20, 383; J. Phys. Chem. Solids 46, 309; Ber. Bunsenges. Phys. Chem. 89, 355.

Maier J (1986) Solid State Ionics 18/19, 1141; Ber. Bunsenges. Phys. Chem. 90, 26.

Maier J (1987) J. Electrochem. Soc. 134, 1524; Solid State Ionics 23, 59; Mater. Chem. Phys. 17, 485.

Maier J and Reichert B (1986) Ber. Bunsenges. Phys. Chem. 90, 666.

Martin S W and Angell C A (1986) J. Non. Cryst. Solids. 83, 185.

Matsui T and Wagner J. B. Jr. (1977) J. Electrochem. Soc. 124, 300.

Maxwell J C (1881) in : *A treatise on electricity and magnetism* vol.1, 2nd ed., Clare Don Press, Oxford, p.435.

Macdonald J R (1984) Solid State Ionics 13, 147.

Melo F E A, Garrett K W, Mendos Filho J and Moreira J E (1979) Solid State Commun. 31, 29.

Morlin Z (1966) Acta Phys. Hung. 21, 137.

Moynihan C T and Lesikar A V (1981) J Am. Ceram. Soc. 64, 40.

Muhlherr S, Lauger K, Nicoloso N, Schreck E and Dransfeld K (1988) Solid State Ionics **28-30**, 1495.

Mundy J N and Jin G L (1986) Solid State Ionics **21**, 305.

Mundy J N and Jin G L (1987) Solid State Ionics **24**, 263.

Nakamura O and Goodenough J B (1982) Solid State Ionics **7**, 119.

Nakamura O and Goodenough J B (1984) solid State Ionics **7**, 125.

Oberschmidt J and Lazarus D (1980) Phys. Rev. B **21(12)**, 5813.

O' Keeffe M (1973) Science **180**, 1276.

O' Keeffe M and Hyde B G (1976) Phil. Mag. **33**, 219.

Olgaard D L and Evans B (1986) J. Am. Ceram. Soc. **69**, C272.

Owens B B and Argue G R (1967) Science **157**, 308.

Owens B B (1971) in : *Advances in Electrochemistry and Electrochemical Engineering*, **Vol.8**, ed. Tobias C W, (John Wiley, Newyork).

Pack S (1979) *Electrical conductivity of* HgI_2 *containing* Al_2O_3 *particles*, Abstract 133, Electrochemical society meeting, Los Angeles.

Pack S, Owens B and Wagner J B Jr. (1980) J. Electrochem. Soc. **127**, 2177.

Pansare A K and Patankar A V (1974) Pramana **2**, 282.

Perrott C M and Fletcher N H (1968) J. Chem. Phys. **48**, 2143, 2681.

Peters C R, Bettman M, Moore J W and Glick M D (1971) Acta Cryst. B **27**, 1826.

Peterson N L, (1983) in : *Character of Grain Boundaries*, ed. Yan M F and Heuer A H, The American Ceramic Society , Columbus, Ohio, pp.236-254.

Phipps J B, Johnson D L and Whitmore D H (1981) Solid State Ionics **5**, 393.

Phipps J B and Whitmore D H (1983) Solid State Ionics **9/10**, 123.

Pierce C B (1961) Phys. Rev. **123**, 744.

Poulsen F W (1982) Solid State Ionics 2, 53.

Poulsen F W (1987) J. Power Sources 20, 317.

Raistrick I D (1986) Solid State Ionics 18/19, 40.

Raleigh Lord (1892) Phil. Mag. 34, 481.

Randles J E B (1947) Discussion Faraday Society 1, 11.

Ratner M A and Nitzan A (1988) Solod State Ionics 28-30, 3.

Ratner M A and Shriver D F (1988) Chem. Rev. 88, 109.

Ravaine D and Souquet J L (1977) Phys. Chem. Glasses 18, 27.

Ravaine D and Souquet J L (1978) Phys. Chem. Glasses 19, 115.

Reuter B and Hardel K (1961) Nature Wissenchaften 48, 161.

Ridgway R, Klein A and O'Leary W (1936) Trans Elektrochem. 70, 71.

Rice M J, Strassler S and Toombs G A (1974) Phys. Rev. Lett. 32, 596.

Roman H E, Bunde A and Dieterich W (1986) Phys. Rev. B 34, 3439.

Roman H E and Yussouff M (1987) Phys. Rev. B 36, 7285.

Schiraldi A (1975) Z. Phys. Chem. N.F. 97, 285.

Schlaikjer C R and Liang C C (1973) in : *Fast Ion Transport in Solids*, ed. Van Gool W, (North Holland, Amsterdam, 1973), p.685.

Schmidt J A, Bazan J C and Vico L (1988) Solid State Ionics 27, 1.

Schottky W (1935) Z. Phys. Chem. B 29, 335.

Schoonman J and Verwey J F (1968) Physica 39, 244.

Schoonman J, Ebert L B, Hsieh C H and Huggins R A (1975) J. Appl. Phys. 46, 2873.

Schreck E, Lauger K and Dransfeld K (1986) Z. Phys. B 62, 331.

Schwab G M and Eulitz G (1967) Z.Physik Chem. (Frankfurt) 55, 179.

Shahi K and Wagner J B Jr.(1981) Solid State Ionics 3/4, 295.

Shahi K and Wagner J B Jr. (1981) J.Electrochem. Soc. 128, 6.

Shahi K and Wagner J B Jr. (1982) J. Solid State Chem. 42, 107.

Shahi K and Wagner J B Jr.(1983) J. Phys. Chem. Solids **44**, 89.

Shilton M G and Howe A T (1977) Mater. Res. Bull. **12**, 701.

Shulze H (1952) Ph.D.Thesis, University of Gottingen, p.249.

Shukla A K, Manoharan R and Goodenough J B (1988) Solid State Ionics **26**, 5.

Simkovich G (1963) J. Phys. Chem. Solids **24**, 213.

Skarstad P M, Merritt D R and Owens B B (1981) Solid State Ionics **3/4**, 277.

Slade R C T and Thompson I M (1988) Solid State Ionics **26**, 287.

Smakula A, (1965) M.I.T. Technical Report no.6.

Stoneham A M, Evelyn Wade and Kilner J A (1979) Mat. Res. Bull. **14**, 661.

Strock L W (1934) Z. Phys. Chem. B **25**, 411.

Teltow J (1949) Ann. Phys. Leipzig **5**, 63, 71.

Teltow J (1950) Ann. Physik **5**, 63; Z. Phys. Chem. **195**, 213.

Toshima S, Kimura N, Niizeki Y and Nikaido T (1968) Denki Kagaku **36**, 69.

Tubandt C and Lorentz E (1914) Z. Phys. Chem. **87**, 513.

Tubandt C (1920) Z. Anorg. Allgem. Chem. **110**, 234.

Tubandt C and Eggert S (1920) Z. Anorg. Chem. **110**, 196.

Tubandt C (1921) Z. Anorg. Allgem. Chem. **115**, 105.

Tubandt C (1923) Z. Anorg. Allgem. Chem. **29**, 313.

Tubandt C, Reinhold H and Liebold G (1931) Z. Anorg. Allgem. Chem. **197**, 225.

Tubandt C (1932) in : *Handbuch der Experimentalphysik* **vol.12**, part I, (Akademische Verlagsgesellschaft M B H, Leipzig), p.383.

Tuller H, Button D P and Uhlmann D R (1980) J. Non-Cryst. Solids **40**, 93.

Ure R W Jr. (1957) J. Chem. Phys. **26**, 1363.

Vaidehi N, Akila R, Shulka A K and Jacob K T (1986) Mat. Res. Bull. **21**, 909.

Van Den Brom W E, Schoonman J and De Wit J H W (1972) J. Solid State Chem. **4**, 475.

Verwey J F and Schoonman J (1967) Physica **35**, 386.

Wagner C (1933) Z. Phys. Chem. **B 22**, 181.

Wagner C and Hantelmann P (1950) J. Chem. Phys **18**, 72.

Wagner J B Jr. and Wagner C (1957) J. Chem. Phys. **26**, 1597.

Wagner C (1972) J. Phys. Chem. Solids **33**, 1051.

Wagner J B Jr. (1980) Mat. Res. Bull. **15**, 1691.

Wang J C and Dudney N J (1986) Solid State Ionics **18/19**, 112.

Wang J C and Bates J B (1986) Solid State Ionics **18/19**, 224.

Watanabe M and Ogata N (1988) Br. Polym. J. **20**, 181.

Wen T L, Huggins R A, Rabenau A and Weppner W (1983) Rev. Chim. Min. **20**, 643.

Wiedersich H and Geller S (1971) in : *The Chemistry of Extended Defects in Non-metallic Solids*, ed. Eyring L and O'Keeffe M, (North Holland, Amsterdam).

Wood L J, Secunda W and McBridge C H (1958) J. Am. Chem. Soc. **80**, 307.

Wright P V (1975) Brit. Polym. J. **7**, 319.

Yan M F, Cannon R M, Bowen H K and Coble R L (1977) J. Am. Ceram. Soc. **60**, 120.

Yao Y F Y and Kummer J T (1967) J. Inorg. Nucl. Chem. **29**, 2453.

LIST OF PUBLICATIONS

(A) IN REFEREED JOURNALS :

1. A. Kumar and K. Shahi (1993) *Enhanced ionic conduction in PbI_2-Al_2O_3 composite solid electrolytes*, J. Mat. Sci. **28**, 1257-1263.

2. Ashok Kumar and K. Shahi (1994) *Conductivity enhancement in NaCl by dispersion of Al_2O_3*, J. Solid State Chem. **108**, (in press).

3. Ashok Kumar and K. Shahi, *The conduction characteristics of $CsCl$-Al_2O_3 composites* (communicated).

4. Ashok Kumar and K. Shahi, *Heterogeneous doping effects in KCl-Al_2O_3 composites* (communicated).

5. Ashok Kumar and K. Shahi, *Enhanced electrical transport in $RbCl$-Al_2O_3 composites (communicated).*

(B) IN SYMPOSIA/CONFERENCES :

1. Ashok Kumar and K. Shahi, (1992) *Enhanced ionic conductivity in $NaCl$-Al_2O_3 composite solid electrolyte system*, Pro. third Asian conference on Solid State Ionics : Materials and Applications, eds. Chowdhari B V R, Chandra S, Shri Singh and Srivastava P C (World Scientific, Singapore) pp.433-439.

2. Ashok Kumar and K. Shahi (1993) *The effect of Al_2O_3 dispersion on the ionic conductivity on the ionic conductivity of CsCl*, 14th Risø International Symposium on Materials Science, Risø National Laboratory, Roskilde, Denmark.